The Effects of Temperature and Carbon Nanotubes on Conducting Polymer Actuator Performance

by

Yenmei (Kerri) Keng

B.E. Biomedical Engineering
State University of New York at Stony Brook, 2008

Submitted to the Department of Mechanical Engineering
in partial fulfillment of the requirements for the degree of

Master of Science in Mechanical Engineering

at the

MASSACHUSETTS INSTITUTE OF TECHNOLOGY

June 2010

Signature of Author: ____
Department of Mechanical Engineering
May 7, 2010

Certified by: _____
Ian W. Hunter
Professor in Mechanical Engineering
Thesis Supervisor

Accepted by: _____
David E. Hardt
Chairman, Department Committee on Graduate Students

The Effects of Temperature and Carbon Nanotubes on Conducting Polymer Mechanical Performance

by

Yenmei (Kerri) Keng

Submitted to the Department of Mechanical Engineering
on May 7, 2010 in partial fulfillment of the
requirements for the degree of
Master of Science in Mechanical Engineering

Abstract

Conducting polymers serve as electrically conductive actuators via ion diffusion in and out of the polymer when voltages are applied. Their actuation performance can be largely affected by deposition setup, post-deposition processing, type of electrolyte, applied voltage for actuation, and temperature. It was shown that increasing temperature caused higher active stress in polypyrrole, an attractive conducting polymer actuator material. However, detailed characterizations were lacking to determine whether the improved active stress was caused by structural change in the polymer and/or charging effect. A temperature-controlled solvent bath was integrated with a custom-built electrochemical dynamic mechanical analyzer to conduct isometric and isotonic tests on polypyrrole under elevated temperature. Experimental results showed that heating increased the charge transport through the polymer and thermal expansion in the polymer allowed more room for charge uptake. As a result, increase in ion movement largely contributed to improvements in actuation stress (rate) and strain (rate), while the decrease in stiffness due to heating had limited effect. Moreover, actuation performance was further improved by choosing large active ion type, BMIM. Although the active stress and strain increased via heating, creep limits the reversibility of conducting polymer actuators. To reduce creep rate, functionalized multi-walled carbon nanotubes (fCNTs) were introduced to fabricate composites with polypyrrole and with PEDOT. Out of four attempted fabrication techniques, drop-casted multilayer structure demonstrated that increasing the amount of fCNTs reduced creep rate, but also decreased active strain, stiffness, and conductivity. Applying higher preload (up to 3 MPa) improved active strain in the composites by providing more space for charge uptake. The amount of sCNTs that provided optimal performance was approximately 20-30% by weight.

Thesis Supervisor: Ian W. Hunter
Title: Professor in Mechanical Engineering

Acknowledgments

Before enrolling in MIT, I had doubts about how I would face new challenges and grow academically. As a biomedical engineering undergraduate, I knew that switching focus to mechanical engineering in this "intimidating" school required significant courage and faith. The BioInstrumentation Laboratory that I joined since July 2008 provided all that I needed to become a more interdisciplinary researcher and a more independent thinker. I would like to thank Professor Ian Hunter for providing this excellent opportunity for me to work in such an inspiring and friendly environment.

During the past two years in the Lab, my work progress had never been limited by the lack of resources. My labmates have been incredibly enjoyable to work with and helpful in any way possible so that I never felt alone. I thank Jean Chang, Ellen Chen, Brian Hemond, Cathy Hogan, Scott McEuen, Eli Paster, Priam Pillai, Shige Tanaka, Bryan Ruddy, and Adam Wahab for their help and support. When I first joined the lab, I was even unfamiliar with simple tasks such as wire stripping, soldering, or operating the milling machine. Special thanks to Priam Pillai for all his guidance throughout my research experience. He has taught me countless skills, from how to clean beakers properly to making contributions in conducting polymer research. I have also enjoyed collaborating with Dr. Ali Shakh, Jan Schnorr, and Dr. Timothy Swagger for the CNT project. Not only that I learned how to be a collaborator and communicator, I also learned to be a mentor of an undergraduate research assistant, Kathy Bui. Her excellent work has facilitated our research smoothly. I would also like to thank Kate Melvin for her great

help in keeping the lab running. The Lab has provided tremendous encouragement and motivation that is indescribable in words.

My family and friends have also been very supportive in the past two years throughout my journey at MIT. It was my father, Jen-Peng Keng's profession as a biology professor in Taiwan who first got me interested in the field of science and engineering. My brother, who just obtained his Ph.D. degree in biomedical engineering in June 2009, has been a role model as a great engineer and unpuzzled many of my doubts in academia. My mother, Shouyu Kuo has been very caring and always made sure that I lived as a healthy graduate student. Furthermore, I thank my boyfriend, Tien-Yun Lee for his love. Without his support, I could have not been able to happily live through the challenging two years at MIT.

Finally, I would like to give many thanks to the Institute for Soldier Nanotechnology and the Warren M. Rohsenow Fellowship funding for supporting my research.

Table of Contents

CHAPTER 1
Introduction **13**
1.1 Polypyrrole and PEDOT Background 16
1.2 Conducting Polymer Actuation and Thermal Effect 20
1.3 Electrochamical Dynamic Mechanical Analyzer 22
1.4 Chapter Overview 24

CHAPTER 2
Temperature Controller for Electrochemical Dynamic Mechanical Analyzer **26**
2.1 Instrumentation: Temperature-Controlled Electrochemical Bath 27
2.1.1 On-Off Controller vs. PID Controller 27
2.1.2 PID-Controlled Electrochemical Bath 29
2.2 Temperature-Controlled Conducting Polymer Actuation 34

CHAPTER 3
Characterizing the Effect of Elevating Temperature on Polypyrrole **36**
3.1 Active Stress and Stress Rate 37
3.1.1 Introduction 37
3.1.2 Stiffness Measurement & Results 37
3.1.3 Isometric Actuation 38
3.1.4 Maximum Charge, Peak Stress, and Maximum Stress Rate 40
3.1.5 Discussion 44
3.2 Actuation in Cation-Driven Electrolyets 47
3.2.1 Introduction 47
3.2.2 Actuation in the Three Electrolytes 48
3.2.3 Actuation in Different Electrolytes at Room Temperature 48
3.2.4 Actuation in Different Electrolytes at Elevating Temperature 49
3.2.5 Discussion 52
3.2.6 Conclusions 54
3.3 Effect of Ion Delivery on Strain and Strain Rate 55
3.3.1 Introduction 55
3.3.2 Temperature Elevated Isotonic Actuation 55
3.3.3 Results 57
3.2.4 Conclusions 60
3.4 Polypyrrole Film Thickness Effect 62
3.5 Thermal Effect Modeling 64
3.6 Conclusions 68

CHAPTER 4
Effect of CNTs on Conducting Polymer and Composite Fabrication Techniques 69
4.1 CNT Specification 70
4.2 Fabrication Techniques 71
4.2.1 Direct Deposition of sCNTs During PPy Polymerization 71
4.2.2 Soaking and Sonicating PPy in sCNT Suspension 71
4.2.3 Electrostatic Self-Assembly of sCNTs 72
4.2.4 Multilayer Conducting Polymer-sCNT Composite by Drop-casting 75
4.3 Properties of the sCNT Drop-casted Composites 83
4.3.1 Thickness, Conductivity, and Stiffness Results 83
4.3.2 Actuation Results 87
4.3.3 Conclusions 92
4.4 Stretching & Rolling Composite Films 94
4.4.1 Actuation at Increasing Preloads 94
4.4.2 Stretched PPy-sCNT Composite 95
4.5 Conclusions and Future Work 100

CHAPTER 5
Summary 101

References 102

Appendix A. Temperature controller code in Visual Basic 105

Appendix B. MATLAB code for mechanical properties calculation 110

List of Figures

1-1 Molecular structure of (a) PPy (b) PEDOT 16
1-2 Doping process during polypyrrole polymerization 18
1.3 Electrochemical deposition of polypyrrole 19
1.4 Polypyrrole film 19
1-5 Polypyrrole actuation mechanism 20
1-6 Electrochemical dynamic mechanical analyzer 23

2-1 The on-off controller resulted in more oscillation than the PID controller 29
2-2 Temperature was controlled by the PID controller 30
2-3 First version of the temperature-controlled bath 31
2-4 With the fans around the bath off, the bath was able to reach to 80°C faster than when the fans were on. 32
2-5 Final version of the temperature-controlled electrochemical bath 33
2-6 Electrochemical bath heating up was observed under a thermal camera 33
2-7 The temperature-controlled bath was integrated with the EDMA setup for thermal actuation studies 34
2-8 User interface in Visual Basic for the temperature-controlled bath 35

3-1 The polypyrrole sample stiffness linearly decreased 38
3-2 Strain of the polypyrrole sample at different temperatures 40
3-3 Isometric results at 55°C 41
3-4 Averaged peak charge per volume for +1V 41
3-5 Peak charge per volume at different temperatures 42
3-6 First half of the averaged stress cycle for 27°C, 35°C, 45°C, 55°C, 65°C, 75°C, and 83°C 43
3-7 Peak stresses at different temperatures 43
3-8 Maximum stress rate increased with temperature 44
3-9 At room temperature, the active stress of polypyrrole was the highest in BMIM-PF_6 in the three salts 49
3-10 Charge per polymer volume increased the most with temperature in BMIM-PF_6 and the least increase in TEAP 52
3-11 (a) BMIM-PF_6 crystal (circular) and (b) TEAP crystal (long strips) residues on polypyrrole surface after actuation 53
3-12 Isotonic results at 27°C 56
3-13 Averaged strain at 27°C, 35°C, 45°C, 55°C, 65°C, 75°C, and 83°C 58
3-14 Peak strain at all temperatures at both +0.8 V and -0.8 V 58
3-15 Both maximum strain rate and charge per volume at +0.8 V and -0.8 V increased with temperature 59
3-16 Before 65°C the strain to volume ratio overlapped, and past this temperature the ratio was higher in the 40 μm film than the 20 μm 63
3-17 The compliance decreases with increasing charge 64
3-18 The solved k/a decreased exponentially with increasing temperature in both

approaches 66
3-19 The solved alpha/a increased until 55°C in Approach 1 and had no obvious change in Approach 2 67

4-1 The cCNTs settled down to the bottom of the beaker within hours after mixing, while the sCNTs stayed stable in propylene carbonate two months after mixing 70
4-2 Surface SEM images showed that soaking polypyrrole films in CNT suspension did not successfully attach sCNTs to the polymer 72
4-3 A free-standing polypyrrole film, stabilized by a plastic frame, was placed in the CNT suspension to attach CNTs to the surface by electrostatic 74
4-4 Applying the polypyrrole base with 0.7 V reduced the creep and strain compared to the control film 75
4-5 (a) The procedure for fabricating layer-by-layer PEDOT-sCNT composite films. (b) The sCNT "control" film consisted four sCNT layers (80%) supported by two PEDOT layers 77
4-6 Cross-sectional SEM images of drop-casted PPy-sCNT films 80
4-7 Surface SEM images of drop-casted PPy-sCNT films 81
4-8 Electrode-side surface of a PEDOT-sCNT composite had sCNT clusters and scattered sCNTs penetrating through 82
4-9 Stiffness of PPy-sCNTs composite decreased with amount of sCNT 85
4-10 Definition of creep rate 87
4-11 Increasing the amount of sCNTs reduced the creep and strain of the PEDOT composite 89
4-12 Increasing the amount of CNTs reduced charge transfer of the PEDOT composite but the charge movement was more reversibe 89
4-13 The illustration shows a speculated mechanism on how the sCNT impeded the composite from actuating freely 90
4-14 Peak stress and peak strain of polypyrrole/CNTs composite decreased when the amount of CNTs increased from 11% to 42%. Past 42%, both reached a plateau 91
4-15 The peak stress in five-layer polypyrrole-CNTs composite increased with increasing preload 95
4-16 The PPy-sCNT composite was manually stretched by approximately 10% 96
4-17 SEM images showed that stretching changed the surface features 97

List of Tables

1-1 Mechanical properties of different actuator materials 15
3-1 Size of ions in BMIM-PF_6, BMIM-BF_4, and TEAP 47
4-1 As the amount of sCNTs increased in the PEDOT-sCNT composites, the thickness increased but the conductivity decreased 84
4-2 As the amount of sCNTs increased in the PPy-sCNT composites, the thickness increased but the conductivity decreased 84
4-3 List of results showed how unstretched PPy-sCNT composite compared to the stretched PPy-sCNT composite in conductivity, stiffness, creep rate, strain, and maximum strain rate parallel to the stretch axis 98

CHAPTER 1

Introduction*

Actuators perform mechanical work by transforming energy input sources. In nature, mammalian skeletal muscles can reach active stress of 0.35 MPa and active strain of up to 20% ([1], [2]). Such mechanical performance has been attempted to be achieved by various "artificial muscle" materials, including dielectric elastomers, carbon nanotube actuators, shape memory alloys, etc. These materials transform electrical, chemical or thermal energy inputs into geometric changes. Table 1-1 describes properties of different actuator materials [12]. Among them, polypyrrole (PPy) is an attractive material that can be actuated at voltages lower than 2 V and reach up to 30 MPa active stress and 39% maximum strain ([3], [4], [5], [6], [7]). Besides polypyrrole, other conducting polymer actuator examples include poly(3,4-ethylenedioxythiophene) (or PEDOT), polyacetylene and polyaniline. Conducting polymer actuators exhibit both the flexibility of plastics and electrical conductivity. Research done for this thesis utilized these unique characteristics to improve actuation of conducting polymers, specifically polypyrrole.

The actuation of polypyrrole is underlined by the volumetric changes caused by ionic diffusion in and out of the polymer. The charge-driven mechanical work has been modeled to describe the coupling of structural and ionic contributions to total strain [10]. The factors that improve actuation can vary from deposition recipe to post-deposition

* Partial content of this chapter reuses relevant materials from paper "Characterizing the Effect of Temperature Increase on Polypyrrole Active Strength and Stress Rate" (SMASIS2009-1258), for the 2009 ASME Conference on Smart Materials, Adaptive Structures and Intelligent Systems.

modifications to the polymer. Prior work done in the BioInstrumentation Lab has shown that heating increased active stress and addition of functionalized multiwall carbon nanotubes (fCNTs) reduced the creep rate of conducting polymers [9]. This thesis further characterizes the actuation of polypyrrole under elevating temperature by comparing the effects of stiffness change and charge uptake. This thesis also discusses different polypyrrole-fCNT composite fabrication techniques and how different fCNT content affects actuation. For material comparison, PEDOT-fCNT composites were also fabricated and analyzed due to the fact that PEDOT can be synthesized and actuated following same methods as polypyrrole [9].

Actuator	Active strain (%)	Active stress (MPa)	Work density (kJ/m^3)	Peak Strain Rate (%/s)	Efficiency (%)	Advantages	Disadvantages
Mammalian Skeletal Muscle	**20**	**0.35**	**8**	**> 50**	**~ 40**	Has systems for heat and waste removal, energy delivery and regeneration	Requires specialized chemical and thermal environment, not synthetically produced
Dielectric Elastomers	Up to **380**	**~ 1**	Up to **3400**	**4,500**	Typically **30**, up to **90**	Very high strains and strain rates	High voltages (>1 kV) and fields (~150 MV/m) required
Liquid Crystal Elastomers (thermally or electrically activated)	**45** in thermal, **2-4** in electrical materials	**0.01-0.5**	**~ 20**	**30** in thermally activated, **1000** in electrically	75 in electrical materials	Large strain for thermal materials, fast strains for electrical. Photo-activation has been achieved	Thermal versions are slow unless very thin or photoactivated. Electrical versions require high fields (1- 25 MV/m)
Polypyrrole (conducting polymer)	Up to **39** reported, **5** reliably	Up to **30**	**100**	**12**	**20**	Low voltage (~2 V) High stress and strain	Slow (often run at several Hz to achieve full strain)
Ionic Polymer Metal Composites	**0.5-3**	**3**	up to **5**	**3**	**1.5-3**	Low voltage (<10 V), mechanical amplification gives large displacements	Only useful for bending (not linear) motion
Carbon Nanotube Actuators	**< 1**	up to **30**	**2**	**20**	**0.1**	Large operating temperature range. Low voltage.	Materials are expensive, active strains are very low
Thermally Activated Shape Memory Alloys	**5**	up to **200**	**> 1000**	**300**	**< 5**	Very high power (>100 kW/kg). Low operating voltage	Difficult to control (run between fully contracted and extended but not between)

Table 1-1. Mechanical properties of different actuator materials. Among these materials, polypyrrole is able to actuate at low voltages with active strain up to 39% and active stress up to 30 MPa. (Taken from [2] and [12])

1.1 Polypyrrole and PEDOT Background

Polypyrrole is the main conducting polymer material studied in this thesis for temperature effect characterizations and fCNT composite fabrication. Besides the attractive properties previously mentioned, polypyrrole's flexibility and conductivity as high as 10^4 S/m are other advantages that highlight the material to serve with potential engineering applications. Polypyrrole turns from an insulating material at its neutral state to a conductive material when it is electrochemically doped during polymerization. When a voltage is applied, doping allows electron to delocalize along the conjugated backbone of polypyrrole, causing it to alternate in single and double bonds (Figure 1-1a) ([10], [11]). Similarly, PEDOT also has a conjugated backbone that makes it conductive via the same mechanism as polypyrrole (Figure 1-1b).

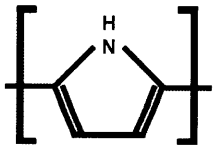

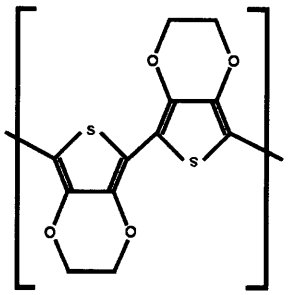

Figure 1-1.
(a) Molecular structure of polypyrrole. (b) Molecular structure of PEDOT.

Pyrrole polymerization protocols have been well developed in the Lab to synthesize robust free-standing films with repeatable mechanical properties (Figure 1-1). The deposition solution was composed of 300 mL propylene carbonate, 50 mM (4.12 g) tetra-ethylammonium hexafluorophosphate, 1% (v/v) water, and 50 mM (or 1.04 ml) pyrrole monomer. Before adding pyrrole monomer the solution was stirred for 10

minutes and then placed in a MicroClimate chamber set to -20°C for half an hour. The cooled solution was then nitrogen saturated before the addition of pyrrole monomer. A glassy carbon crucible was used as the working electrode. A copper sheet served as both the counter and reference electrodes. A constant current density of 1 A/m^2 (or total current of 16 mA) was applied to the crucible which was held at -40°C for ten hours (Figure 1-3). This setup allowed pyrrole to oxidize and polymerize onto the surface of the crucible. After the deposition polypyrrole film surface was rinsed with propylene carbonate and air-dried for about a day ([11], [12]). The film could then be easily peeled off from the crucible with thickness of about 20 μm (Figure 1-4). PEDOT polymerization can be achieved following the same protocol, substituting pyrrole with EDOT monomer.

Polypyrrole and PEDOT can be repeatedly synthesized in large quantities and exhibit stable properties [8]. "Free-standing films" mentioned in this thesis were all synthesized following the protocol described above.

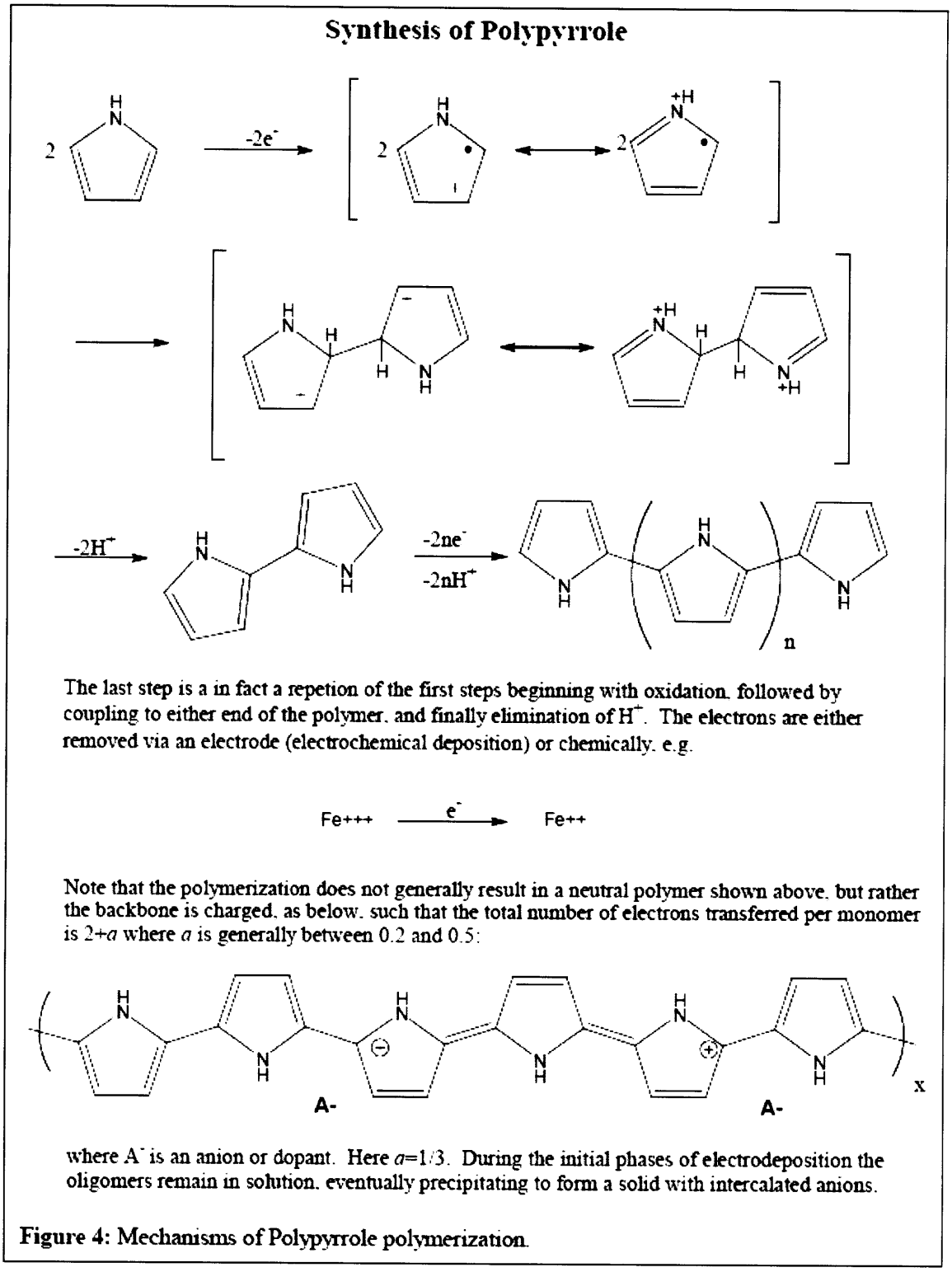

Figure 4: Mechanisms of Polypyrrole polymerization.

Figure 1-2. The doping process occured during pyrrole polymerization and turned polypyrrole into a conductive material (Taken from [10]).

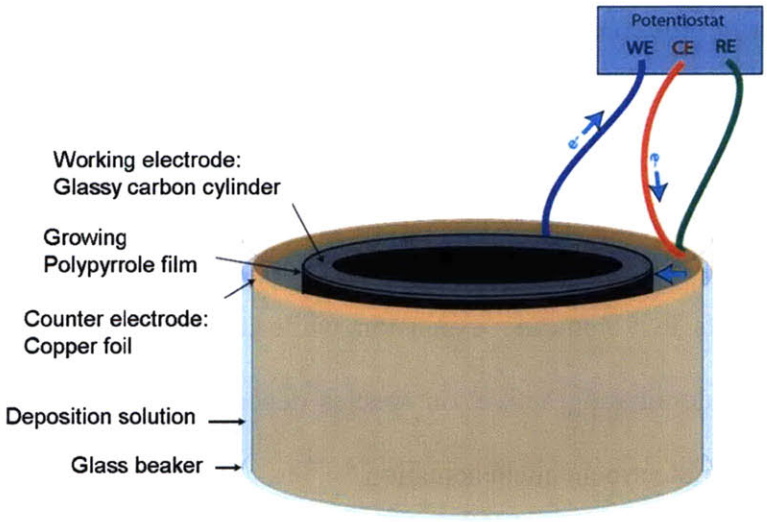

Figure 1-3. Electrochemical deposition of polypyrrole required a constant current density of 1 A/m^2 applied to the glassy carbon working electrode versus the copper foil that served as the counter (and reference) electrodes. (Taken from [12])

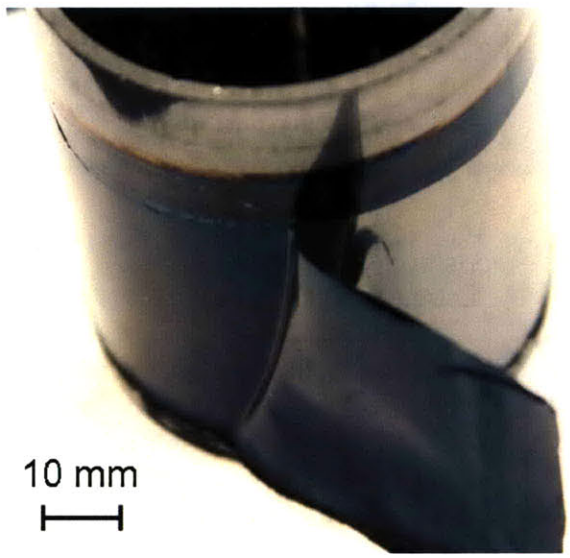

Figure 1-4. A 20 μm polypyrrole film formed on the glassy carbon surface after a ten-hour deposition.

1.2 Conducting Polymer Actuation & Thermal Effect

Conducting polymer actuation is achieved via ionic diffusion in and out of the polymer as it is electrochemically stimulated. As a potential difference is created between the polymer strip and a nonreactive counter electrode across an electrolyte, ionic movement takes place in order to maintain charge neutrality in the polymer. Ion flux into the polymer results in volumetric expansion while ion outflow results in contraction (Figure 1-5). The dominating active ion species depend upon the solvent used and the voltages applied for electrochemical actuation.

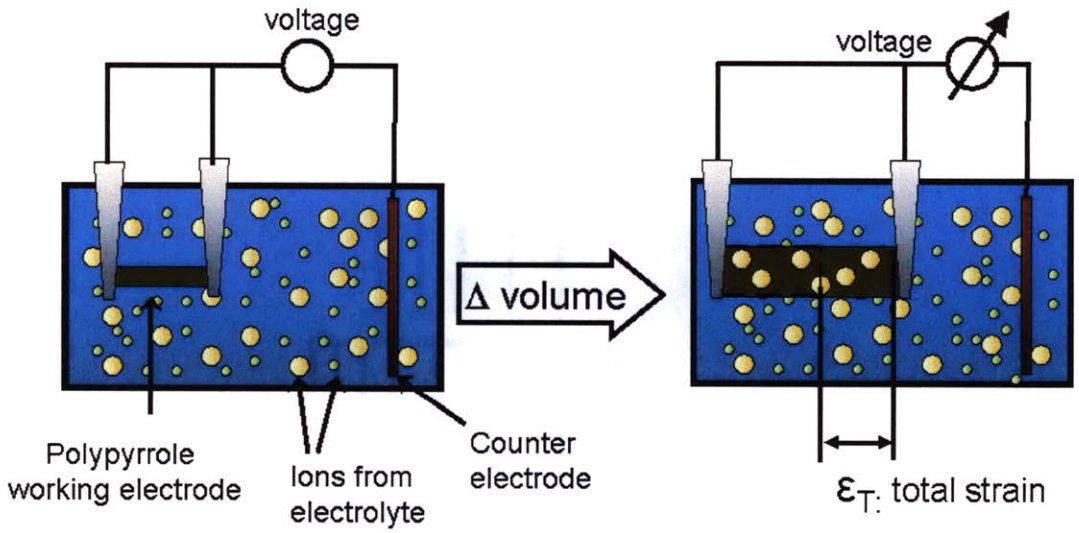

Figure 1-5. As voltages are applied, conducting polymer actuation is achieved via ionic movement in and out of the polymer. Ion diffusion into the polymer causes it to expand while ions moving out from the polymer causes it to contract.

A model was developed by John Madden to characterize the response speed of conducting polymers [10]. The model consists of two critical time constants. One is the charging time constant $\tau_{RC} = RC_v$, in which R is the solution resistance and C_v is the

polymer volumetric capacitance. The other time constant is the diffusion time constant $\tau_D = \frac{a^2}{4D}$, in which a is the polymer thickness and D is diffusion coefficient. Both resistance and diffusion coefficient are dependent upon various factors, including temperature. As the temperature is increased, the solution resistance R would decrease and the diffusion coefficient D would increase, causing both time constants to decrease [10]. Smaller time constants imply that the polymer undergoes quicker charge transport and diffusion, and thus make it a faster actuator.

Besides the charging effect, the stiffness also contributes to actuation performance of the polymer. Equation (1) describes how charge and stiffness relate to mechanical properties [10]:

$$\varepsilon_T = \frac{\sigma}{E} + \alpha\rho \ , \qquad (1)$$

in which ϵ_T is total strain, σ is stress, E is stiffness, α is a strain to charge coefficient, and ρ is the charge per unit polymer volume. The term $\alpha\rho$ is the volumetric strain generated by swelling of the polymer from charging effect. Both charge uptake and stiffness may vary with temperature to affect overall strain.

Prior studies done in the Lab have shown that the active stress of polypyrrole increased with elevated temperature but did not provide detailed information about whether the stiffness or the ion transfer contributed to the stress increase more dominantly (or equally). Chapter 3 of this thesis characterizes how dominating ion species and stiffness contribute to polypyrrole actuation under elevated temperature.

1.3 Electrochemical Dynamic Mechanical Analyzer

To characterize conducting polymers, an electrochemical dynamic mechanical analyzer (EDMA) was constructed that simultaneously performs electrochemistry and mechanical analyses [9]. The EDMA is composed of a potentiostat (AMEL Instruments, Model 2051), single axis stage (Aerotech, ALS 130 Linear Stage), strain gauge force sensor (Futek, FSH00104-A), electrochemical bath, electrodes, and computer interface in Visual Basic. The potentiostat supplies voltage to the polymer sample versus a silver wire reference electrode. The electrochemistry occurs in a solvent bath, with a counter electrode attached to the bath wall (Figure 1-6a).

As the polymer sample is electrochemically stimulated the stress generated by the sample can be measured by the force sensor. As the sample volume decreases the force sensor is pulled towards the sample which is then registered as a positive force. Change in sample length, or strain can be sensed or controlled by the single axis motorized stage mounted with an encoder (Figure 1-6b).

A temperature-controlled solvent bath was integrated with the EDMA for temperature studies. Details about the controller setup and how it integrates with the EDMA are included in Chapter 2.

(a)

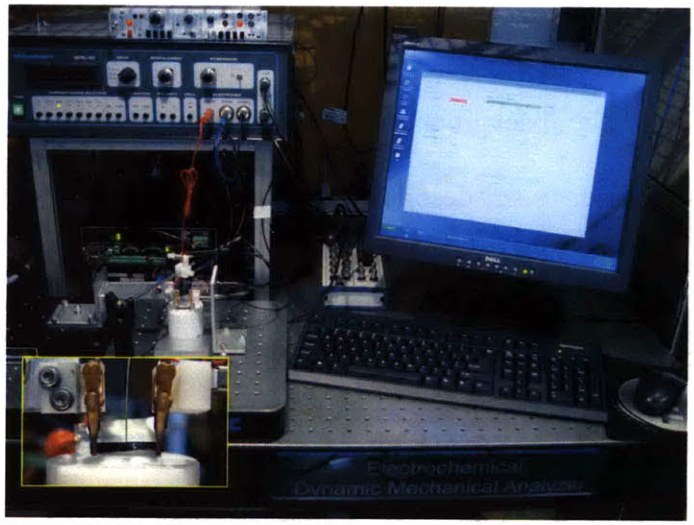

(b)

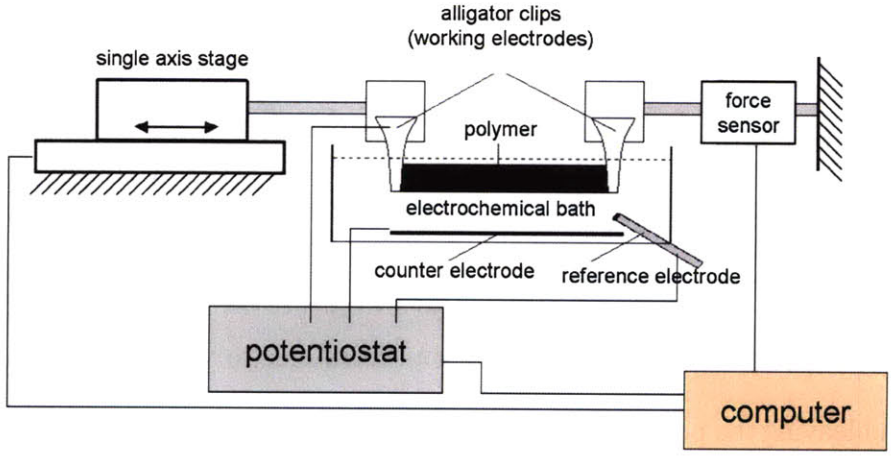

Figure 1-6. Custom built electrochemical dynamic mechanical analyzer (EDMA) (a) experimental set up; (b) system schematic. Lower left corner in (a): The polymer is clamped by two conductive alligator clips, which is the working electrode for actuation. The sample is actuated in a solvent bath, which includes a silver wire as the reference electrode and stainless steel foil as the counter electrode. The potentiostat supply voltage is controlled by the computer. An encoder on the single axis stage senses and controls sample strain, and the strain gage force sensor measures force. Overall, the system applies and measures potential, current, stress, and strain to and from the polymer sample for material characterization. (Taken from [9])

1.4 Chapter Overview

Chapter 1 introduces the background of conducting polymers and their actuation mechanism. This chapter also describes the electrochemical dynamic mechanical analyzer that the Lab built to characterize conducting polymer actuators. This thesis focuses on characterizing the effect of temperature and fCNTs on polypyrrole and PEDOT actuation performance.

Chapter 2 covers how the temperature-controlled solvent bath was constructed as a part of the EDMA and how it can be used in-parallel with other functions for polymer actuator characterization.

Chapter 3 characterizes active stress and strain, and investigates the effect of stiffness versus charge transfer under elevated temperature. This chapter also describes performance of polypyrrole in different cation-driven electrolytes, and how rate of ions entering and leaving the polymer differed at increasing temperature.

Chapter 4 compares different conducting polymer-fCNT composite fabrication techniques and how fCNTs affected actuation of conducting polymers – polypyrrole and PEDOT. The drop-casted multilayer composites and their actuation results are discussed specifically. Effect of preload and stretching on the composites are also included.

Chapter 5 summarizes the characterizations of polymer-fCNT composites and heated conducting polymer, and also provides direction to future research.

MATLAB code used to calculate stiffness, strain, charge, and creep for this thesis is included in Appendix B.

CHAPTER 2

Temperature Controller for Electrochemical Dynamic Mechanical Analyzer

Dynamic mechanical analyzers (DMA) are used to test mechanical properties of materials, mostly polymers. Commercialized DMA's have functions including applying a stress or strain scans to materials in order to measure their modulus or perform fatigue tests. DMA's can also sweep through a wide range of temperature for dynamic mechanical thermal analysis. For example, the Perkin Elmer Pyris DMA 7e has a temperature range of -170°C to 500°C for 3-point bending, extension testing, parallel plate, and single cantilever measure systems [13]. However, there has been no commercialized DMA available that conducts simultaneous electrochemistry and thermal mechanical testing for conducting polymer actuation tests.

The electrochemical DMA (or EDMA) built in the Lab performs single axial extension tests and electrochemical controls to the polymer. Details about the EDMA were included in Section 1.4 and Nate Vandesteeg's Ph.D. thesis. Since very little work has been done to characterize the effect of temperature on conducting polymer actuation, a temperature-controlled electrochemical bath was added to the EDMA for thermal mechanical studies.

2.1 Instrumentation: Temperature-Controlled Electrochemical Bath

The temperature controller consisted of four major units:

(1) Power supply (Hewlett Packard E3631A) for heating/cooling

(2) Controller written in Visual Basic

(3) Resistive thermal device (Surface Mount Teflon RTD) with data acquisition device (Agilent 34970A)

(4) Chemical bath with attached Peltierheaters/coolers

The temperature supply sources of the chemical bath were chosen to be Peltier thermoelectric devices because they function as both heaters and coolers. The heat flux created in between two heat spreaders allows one side of the device to be hot and the other side to be cold. The hot side becomes cold and the cold side becomes cold while the applied voltage polarity is switched. In this thesis, the "hot side" of the device at positive voltage is referred as the "effective surface" in contact with the bath.

2.1.1 On-off controller vs. PID controller

The temperature controller was first written in Visual Basic for both an on-off controller and a proportional-integral-derivative (PID) controller to compare their performance. The comparison was made by controlling the temperature measured directly on the effective side of a Peltier device. In the on-off controller, if the measured temperature was lower than the desired temperature, 6 V was applied to the Peltier device to heat up the effective surface. If the measured temperature was higher than the desired

temperature, the voltage supply was turned off so that air cooling decreased the temperature of the effective surface.

In the PID controller, the output temperature (or voltage) was a combined effect of multiplying, differentiating, and integrating the error between the measured and the desired temperature (Equation 2) [14]. If the measured temperature was lower than the desired temperature, positive voltage was applied so that the effective side was heated up. Similarly, if the measured temperature was higher than the desired temperature, negative voltage was applied so that the effective side was cooled down. The desired temperature can be reached by supplying constantly changing voltage, being the summed effect from the properly tuned gains of the PID controller – K_p, K_i, and K_d,

$$Voltage(t) = K_p e(t) + K_i \int_0^t e(\tau)d\tau + K_d \frac{d}{dt}e(t). \qquad (2)$$

If the proportional term K_p is too high, the output can result in large oscillation leading to unstable temperature output. If the integral term K_i is too high, the output can accelerate and overshoot to a much higher temperature than the desired value. However, large integral term eliminates steady state error quickly. Temperature overshooting over 5°C should be avoided for this electrochemical bath because over-heated electrolyte can change solvent property and deteriorate the mechanical properties of the polymer sample.

Comparing the on-off controller to the PID controller, the on-off controller allowed the Peltier heater to reach the desired temperature faster than the PID controller, because the constantly applied 6 V in the on-off controller quickly heated up the Peltier while in the PID controller the voltage was constantly changing corresponding to the errors. With the gains properly tuned, the oscillation in PID controller was smaller than in the on-off controller. Figure 2-1 shows how the on-off controller compared with the PID

controller, with different K_d values chosen. Figure 2-2 shows how the PID controller ($K_p = 6$; $K_i = 0.002$; $K_d = -100$) could quickly bring the device to the desired temperatures varying between 40°C and 45°C.

2.1.2 PID-controlled electrochemical bath

The PID controller was selected over the on-off controller because of its tunability and showed no oscillations. The PID controller was then tuned for the electrochemical bath, including an outer and inner bath. The outer bath was milled from a 6061 T6 aluminum block with dimensions of 50 mm × 30 mm × 35 mm and the bath thickness was 5 mm. The inner bath, serving as an electrical insulation layer, was milled out of Teflon and fit right into the aluminum bath (Figure 2-3).

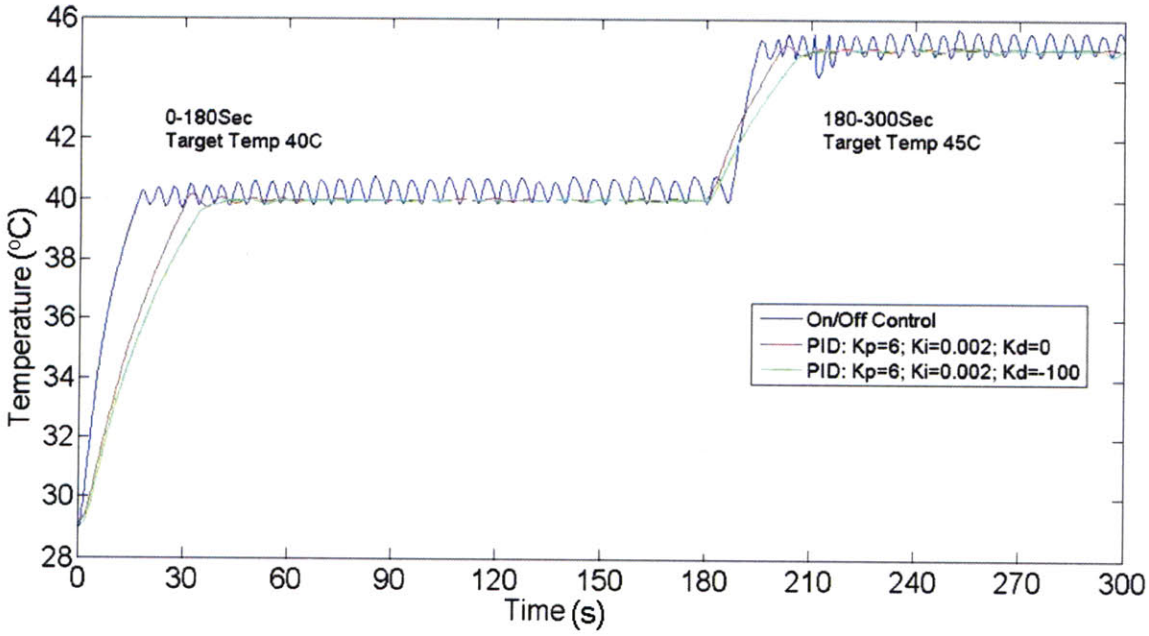

Figure 2-1. The on-off controller resulted in more oscillation than the PID controller. Also, tuning the gains of PID from $K_d = 0$ to $K_d = -100$ reduced the oscillation further.

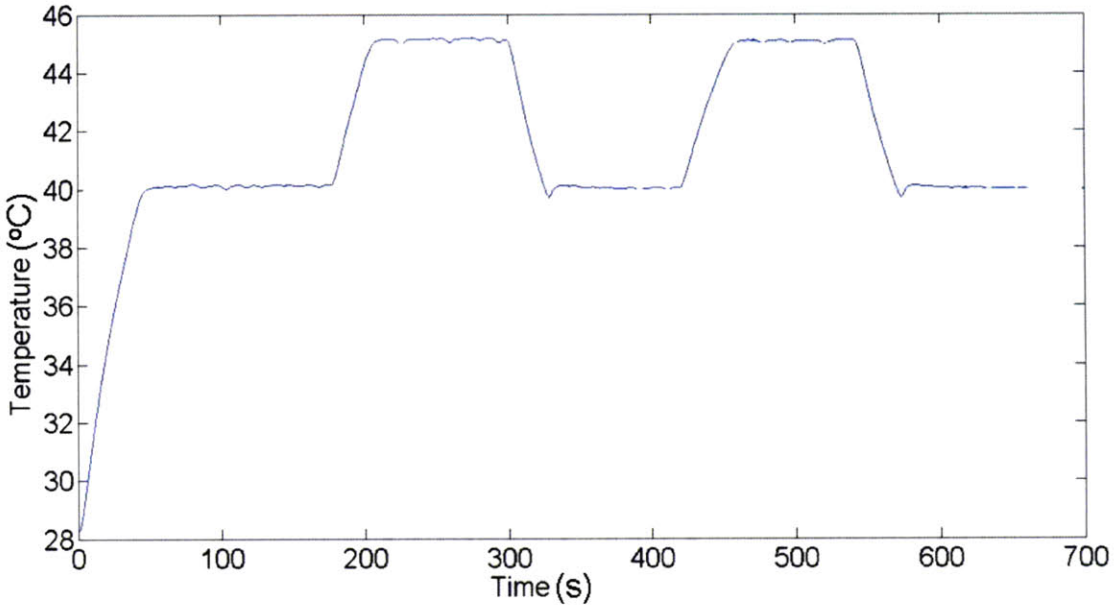

Figure 2-2. Temperature was controlled by the PID controller with temperature measured and controlled directly from a Peltier device surface.

The first version of the temperature-controlled bath had a 30 mm × 30 mm Peltier device (TE Technology, VT-127-1.0-1.3-71P) on each long side of the bath and one 40 mm × 40mm (TE Technology, VT-127-1.4-1.15-71PR) on the bottom, with the "effective side" attached to the bath. The baths and the Peltier thermoelectric devices were attached together using a High Temperature High Thermal Conductivity Paste (Omegatherm "201"). Heat sinks and fans were used to facilitate dissipating heat from the "cold side" of the device to the ambient environment (Figure 2-3).

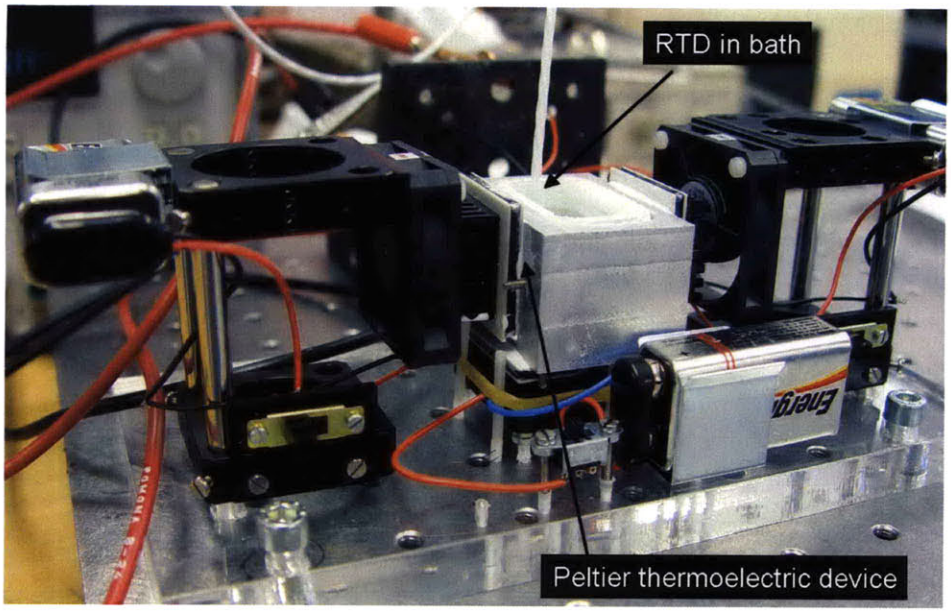

Figure 2-3. First version of the temperature-controlled bath had fans facing the Peltier devices to help dissipate heat.

With one Peltier thermoelectric device under the bath, the water filled in the bath could not heat up to as high as 80°C. Therefore, two Peltier devices were then stacked on top of one another under the bath. This configuration allowed the effective side of the bottom-most device to heat the cold side of the top device, and via heat-transfer, the top device's effective side that is in contact with the bath will consequently be heated up. With this setup, experiments were done to heat the bath filled with water from room temperature to 80°C. The results showed that with the fans on, the bath was over-cooled and could not reach to high temperature as fast as when the fans were off (Figure 2-4). The fans were then replaced by heat sinks for the final setup (Figure 2-5). Figure 2-6 shows the distribution of heat of the electrochemical bath using a Flir Systems Thermovision A40 thermal camera. The top view shows that the center of the bath appeared to be cooler than the area near the heating sources. In thermal actuation tests,

the polymer sample would be placed at the center of the bath, so the RTD should be placed as close to the sample as possible to ensure that the measured temperature was the temperature of the polymer sample. The temperature range of the bath is 25°C to 85°C, with a heating/cooling rate of about 1.5°C per minute. The steady state error is approximately +/-1°C.

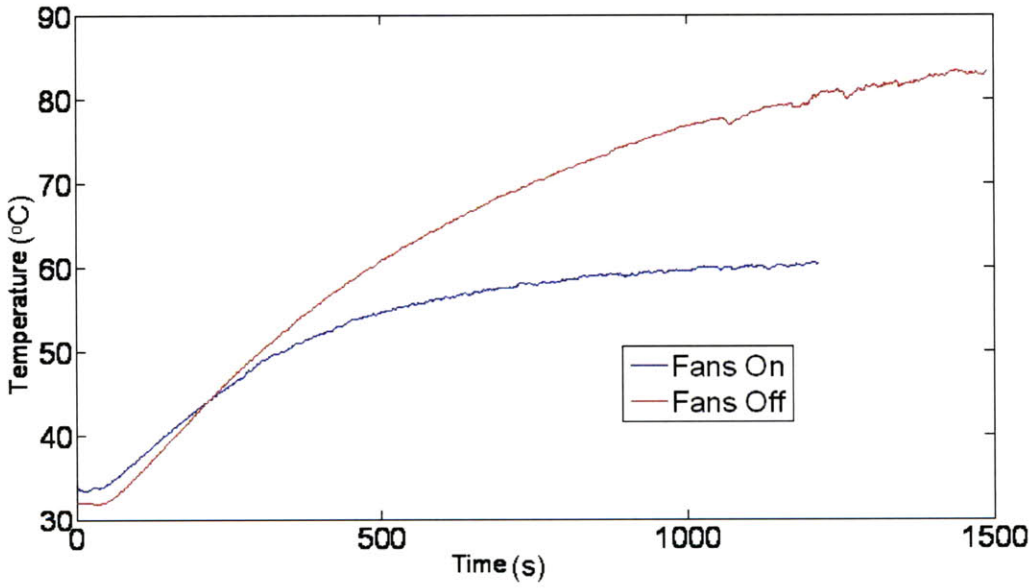

Figure 2-4. With the fans around the bath off, the bath was able to reach to 80°C faster than when the fans were on.

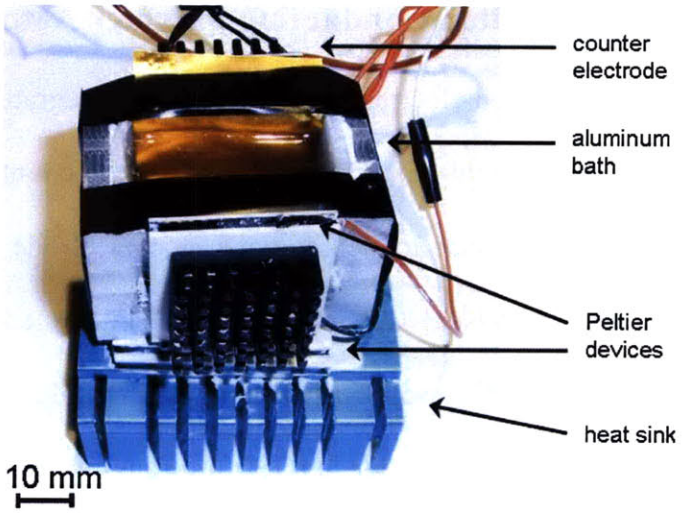

Figure 2-5. Final version of the temperature-controlled electrochemical bath for the EDMA has two Peltier thermoelectric devices stacked on the bottom and one on each side of the bath. The sides facing out had heat sinks attached to them.

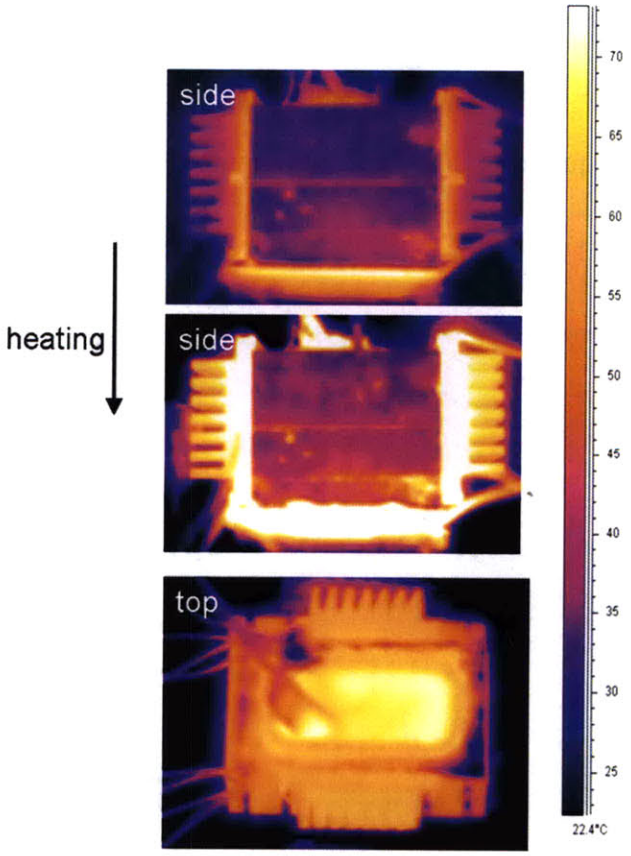

Figure 2-6. The electrochemical bath heating up was observed under a thermal camera.

2.2 Temperature-Controlled Conducting Polymer Actuation

The temperature-controlled electrochemical bath was integrated with the EDMA (Figure 2-7). The bath had a gold-coated foil to serve as the counter electrode and a silver wire inserted into the bath to be the reference electrode (Figure 2-5). The temperature controller in Visual Basic was also integrated and could run independently with other functions of the EDMA. For example, isometric, isotonic, and stochastic tests could be done under temperature ranging from 25°C to 85°C. To operate the temperature controller, the user only needs to start the controller and does not need to change the gain values if the electrolytes are liquid salts or aqueous solutions. The gains were tuned to be $K_p = 2$, $K_i = 0.0003$, and $K_d = -1200$ for these liquids. If the viscosity of the liquid used is much different, then the gains need to be adjusted. The user interface in Visual Basic is shown in Figure 2-8 and its source code is in Appendix A, including commands required to connect the computer to the power supply and the data acquisition unit.

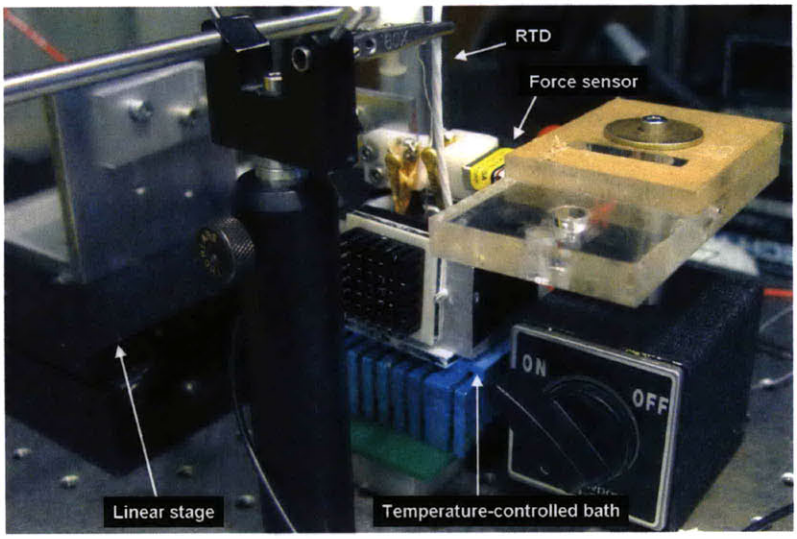

Figure 2-7. The temperature-controlled bath was integrated with the EDMA setup for thermal actuation studies.

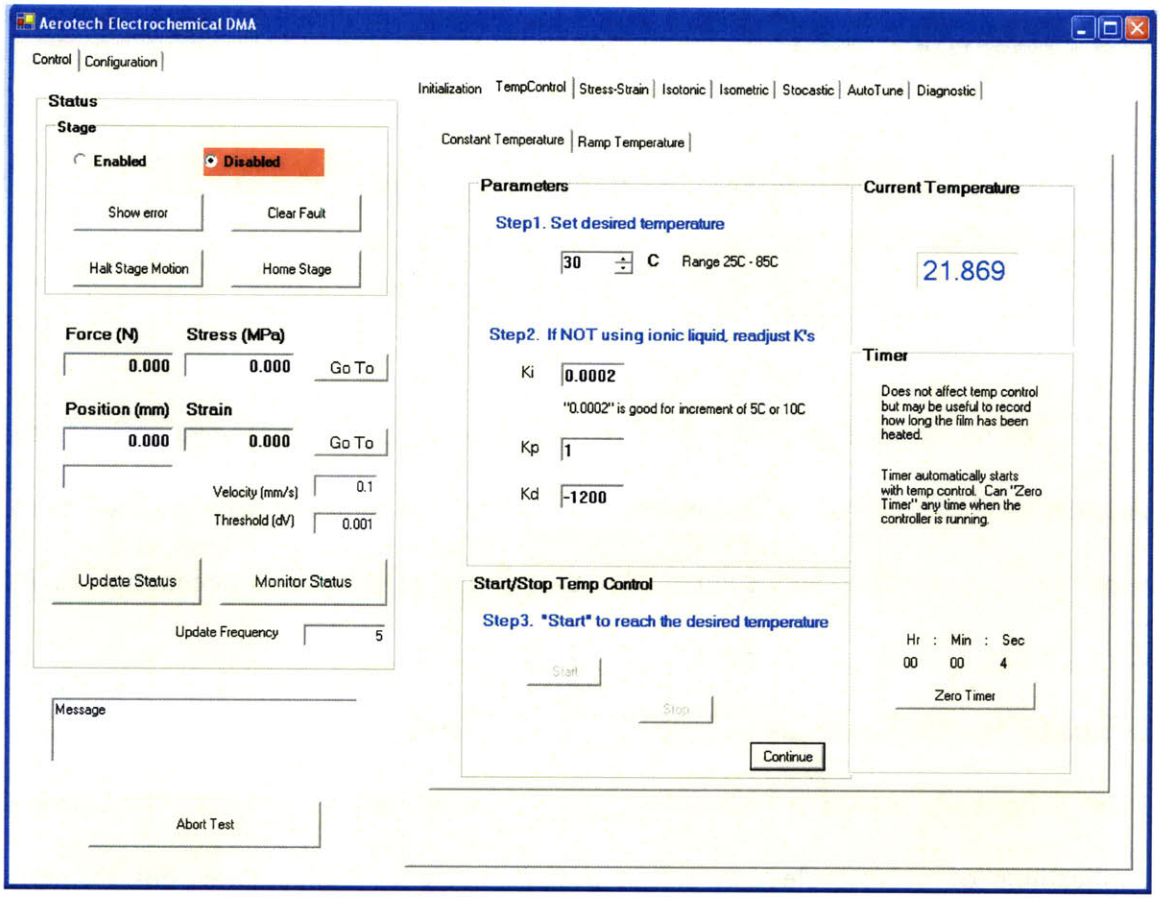

Figure 2-8. The user interface in Visual Basic for the temperature-controlled bath allows the user to set the desired temperature and tune the gain values for different solutions used.

CHAPTER 3

Characterizing the Effect of Elevating Temperature on Polypyrrole

The mechanical properties of polypyrrole could be altered by changing: (1) the polymer synthesis formula and deposition conditions; (2) actuation settings, such as the applied voltage window, applied preload to the polymer, electrolyte concentration, active ion type/size, and rate of ion transfer ([10], [15]). The charging rate can be improved by increasing the ionic mobility, which can be achieved by increasing temperature [20]. Most polypyrrole actuation studies have been done at room temperature but potential applications of polypyrrole may be in a wide range of temperature. For example, polypyrrole actuators may be used for medical devices that operate inside human bodies. This chapter characterizes how elevated temperature affects polypyrrole actuation from the perspective of ionic movements.

3.1 Active Stress and Stress Rate[†]

3.1.1 Introduction

In this study, polypyrrole was actuated under isometric conditions, in which the polymer was kept at a constant strain and the stress was measured during a simultaneous electrochemical stimulus. Rewriting Equation (1) from Chapter 1, Equation (3) describes how charge is related to mechanical properties in isometric mode [20]:

$$\sigma = E(\varepsilon_T - \alpha\rho) \ , \qquad (3)$$

in which ϵ_T is total strain, σ is stress, E is stiffness, α is a strain to charge coefficient, and ρ is the charge per unit polymer volume. This equation suggests that stress is proportional to the stiffness and charge per polymer volume.

3.1.2 Stiffness Measurement & Results

A polypyrrole strip (length 11.2 mm; width 1.5 mm; thickness 20 μm) was cut for stiffness measurements. The sample was clamped at the sample's two ends and submerged in 1-Butyl-3-methylimidazolium hexafluorophosphate (BMIM-PF_6). To avoid buckling, the polymer was pre-loaded at 5 MPa. Sinusoidal strain of 1% was applied for 12 cycles at 1 Hz, without any electrochemical stimuli. The amplitudes of the obtained sinusoidal stress cycles were averaged and divided by strain amplitudes to calculate stiffness. This procedure was repeated isothermally at 25°C, 50°C, 55°C, 65°C, 70°C,

[†] This section reuses relevant sections from paper "Characterizing the Effect of Temperature Increase on Polypyrrole Active Strength and Stress Rate" (SMASIS2009-1258), for the 2009 ASME Conference on Smart Materials, Adaptive Structures and Intelligent Systems.

75°C, 80°C and 83°C in sequence using the same sample. The sample remained in the solvent bath during heating. Stiffness data was analyzed in MATLAB. Results showed that the stiffness decreased by 21% as the temperature was elevated from 25 to 80°C and started to level off past 80°C (Figure 3-1).

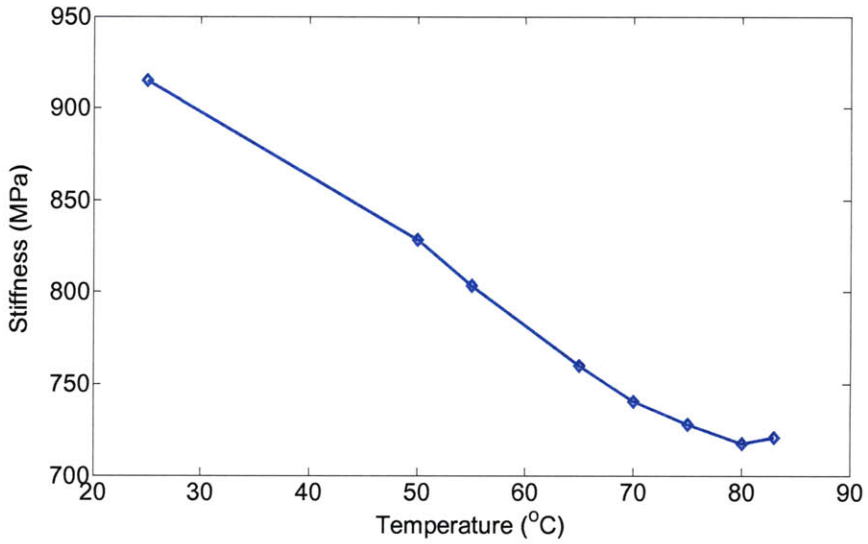

Figure 3-1. The polypyrrole sample stiffness linearly decreased by 21% 25 to 80°C. The stiffness was obtained by applying the sample with sinusoidal strain of 1% at 1 Hz for 12 cycles at 25°C, 50°C, 55°C, 65°C, 70°C, 80°C, and 83°C.

3.1.3 Isometric Actuation

Another polypyrrole strip cut from the same film was used for isometric actuation testing. This sample had approximately the same size as the sample used for stiffness measurements. The sample was held at the two ends by gold-coated clamps that served as the working electrodes. Stainless steel foil was used as the counter electrode and a silver wire served as the reference electrode. The silver wire was placed as close to the sample as possible.

The sample was held at a constant strain and preloaded to about 4 MPa. Square shaped electrical pauses +/-1 V were applied at 0.025 Hz for ten cycles. The same isometric test was repeated isothermally at 27°C, 35°C, 45°C, 55°C, 65°C, 75°C, and 83°C in sequence using the same sample. Current, potential, strain and stress data were recorded at each temperature.

In this study, BMIM-PF_6 was used as the electrolyte. With this solvent $BMIM^+$ ions are the species that diffuse through the polymer. As a positive potential is created across the sample, the $BMIM^+$ ions are expelled from the polymer bulk into the electrolyte. Such ion outflow causes the polymer to decrease in volume. Similarly, as a negative potential is created the $BMIM^+$ ions are attracted into the polymer bulk and this ion influx causes the polymer to increase in volume [15].

Isometric results at different temperature showed that as the temperature increased the sample slowly expanded. The strain needed to provide the sample a 4 MPa preload increased by 230% from 27°C to 83°C (Figure 3-2).

Applying a potential across the sample caused ions to diffuse in and out of the polymer causing the load on the sample to change. As +1 V was applied both the sample charge and stress increased. The opposite occurred as -1 V was applied. The stress saturates around 20 s. Figure 3-3 shows the isometric results obtained at 55°C. At this temperature the strain was held at constant 1%. The shape of the first two charge and stress cycles appeared slightly different form the rest since the sample takes a few cycles to equilibrate.

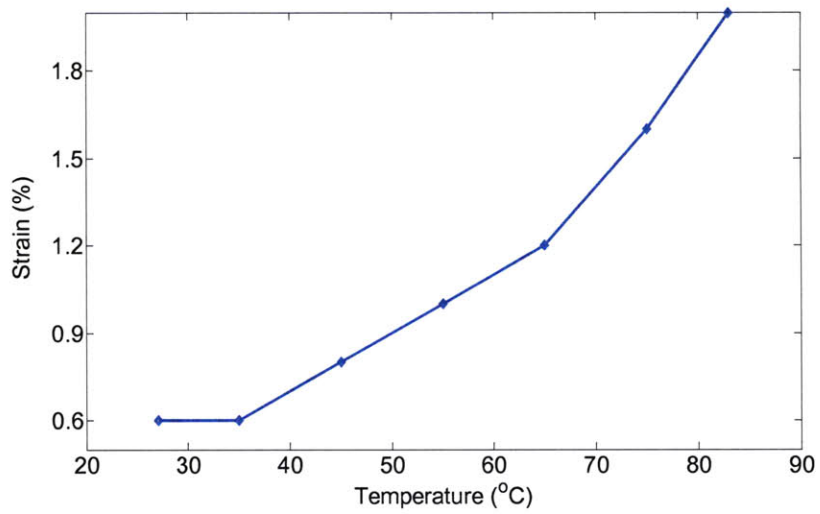

Figure 3-2. Strain of the polypyrrole sample at different temperatures. The strain increased from 0.6% at 27°C to 2.0% at 83°C.

3.1.4 Maximum Charge, Peak Stress, and Maximum Stress Rate

For 27°C, 35°C, 45°C, 55°C, 65°C, 75°C and 83°C, the charge was calculated by integrating the current that was generated (Figure 3-3). The sample took a few cycles to equilibrate so the first two cycles were eliminated for data analyses. The last eight charge cycles were averaged, in which the amplitude corresponded to the peak charge. The ratio of peak charge to the original sample volume (before any heating or electrochemical activity) gave peak charge per volume. The peak charges per volume at each temperature were compared (Figure 3-5).

As the temperature increased, charge per volume increased and reached plateaus (Figure 3-4). The amplitudes of these curves were calculated. Figure 3-5 shows the first half cycle (when +1 V was applied) of the average charge per cycle for the seven different temperatures. The peak charge per volume increased by 983% from 27-75°C, and past 75°C the peak charge started to level off.

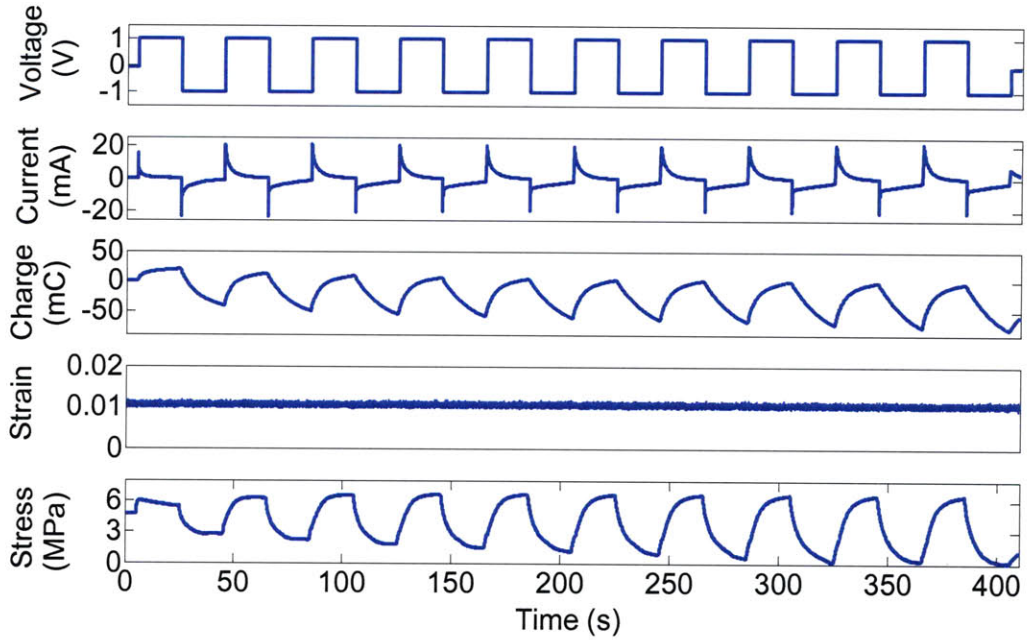

Figure 3-3. Isometric results at 55°C that show potential, current, charge, strain, and stress versus time. Ten cycles of +/-1 V (40 seconds each cycle) were applied to the sample and strain was maintained at about 1%. Applying +1 V caused the stress and charge to increase, while applying -1V caused them to decrease.

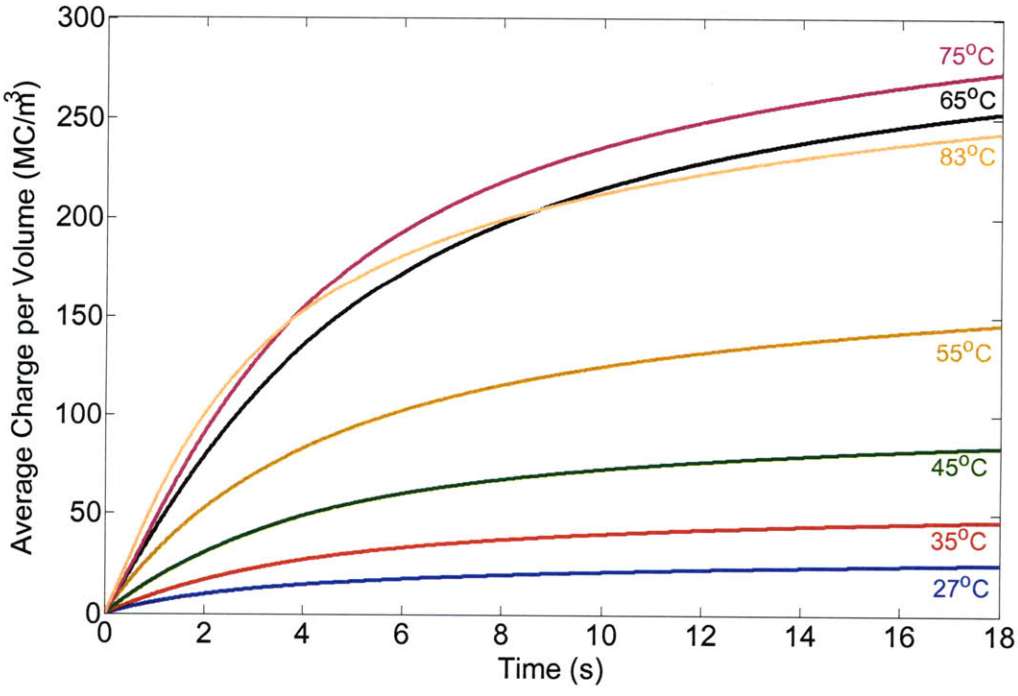

Figure 3-4. Averaged peak charge per volume for +1V. The charge increased parabolically with time for 27°C, 35°C, 45°C, 55°C, 65°C, 75°C, and 83°C.

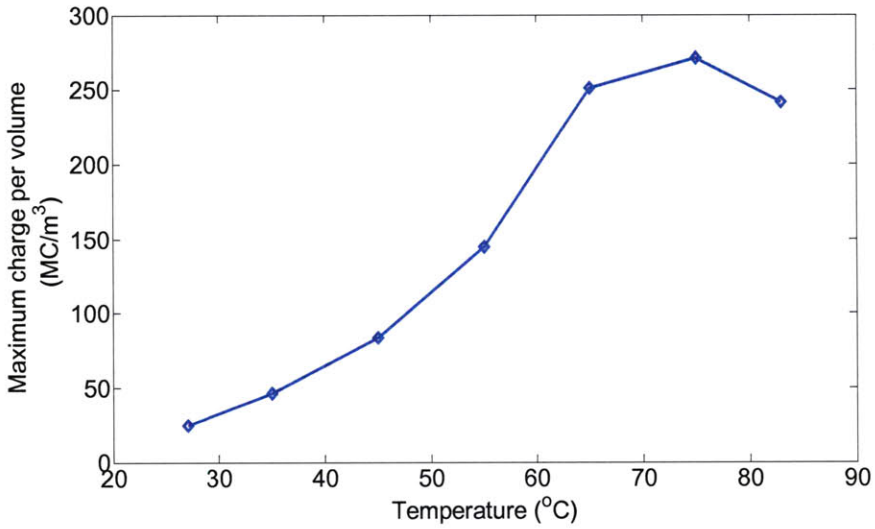

Figure 3-5. Peak charge per volume at different temperatures. At 27°C the charge per volume was 25 MC/m^3. As the solvent bath (and the sample) was heated to 75°C the value increased to 271 MC/m^3, and at 83°C the stress dropped by 30 MC/m^3.

The same procedure that was used to obtain the peak charges was followed to obtain peak stresses. Stress rates were calculated by taking the peak stress differences between each second. Both peak stresses and maximum stress rates were compared for different temperatures (Figure 3-7; Figure 3-8). At 27°C, 35°C, 45°C, 55°C and 83°C the stress increased with time and reached plateaus. However, at 65°C and 75°C the stress stayed flat for the first two seconds due to sample buckling, and then increased in the same way as at other temperatures (Figure 3-6). The maximum values of the curves in Figure 1-6, i.e. the averaged stress amplitudes, gave peak stresses. Figure 3-7 shows that the peak stress increased with temperature until 75°C. Peak stress increased with the temperature following the same trend as the peak charge per volume.

The maximum stress rate increased parabolically with temperature up to 75°C. The maximum stress rate at 83°C was 23 times higher than the rate at 27°C. The increase with temperature had no saturation (Figure 3-8).

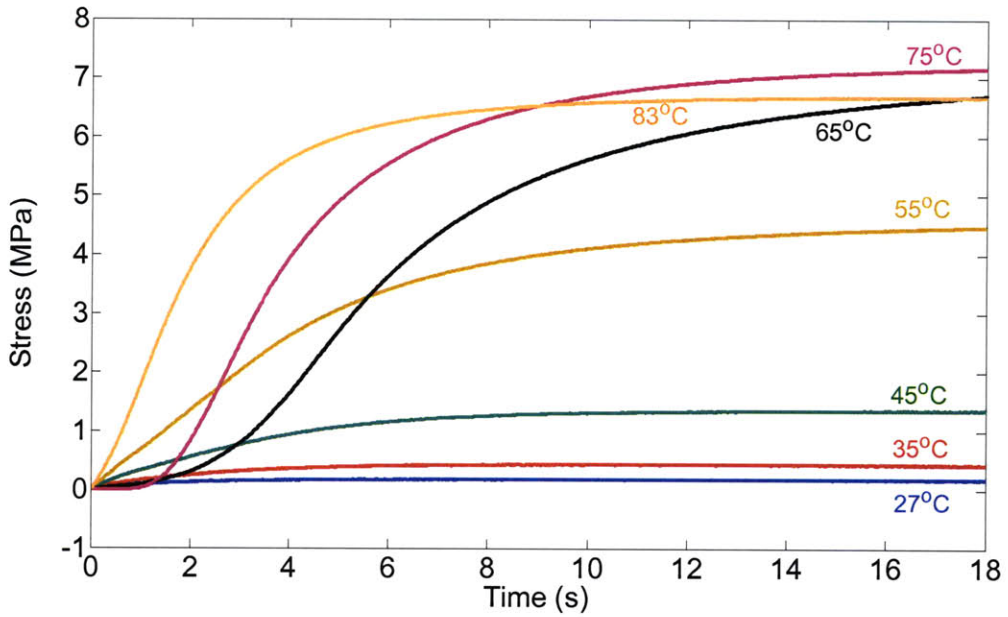

Figure 3-6. First half of the averaged stress cycle for 27°C, 35°C, 45°C, 55°C, 65°C, 75°C, and 83°C. As the temperature increased the stress amplitude also increased and reached plateaus. At 65°C and 75°C the stress stayed flat for the first two seconds and then started to increase.

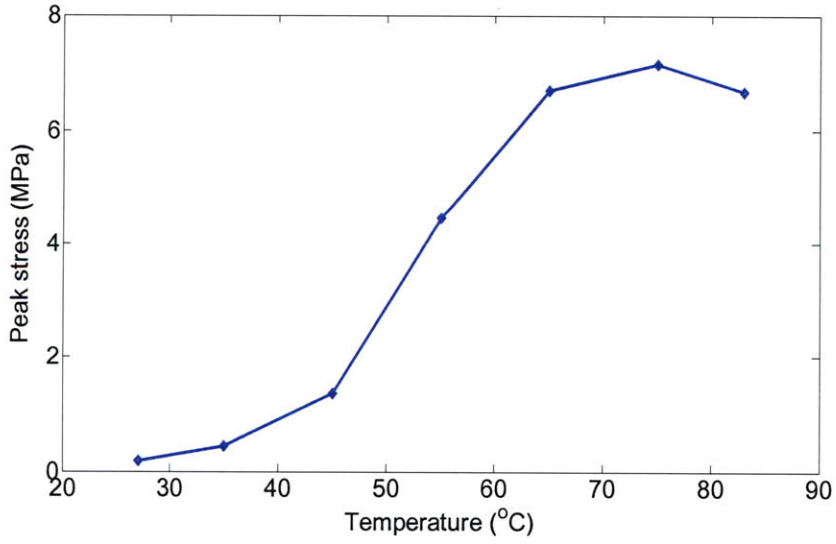

Figure 3-7. Peak stresses at different temperatures. At 27°C the stress amplitude was 0.2 MPa. As the temperature was increased to 75°C the stress amplitude increased to 7.2 MPa.

3.1.5 Discussion

This section describes (1) how increasing temperature can improve polypyrrole actuation strength and stress rate; and (2) what factor dominantly affects the stress change with temperature increase. Stiffness measurements and isometric tests were conducted at different temperatures from room temperature to around 83°C. Results showed that stiffness decreased by 21% from 25 to 80°C. Strain results showed that the sample expanded slowly after heating as strain increased with temperature. As the temperature increased from 27 to 75°C the maximum charge per volume increased by 983%. Like the maximum charge per volume, peak stress reached a plateau at 75°C. The maximum stress rate increased until 83°C.

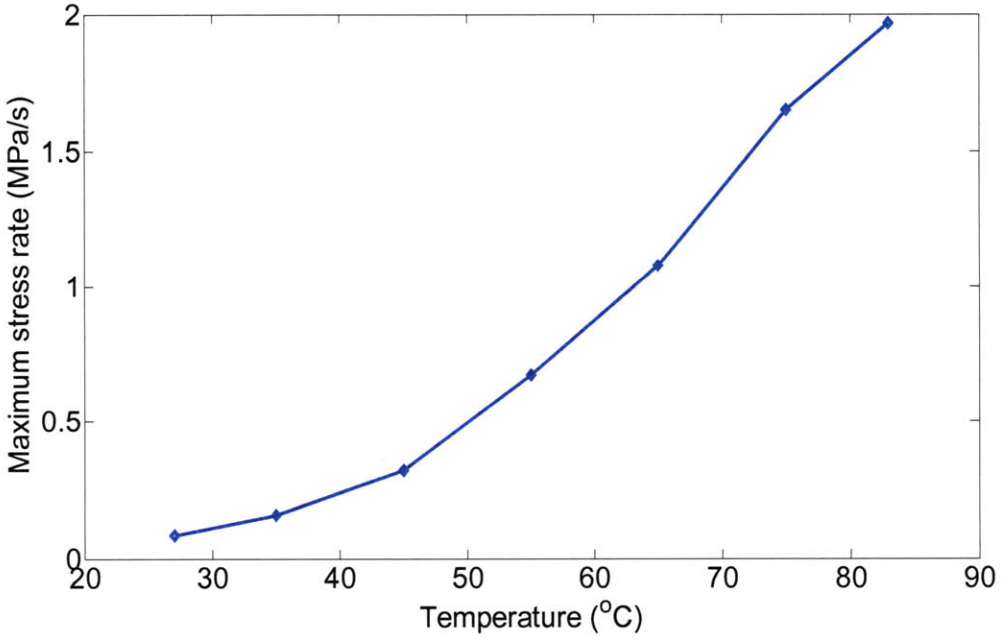

Figure 3-8. Maximum stress rate increased with temperature. As the solvent bath and the sample were heated from 27°C to 83°C, the peak stress rate increased from 0.08 MPa/s to 1.97 MPa/s.

While voltage was applied to the sample, both charge and stress changed in very similar ways, such as the trends shown in Figure 3-3. At +1 V ion movements caused the sample to pull inward and increase in stress. This decrease in volume suggested outflow of the $BMIM^+$ ions. At -1 V the sample expanded by attracting the same ions into the sample bulk. The results suggested that the movements of positive ions were more dominant than that of the negative ions to cause stress changes, as mentioned earlier.

Based on the charge per volume results, increasing the temperature caused $BMIM^+$ ions to flow out faster from the sample and in higher quantities. The faster ion flow suggested that heating lowered the solvent resistance. As the larger amount of ions left the sample, the sample shrunk and pulled harder on the force sensor. Since the charge increased by almost 1000% with the temperature while the stiffness only had 21% decrease, based on Equation (1) the increase in peak stress resulted more from the charging effect than from changes in stiffness. However, there are studies that have shown the charging effect on stiffness which we have not explored ([17], [18]).

The peak stress results showed an optimal temperature of 75°C. Peak stress corresponds exactly to the amount of charge injected into the polymer since they both peaked at the same temperature. The peak charges started to level off may be due to the limited volumetric capacity for ions past 75°C. And the amount of ions that the polymer can hold depends upon the ion size. Thus, polypyrrole actuation strength at different temperatures may be solvent/ion dependent. To verify this conclusion, next section is followed by repeating the same experiments using different solvent/ion combinations.

The strain results showed volumetric expansion as the sample was heated. The sample volumetric expansion that occurred with heating caused it to buckle at 65°C and

75°C. The stress curves for these two temperatures in Figure 3-6 stayed flat for the first two seconds. Until the sample had enough ions flowing outward it started to straighten up and pull on the force sensor. Although these two stress curves reached plateau within 18 seconds, buckling could possibly be eliminated by increasing the preload. Besides buckling, volumetric expansion should have also been considered for peak charge per volume calculation. Rather than taking ratio of charge per current volume, original volume of 0.336×10^{-9} m^3 was used for all temperatures. Remeasuring the sample length (perhaps as well as the width) at each temperature would have been necessary to allow more accurate peak charge to volume ratios, although the overall charge versus temperature trend would not change much (Figure 3-6).

Without the data at temperatures higher than 83°C, it is unclear what would happen past 83°C. The general trend suggests that actuating polypyrroe at high temperatures had significantly higher maximum stress rate. Although actuating polypyrrole at temperature as high as 75°C improved strength and stress rate, the performance of the sample is limited to the electrolyte used.

3.2 Actuation in Cation-Driven Electrolytes

3.2.1 Introduction

Section 3.1 discussed that increasing temperature increased the ionic mobility and charging rate to cause higher active stress in polypyrrole. The charging rate can also be improved by increasing the ionic conductivity with choice of electrolytes and mobile ion species. For example, actuation in sodium hexafluorophosphate gives higher strain than in tetraethyammonium hexafluorophosphate (TEAP) [20].

The polypyrrole actuator is more efficient with one dominant ion type than with two, because the movement of one ion type can be counteracted by the other ion type that moves in opposite direction. This study characterized and compared how cation-dominated actuation by different ion types and sizes can be improved under elevating temperature. Actuation in 1-Butyl-3-methylimidazolim hexafluorophosphate (BMIM-PF_6) and 1-Butyl-3-methylimidazolim tetrafluoroborate (BMIM-BF_4) has been shown to be driven by the BMIM cation, and actuation in TEAP is also driven by the cation (TEA) at negative voltage [15]. Table 3-1 lists the ion species and their sizes (longest distance between two ends) of these three salts.

Ion type	Size (nm)
$BMIM^+$	0.92
TEA^+	0.67
PF_6^-	0.32
BF_4^-	0.25

Table 3-1. Size of ions in BMIM-PF_6, BMIM-BF_4, and TEAP

3.2.2 Actuation in the Three Electrolytes

In both BMIM-PF_6 and in BMIM-BF_4 voltage between -0.8 V and +0.8 V was applied to the polymer, and in TEAP/PC the voltage window was -0.8 V to 0 V to ensure only the cation was transferred.

In stress studies, polypyrrole samples were first excited sinusoidally in electrolyte for 1% at 1 Hz for 10 cycles with sample preloaded to 5 MPa. Upon polymer submersion in the electrolytes, the samples were "warmed up" with square voltage pulses at about 0.038 Hz for 10 cycles without any tension in the samples to finalize initial ion uptake from the electrolyte. The polymer was then preloaded to 8 MPa and actuated isometrically using the same electrochemical settings as the warm-up procedure. Isometric tests were conducted isothermally in BMIM-PF_6, BMIM-BF_4, and TEAP/PC.

3.2.3 Actuation in Different Electrolytes at Room Temperature

Applying polypyrrole with +0.8 V in both BMIM-PF_6 and BMIM-BF_4 caused more positive stress in the polymer, meaning that the polymer was under contraction resulting from the $BMIM^+$ cations leaving the polymer bulk (Figure 3-9). Similarly, applying polypyrrole with -0.8 V in these two electrolytes caused the polymer to expand, resulting from the cations entering into the polymer bulk. Although both electrolytes had the cations being the dominant ion type, in BMIM-BF_4 the stress reached a plateau soon after the voltage was applied, while in BMIM-PF_6 the stress was still slowly increasing towards the end of the cycle. The difference might be due to the fact that $BMIM^+$ disassociates easier from PF_6^- compared to BF_4^- at the applied voltage so that more $BMIM^+$ ions were free to enter the polymer bulk from the surface in BMIM-PF_6 than in

BMIM-BF_4. In TEAP/PC, like in the previous two liquid salts, the cations TEA^+ left the polymer at 0 V and entered the polymer at -0.8 V.

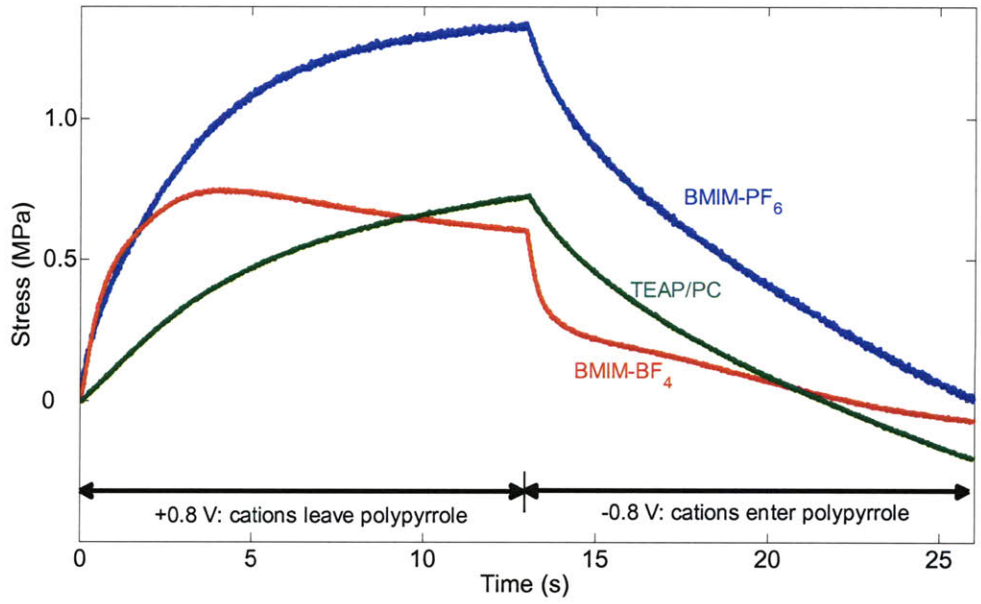

Figure 3-9. At room temperature, the active stress of polypyrrole was the highest in BMIM-PF_6 in the three salts. Although both BMIM-PF_6 and BMIM-BF_4 had the BMIM ions dominating the actuation, the shape in stress appeared differently.

3.2.4 Actuation in Different Electrolytes at Elevating Temperature

At all temperatures polypyrrole had the most charge while being actuated in BMIM-PF_6 and the least charge per polymer volume in TEAP/PC. Charge increased nearly linear with temperature by approximately 4.30 $MC/m^3/^oC$ in BMIM-PF_6, 1.92 $MC/m^3/^oC$ in BMIM-BF_4, and only 1.33 $MC/m^3/^oC$ in TEAP/PC (Figure 3-10 a). Elevating the temperature resulted in higher ionic mobility and polymer volumetric expansion, causing ion transfer through the polymer in faster rates and higher quantities.

The peak stress depended upon the amount of charge transferred to the polymer. Actuation in BMIM-BF_6 resulted in higher change in peak stress with increasing

temperature than in BMIM-BF_4 and in TEAP/PC (Figure 3-10 b). In BMIM-PF_6 peak stress started to reach a plateau of about 6.1 MPa at 75°C, and in TEAP/PC peak stress increase with temperature started to plateau past 55°C. For isometric tests in BMIM-BF_4, polypyrrole samples buckled at temperatures above 55°C. In BMIM-PF_6 the polymer also buckled but not until 75°C. Buckling occurred because high temperatures caused thermal expansion in the polymer, even though the polymer was preloaded at 8 MPa. The polypyrrole thermal expansion was greater in BMIM-BF_4 than in BMIM-PF_6, causing the sample to start buckling at lower temperature in BMIM-BF_4 compared to BMIM-PF_6.

The maximum stress rate also increased with temperature in all three electrolytes because heating facilitated ion transfer through the polymer bulk. In BMIM-PF_6 polypyrrole had the highest increase in peak stress rate with temperature for about 23 kPa/s/°C, approaching to a plateau. In PC/TEAP polypyrrole had the lowest increase in peak stress rate with temperature for about 9.4 kPa/s/°C, in a more linear manner than in BMIM-PF_6 (Figure 3-10 c). Similar to maximum charge per volume, at all temperatures the maximum stress rate was the highest in BMIM-PF_6, lowest in TEAP/PC (Figure 3-10 c). The stress rates were affected by the amount of charge transferred to the polymer. In BMIM-PF_6 the polymer had the highest stress rate compared to the other two electrolytes because it had the highest maximum charge per polymer volume.

(a)

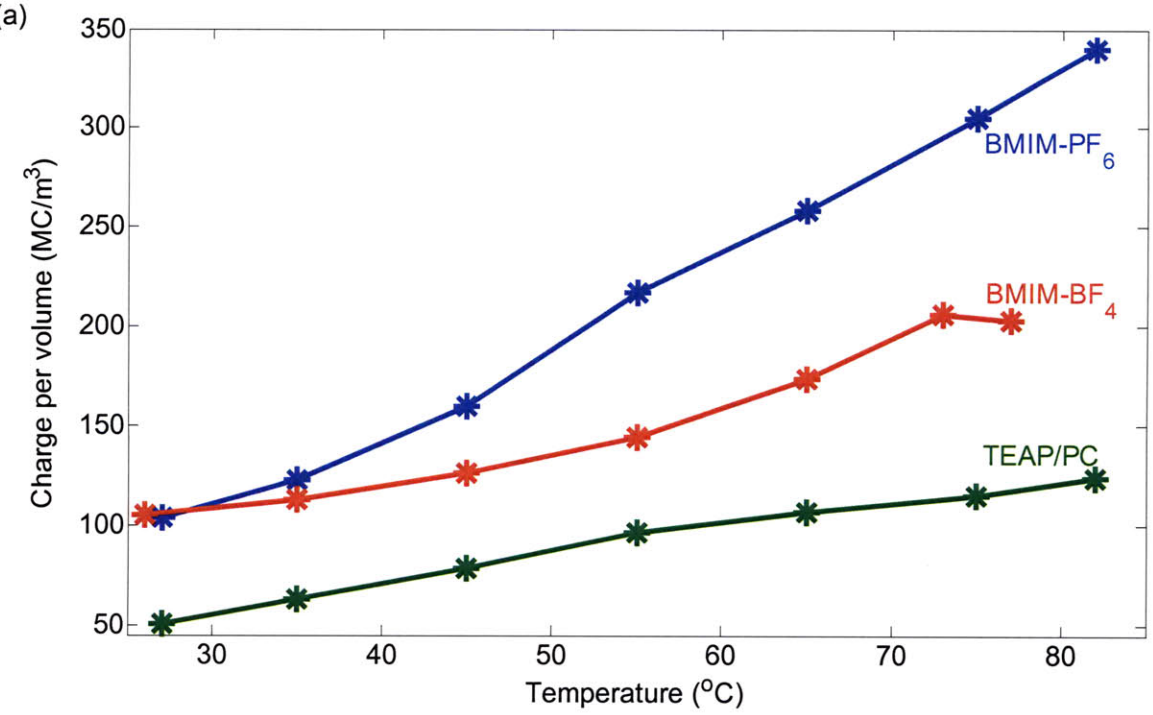
Charge per volume (MC/m^3)
Temperature (^{o}C)
BMIM-PF$_6$
BMIM-BF$_4$
TEAP/PC
350
300
250
200
150
100
50
30
40
50
60
70
80

(b)

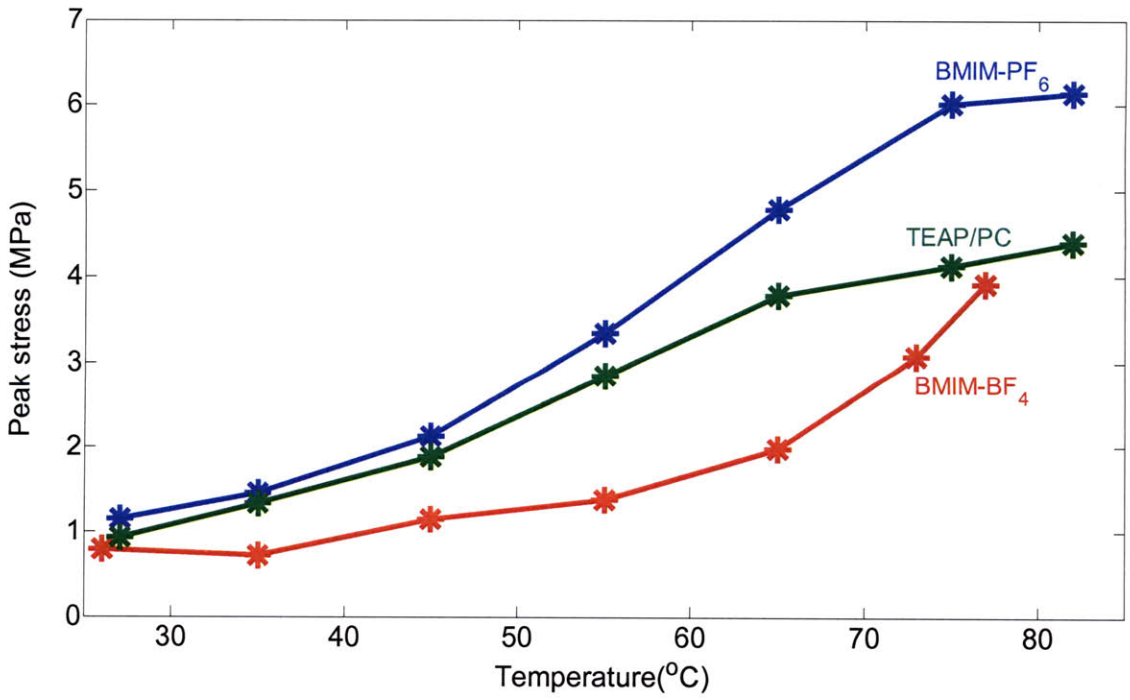
Peak stress (MPa)
Temperature(^{o}C)
BMIM-PF$_6$
TEAP/PC
BMIM-BF$_4$
7
6
5
4
3
2
1
0
30
40
50
60
70
80

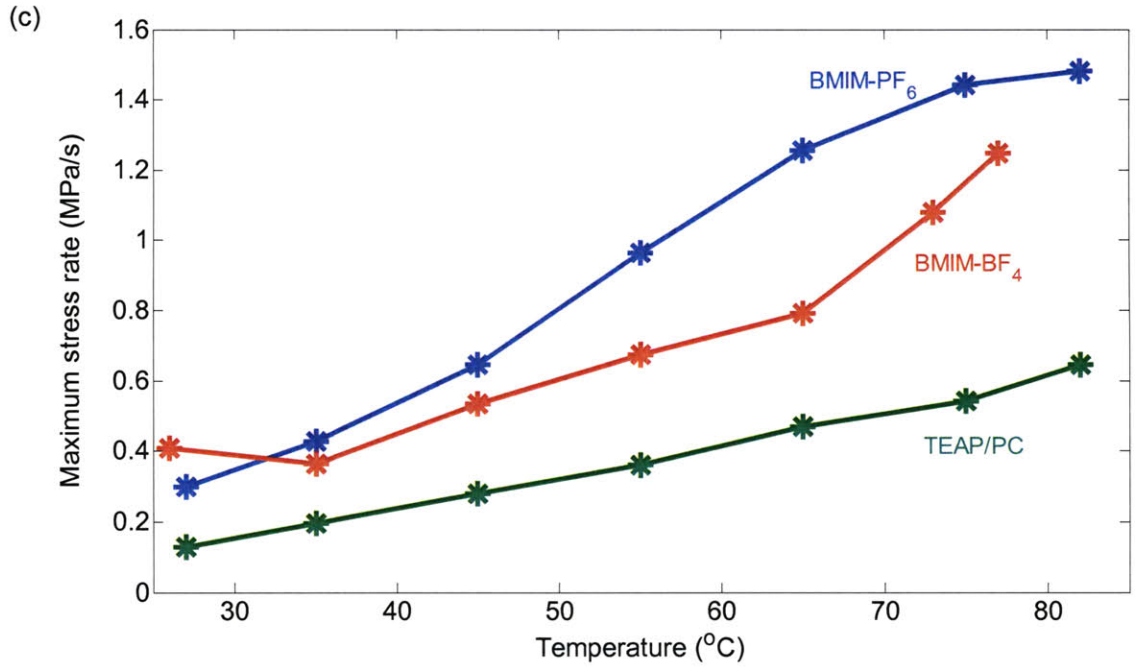

Figure 3-10. (a) In the three electrolytes used, charge per polymer volume increased the most with temperature in BMIM-PF_6 and the least increase in TEAP. (b-c) The peak stress and maximum stress rate also increased the most in BMIM-PF_6.

3.2.5 Discussion

The BMIM-PF_6 and BMIM-BF_4 ionic liquids provided better actuation results than TEAP/PC due to the fact that $BMIM^+$ ions were larger than TEA^+ ions, and thus resulted in higher actuation stress and strain. Besides the effect of ion size, the amount of ions transferred also affected actuation. The BMIM-PF_6 crystals appeared to be circular with average diameter of approximately 0.5 to 1 μm while the TEAP crystals were thin strips that were 2 to 3 μm long (Figure 3-11). The circular BMIM-PF_6 crystal shape might have allowed easier separation of the ions under the applied voltages than the TEAP long crystals. Besides, the electrolyte concentrations of neat BMIM-PF_6 and BMIM-BF_4 were higher than 0.05 M TEAP/PC so there was nearly constant $BMIM^+$ ions availability near

the polymer surface. As the temperature was increased, the $BMIM^+$ ions separated from the ionic liquids to transfer through the polymer was increased in quantity and contributed in even better actuation performance than the actuation caused by TEA^+ under the same temperature. Therefore, the higher charge per polymer volume and better actuation strain by the $BMIM^+$ ions than TEA^+ resulted from both large ion size and higher quantity.

The reasons to why having $BMIM^+$ rather than PF_6^- being the dominant species have not yet been fully understood. The mobile species theoretically can be the cations and/or the anions to neutralize the charge in polymer bulk. Since electrochemical polymerization of polypyrrole left the chains positive and PF_6^- anions (32 nm) were smaller than $BMIM^+$ cations (92 nm), intuitively PF_6^- should be the mobile ion but not $BMIM^+$. $BMIM^+$ might have higher diffusivity through the polypyrrole surface than PF_6^- to be active in the electrochemical responses.

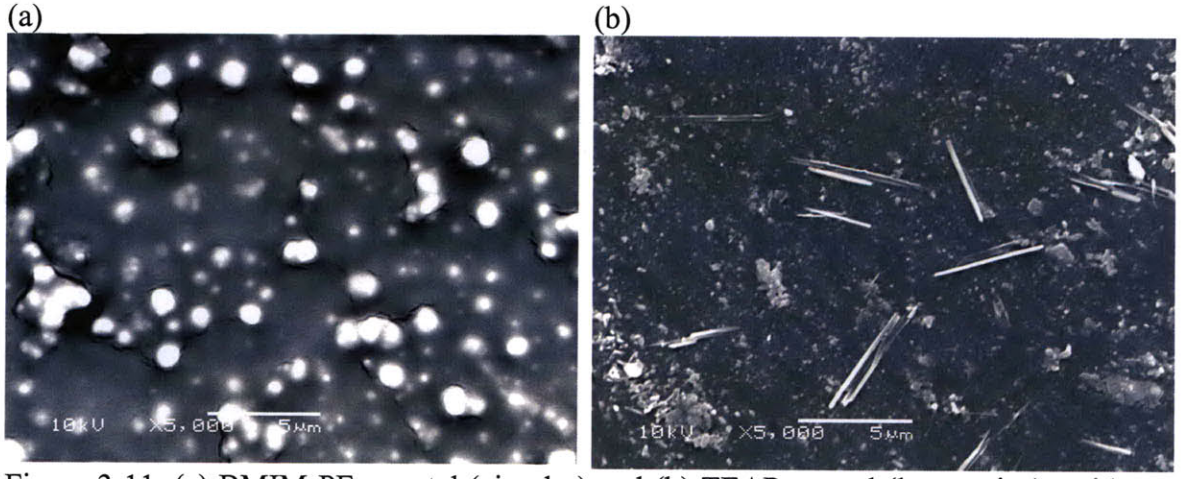

Figure 3-11. (a) BMIM-PF_6 crystal (circular) and (b) TEAP crystal (long strips) residues on polypyrrole surface after actuation.

3.2.6 Conclusions

The actuation performance is largely determined by the ion type as well as the amount of charge present in the polymer. This work investigated how different electrolytes – BMIM-PF_6, BMIM-BF_4, and TEAP/PC – affected polypyrrole actuation under elevating temperature. The results showed that overall BMIM-PF_6 was the best electrolyte to generate actuation because the polymer possessed the combined advantages of (1) having only one ion type $BMIM^+$ as the active species so that charge transfer could be easily observed; (2) having highest charge per polymer volume, thus highest actuation stress and strain, compared with the other two electrolytes; (3) highest stress rate increase with elevating temperature among the three electrolytes; (4) less sample buckling at high temperatures compared with actuation in BMIM-BF_4.

3.3 Effect of Ion Delivery on Strain and Strain Rate[‡]

3.3.1 Introduction

Previous sections showed that isometric tests at temperatures above 65°C in BMIM-PF_6 became difficult because thermal expansion caused the polymer to buckle. Therefore, the true peak stress at high temperatures might have been larger than what we measured. To resolve the buckling problem and further investigate strain change with temperature, this work includes isotonic actuation of polypyrrole between 27°C and 83°C. In addition, since little work has been done to demonstrate how actuation performance can be affected by ionic flow into versus out of polymer under gradually increasing temperature, here we also compare the actuation performance at both positive and negative voltages. Liquid salt BMIM-PF_6 was particularly chosen for this study because it was shown to give the best actuation results in Section 3.2.

3.3.2 Temperature Elevated Isotonic Actuation

The polypyrrole film was electrochemically synthesized using the same method as described in Chapter 1. Samples were cut from the polypyrrole film and held in between two gold-coated clamps for isotonic actuation tests. The sample between the clamps was measured to be 8.6 mm in length and 2 mm in width on average. Isotonic testing was done on the EDMA and the integrated temperature controlled solvent bath was used for heating up the electrolyte BMIM-PF_6 [19]. For approximately every increment of 10°C from 27°C to 83°C, the polymer was applied with +/-0.8 V square electrical pulses at

[‡] This section reuses relevant sections from paper "The Effect of Ion Delivery on Polypyrrole Strain and Strain rate under Elevated Temperature" (1222-DD02-10), for the 2009 MRS Fall Meeting.

0.05 Hz for 20 cycles. For each isotonic test, the polymer was held at a constant stress of 1.5 MPa.

For 27°C, 35°C, 45°C, 55°C, 65°C, 75°C, and 83°C, the charge was obtained by integrating the current generated in the polymer. The first five cycles of strain were eliminated because electrochemical activity in the polymer took some time to equilibrate. Hence for data analysis only the last 15 cycles of strain were averaged. The amplitude was the peak strain and the steepest slope per second was the maximum strain rate. Furthermore, in order to investigate the effect of positive and negative voltages, maximum strain rates of each sample were determined separately for each temperature. The maximum charge per polymer volume was also obtained by averaging the last 15 cycles of the charge curve, with the polymer volume being the measured dimensions 0.688×10^{-9} m^3. Peak strain, maximum strain rate, and maximum charge per volume were plotted as functions of temperature.

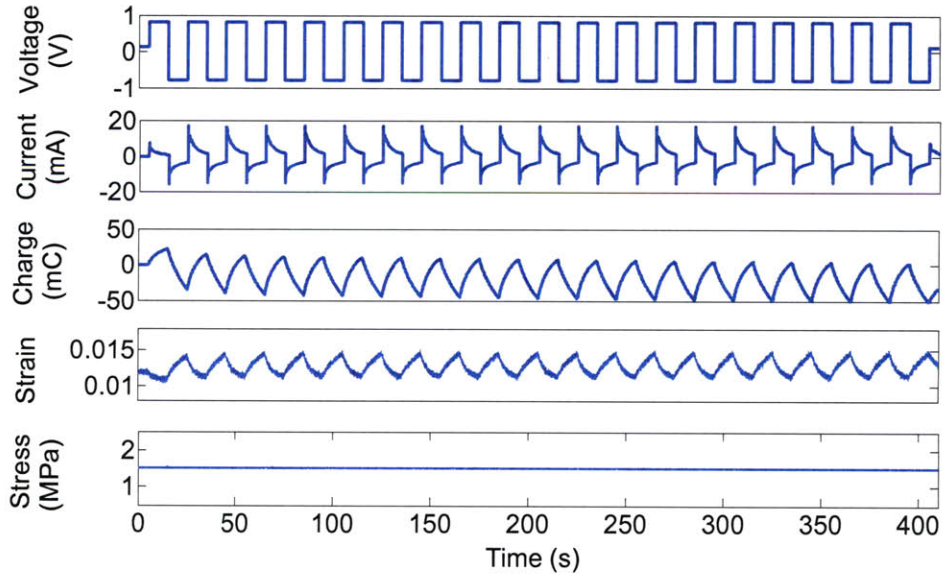

Figure 3-12. Isotonic results at 27°C that shows voltage, current, charge, strain, and stress versus time. Twenty cycles of square pulses of +/-0.8 V were applied to the polymer.

3.3.3 Results

As +0.8 V was applied to the polymer, the $BMIM^+$ ions were expelled from the sample causing the strain to decrease. As -0.8 V was applied, the $BMIM^+$ ions were attracted to the polymer. The ion influx caused strain to increase. Figure 3-12 shows the isotonic results obtained at 27°C. Isotonic results at other temperatures had the same trends in current, charge, and strain.

At +0.8 V the averaged strain increased with temperature by 4.8 times, from 0.35% at 27°C to 2.03% at 83°C. At -0.8 V the peak strain increased with temperature by 4.9 times, from 0.34% at 27°C to 2.02% at 83°C (Figure 3-13; Figure 3-14). The averaged strain amplitudes at both positive and negative voltages at all temperatures were approximately the same and increased with temperature in an exponential trend (Figure 3-14).

Similar to peak stress, the maximum strain rate also increased with temperature but with different trends (Figure 3-14 a). At +0.8 V the maximum strain rate increased exponentially by 5.7 times, from 0.1 %/s at 27°C to 0.67 %/s at 83°C. At -0.8 V the maximum strain rate increased by 3.1 times, from 0.06 %/s at 27°C to 0.23 %/s at 83°C. Past 75°C the maximum strain rate at -0.8 V started to level off. For all temperatures the maximum strain rate at +0.8 V was higher than that at -0.8 V, and the difference increased with temperature. At 27°C the maximum strain rate at +0.8 V was 0.044 %/s higher than at -0.8 V, and at 83°C the difference increased to 0.44 %/s (Figure 3-15 a).

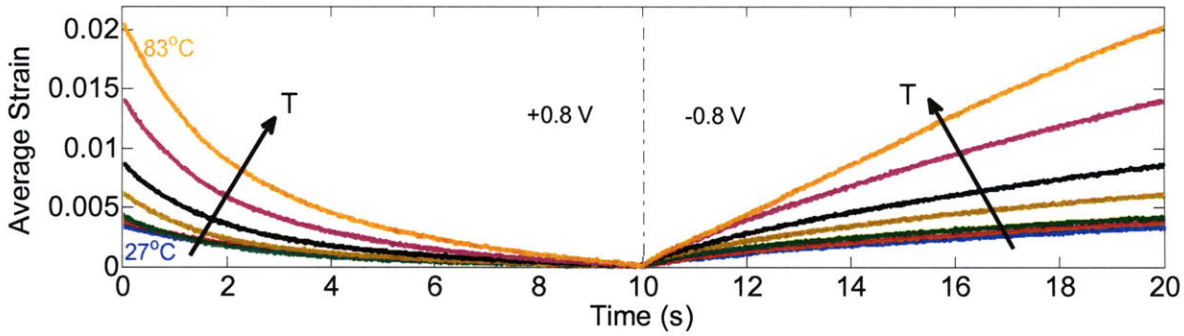

Figure 3-13. Averaged strain at 27°C, 35°C, 45°C, 55°C, 65°C, 75°C, and 83°C. As the temperature increased the average strain increased. The strain decreased at +0.8 V due to the $BMIM^+$ ions leaving the polymer and the strain increased at -0.8 V due to the $BMIM^+$ ions entering the polymer.

Similar to maximum strain rate, maximum charge per polymer volume was higher at +0.8 V than at -0.8 V for all temperatures (Figure 3-15 b). At 27°C the maximum charge per volume at +0.8 V was 4.5 MC/m^3 higher than at -0.8 V, and at 83°C the difference was 11.8 MC/m^3. At +0.8 V the maximum charge per volume increased with temperature by 2.4 times, from 11.2 MC/m^3 to 38.5 MC/m^3. And at -0.8 V it increased by 2.9 times, from 6.8 MC/m^3 to 26.7 MC/m^3 (Figure 3-15 b).

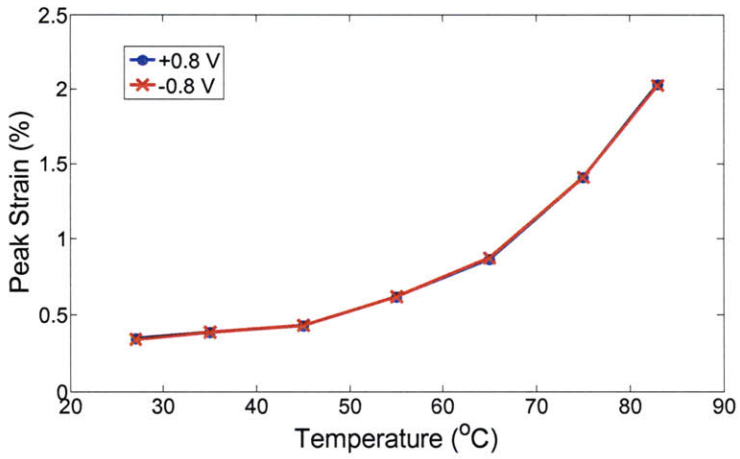

Figure 3-14. Peak strain at all temperatures at both +0.8 V and -0.8 V were on top of each other. As the temperature increased, peak strain increased by 4.9 times exponentially.

The increases in maximum charge per volume with temperature suggest that heating caused higher ionic mobility, and also allowed more ions to flow in and out of the polymer within the same time frame. Therefore, at high temperatures when the polymer held more ions, the strain was higher than at lower temperatures. And at high temperatures when the ions moved faster in and out of the polymer, the actuation strain rate was higher than at lower temperatures. The exponential temperature-dependent behavior of the polymer can be further explained quantitatively using the charging and the diffusion time constants. The charging time constant is proportional to the solution resistance while the diffusion time constant is inversely proportional to the diffusivity. Both constants were shown previously to decrease with increasing temperature, meaning that the solution resistance decreased and the diffusivity increased [16].

Figure 3-15.

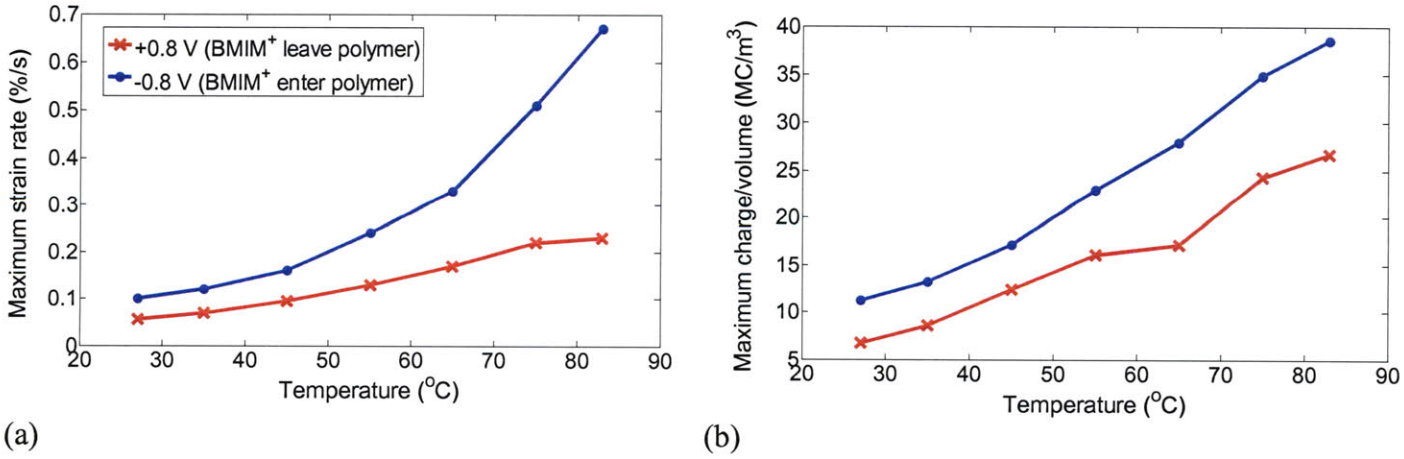

Figure 3-15 (a-b). Both maximum strain rate and charge per volume at +0.8 V and -0.8 V increased with temperature. For all temperatures, at +0.8 V both had higher values than that at -0.8 V. Figure 4 shows that maximum strain rate at +0.8 V increased much faster with temperature than at -0.8 V.

Based on Figure 3-15 (a) and (b), both maximum strain rate and maximum charge per volume had greater values at +0.8 V than at -0.8 V. Since the active ion species was $BMIM^+$, the results suggest that at +0.8 V the ions preferentially left the polymer to stay in ionic liquid. As the temperature increased, i.e. as the ionic mobility increased, at +0.8 V the $BMIM^+$ ions left the polymer even faster than entering the polymer. This explains why the difference in maximum strain rate and maximum charge per volume between +0.8 V and -0.8 V increased with temperature.

3.3.4 Conclusions

This study showed that with increasing temperature peak strain exponentially increased, and that maximum strain rate increased much faster when ions were diffusing out rather than into the polymer. We did not demonstrate coupling of stiffness and charge effect under increasing temperature because Section 3.1 showed that charge effect more dominantly determined actuation performance [19]. Compared with our previous isometric results, both peak stress and strain exponentially increased with temperature up to about 65°C. The stress trend past 65°C was not conclusive because isometric tests resulted in polymer buckling past this temperature. Moreover, the previous isometric results showed a charge to volume ratio plateau past 75°C, but the isotonic results did not have a plateau. Such discrepancy perhaps results in different thicknesses of the samples and possible variations in deposition process. The average thickness of the polymer for isotonic tests was twice as thick as the film used for previous isometric studies. It is speculated that a thicker film has relatively larger charge capacity and thus allows ion

diffusion in higher quantities when temperature was increased while a thinner sample can saturate faster. Section 3.4 is followed to investigate the effect of polymer film thickness.

3.4 Polypyrrole Film Thickness Effect

Sections 3.1 to 3.3 have shown that temperature elevation caused exponential increase in active stress and strain due to the fact that heating increased ion movement. Besides the charging effect, heating also caused the polymer bulk to undergo thermal expansion, creating more room for ion diffusion. This experiment investigated how polypyrrole films with different thicknesses affected active strain under increasing temperature.

Polypyrrole films were fabricated following the procedures described in previous sections. The deposition time was set to 10 and 12 hours to form 20 μm and 40 μm films, respectively. Samples from these two films were cut in the same width and length and actuated isotonically using the same settings throughout the same temperature range as in Section 3.3. The maximum strain obtained was normalized to the sample volume that was measured before heating. The strain to volume ratio was compared for different temperatures and offset to the same starting point for both films.

Results showed that the strain to polymer volume ratio exponentially increased with temperature in both the 20 and 40 μm films (Figure 3-16). Before 55°C both curves overlapped on top of each other, but past this temperature strain per volume increased more with temperature in the 40 μm film than the 20 μm film.

This result implied that at high temperatures the thick film underwent more volumetric thermal expansion relative to the thin film, so the thick film got thicker and the expanded space allowed more ion diffusion into the polymer to cause higher strain. This result therefore explained that due to the limited space the charge reached a plateau in a 20 μm film in Section 3.1 but did not in a 40 μm in Section 3.3. For application

purpose, a film as thick as 40 μm can be used at high temperatures to generate high active strain. If the thickness is further increased, the stiffness may also increase and impede the polymer to actuate well.

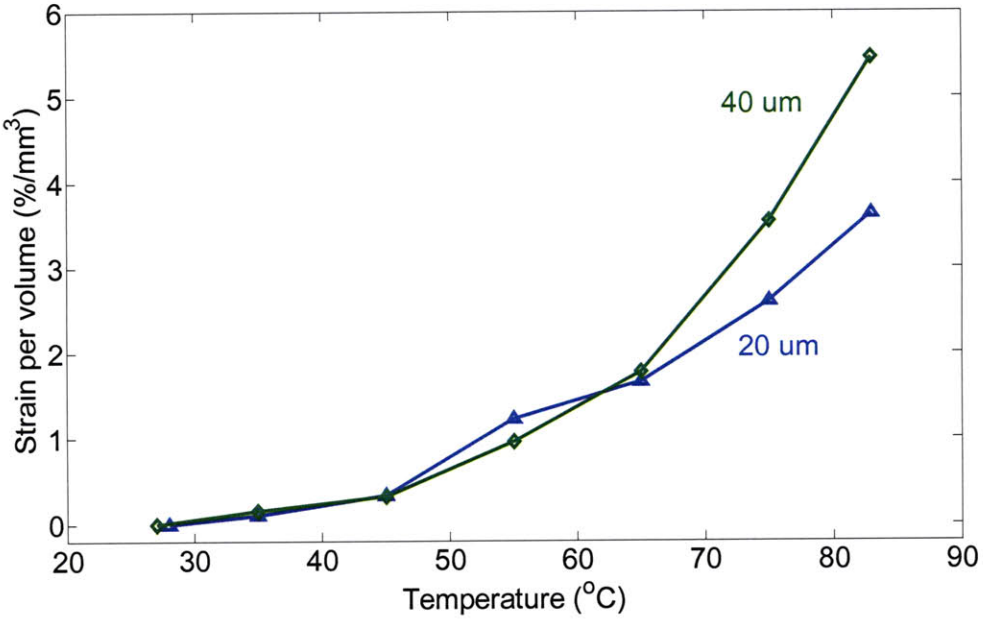

Figure 3-16. Before 65°C the strain to volume ratio overlapped, and past this temperature the ratio was higher in the 40 μm film than the 20 μm.

3.5 Thermal Effect Modeling

Experiments showed that increasing the temperature increased the charge uptake in the polymer bulk. According to Figure 3-5, the charge increased from 25 MC/m^3 at room temperature to 270 MC/m^3 at 75°C. As discussed in Section 3.1, this change did not significantly affect stiffness to cause the increase in stress. Pillai showed that with a bigger change in charge, the inverse of stiffness (or compliance) linearly decreases with increasing charge (Figure 3-17) [18]. The compliance can therefore be written as $y = a - k\rho$ (Equation (4)), in which y is the compliance, ρ is charge, and a and k are constants.

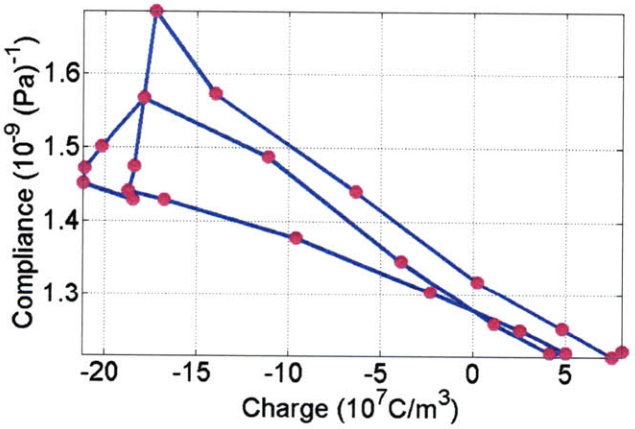

Figure 3-17. The compliance decreases with increasing charge. The change can be approximated as linear (Taken from [18]).

Rearranging Equation (1) and plugging in Equation (4), we got $\varepsilon_T = \frac{\sigma}{E} + \alpha\rho = y\sigma + \alpha\rho = (a - k\rho)\sigma + \alpha\rho$ (Equation (5)). Using isometric data to

calculate k, a, and α, we took first derivative of Equation (5) with respect to time using two approaches – setting y to vary (Approach 1) and not vary (Approach 2) with time:

- Approach 1 – y varies with time:

  $\dot{y} = -k\dot{\rho} = -kI \quad (\dot{\rho} = I)$, in which I is the current.

  Take the first derivative, Equation (5) becomes,

  $\dot{\varepsilon}_T = \dot{y}\sigma + y\dot{\sigma} + \alpha\dot{\rho} = (-kI)\sigma + (a - k\rho)\dot{\sigma} + \alpha I \quad (\dot{\varepsilon}_T = 0$ for isometric tests),

  $\therefore (-kI)\sigma + (a - k\rho)\dot{\sigma} + \alpha I = 0$.

  Rearranging the terms, $\dot{\sigma} = (\rho\dot{\sigma} + I\sigma)\frac{k}{a} + (-I)\frac{\alpha}{a}$,

  $\frac{k}{a}$ and $\frac{\alpha}{a}$ were solved using the measured ρ, σ, $\dot{\sigma}$, and I.

- Approach 2 – y does not vary with time:

  Equation (5) becomes $(a - k\rho)\dot{\sigma} + \alpha I = 0$.

  Rearranging the terms, $\dot{\sigma} = (\rho\dot{\sigma})\frac{k}{a} + (-I)\frac{\alpha}{a}$,

  $\frac{k}{a}$ and $\frac{\alpha}{a}$ were solved using the measured ρ, σ, $\dot{\sigma}$, and I.

The $\frac{k}{a}$ and $\frac{\alpha}{a}$ terms were solved in MATLAB and plotted against increasing temperature for both approaches. The results showed that both approaches had $\frac{k}{a}$ exponentially decreasing with temperature, but the magnitudes were higher in

Approach 2. Results also showed that $\frac{\alpha}{a}$ increased with temperature until 55°C in Approach 1 but stayed nearly constant in Approach 2.

Comparing the two methods, Approach 1 had total squared error that was on average 20% smaller in stress rate than Approach 2. Therefore, having the compliance to vary with time more accurately estimated ratios $\frac{k}{a}$ and $\frac{\alpha}{a}$ than having the compliance constant. Besides, Figure 3-19 showed that in Approach 1 the ratio $\frac{\alpha}{a}$ increased with temperature, meaning that strain per charge increased as the polymer was heated. This result made more physical sense than having the constant $\frac{\alpha}{a}$ in Approach 2.

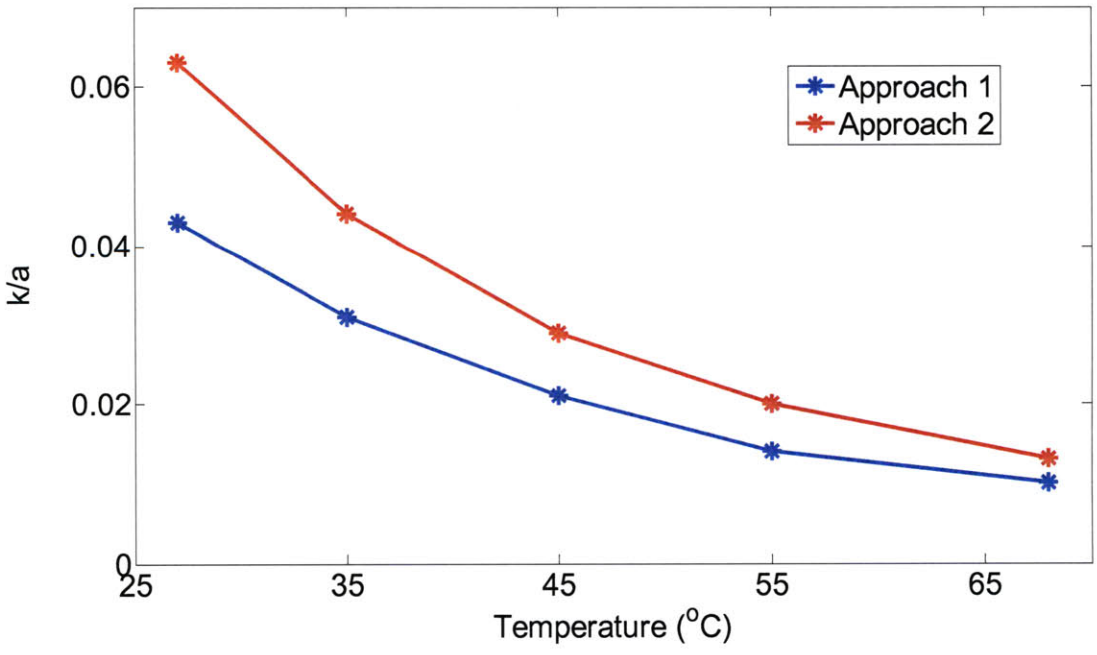

Figure 3-18. The solved $\frac{k}{a}$ decreased exponentially with increasing temperature in both approaches.

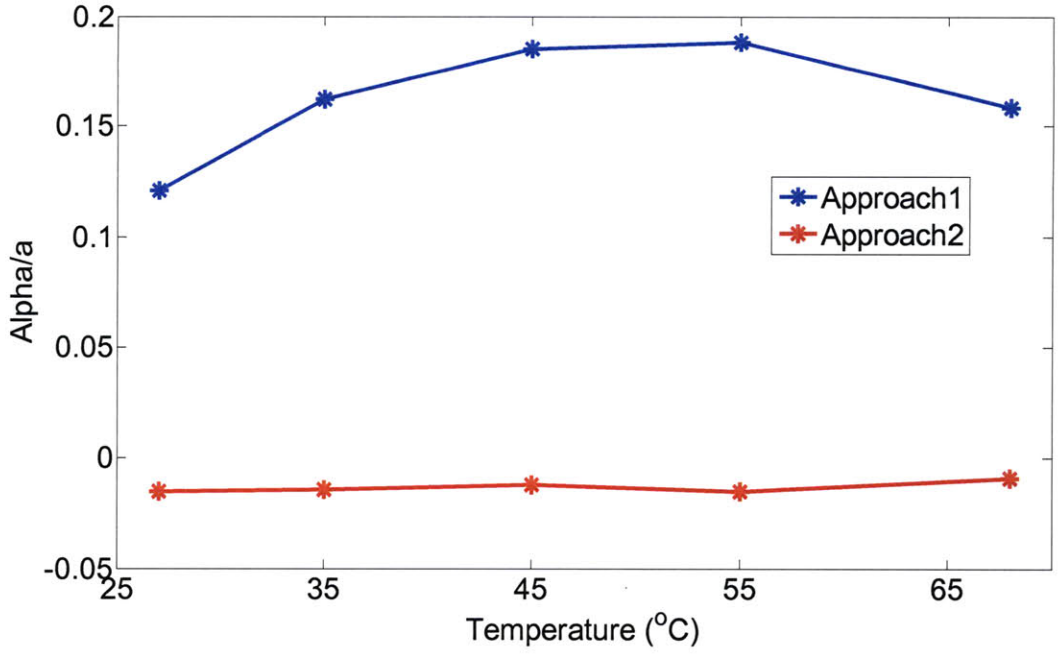

Figure 3-19. The solved $\frac{\alpha}{a}$ increased until 55°C in Approach 1 and had no obvious change in Approach 2.

Having $\frac{k}{a}$ to decrease with temperature implied that the compliance does not change with charge as much in high temperature as in low temperature. Therefore, although at high temperature the ions that diffused into the polymer increased, the stiffness change was not relatively significant to affect actuation performance. This conclusion further verifies that the effect of charge was more influential than the change in stiffness to cause the increase in active stress after heating.

3.6 Conclusions

This chapter showed that polypyrrole actuation highly depended upon the size of the active ion species, rate of diffusion, and the amount of charge uptake. BMIM-PF_6 was proven to give better active stress than TEAP due to the fact that $BMIM^+$ ions were larger than TEA^+ ions. As the temperature of the polymer in BMIM-PF_6 was increased, isometric results showed an optimal temperature of 75°C and isotonic results showed an exponential increase in active strain. Heating not only caused more active ion movement but also expanded the polymer volume to allow more charge uptake. Therefore, larger ions and higher temperature improved actuation performance of polypyrrole.

Although the effect of charging was more significant than the change in stiffness due to short-term heating in the range of 25 to 83°C, it is important that the polymer can sustain high temperature for long terms. Cole et al. showed that cycling the temperature from room temperature to 80°C decreased the active strain in $NaPF_6$ and $TBAPF_6$ due to a possible structural change [20]. Therefore, in the future longevity studies can be done at high temperatures to investigate how polypyrrole sustains in different electrolytes.

CHAPTER 4

Effect of Carbon Nanotubes on Conducting Polymer and Composite Fabrication Techniques [§]

Conducting polymers can be attractive actuator materials due to their mechanical properties. However, creep in these materials limits their reversible performance that is important for potential applications. Preliminary studies done by Dr. Nate Vandesteeg and Priam Pillai from the Lab demonstrated that functionalized multiwall carbon nanotubes (fCNTs) were capable of reducing creep in PEDOT and polypyrrole actuation [16]. Their studies have been continued, adopting modified fabrication techniques and comprehensive actuation analyses. The conducting polymer-fCNTs composite fabrication techniques included soaking/sonicating polypyrrole films in fCNT suspension, nine-layer PEDOT-fCNTs sandwiches by dropcasting, and five-layer polypyrrole-fCNTs sandwiches by dropcasting. The CNTs used in these techniques were more stable in polar solvents than the CNTs previously used by Dr. Vandesteeg and Pillai. And the composites made were analyzed for thickness, conductivity, stiffness, active stress, active strain, and creep.

[§] This chapter reuses relevant sections from a pending manuscript "Effects of Functionalized Carbon Carbon Nanotubes on Poly(3,4-ethylenedioxythiophene) and Polypyrrole Actuation", for the Polymer Journal.

4.1 CNTs Specification

The CNTs that were first used in Dr. Vandesteeg and Pillai's conducting polymer-CNTs composites had carboxyl functional groups (cCNT). These CNTs were slightly soluble in solvents like water or propylene carbonate. Developments by Jan Schnorr and Dr. Timothy Swager's group improved stability of multiwall CNTs (MWNTs) in polar solutions by attaching sulfonate groups (sCNT) instead of the previously used carboxylate groups to their surface. These sCNTs formed much more stable dispersions in propylene carbonate than the cCNTs. Figure 4-1 shows that cCNTs separated out of solution within hours after mixing while the sCNTs stayed stable in propylene carbonate two months after mixing. The sCNTs with sulfonate groups would be ideal for fabrication since soaking polymer in sCNTs suspension and multilayer deposition requires hours of processing time.

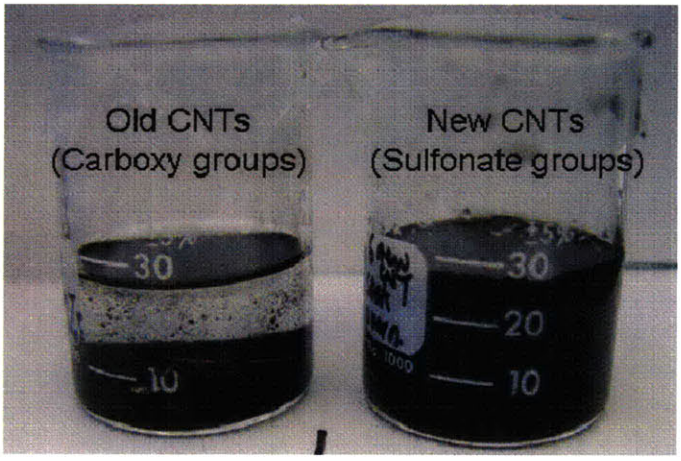

Figure 4-1. The cCNTs settled down to the bottom of the beaker within hours after mixing, while the sCNTs stayed stable in propylene carbonate two months after mixing. The concentration was 1 mg/ml.

4.2 Fabrication Techniques

The fabrication techniques that have been adopted to incorporate sCNTs include direct deposition of sCNTs during polymer polymerization, soaking/sonicating polymer films in sCNT suspension, and multilayered polymer-sCNT sandwiches with total five and nine layers.

4.2.1. Direct Deposition of sCNTs during Porryole Polymerization

Deposition of polypyrrole with the sCNTs blended in the deposition solution did not result in free-standing films. The sCNTs degraded the polymerization of the polypyrrole so the film developed poor mechanical properties. Therefore, successful composite fabrication required separation of polymer deposition and sCNT addition to different steps.

4.2.2 Soaking and Sonicating Polypyrrole Films in sCNT Suspension

Free-standing polypyrrole films were soaked in sCNT suspension for 30 minutes and overnight. They were also soaked in the same suspension, sonicated in a bath sonicator for 30 minutes and one hour. Neither method resulted in successful attachment of the sCNTs onto the polymer surface. SEM (JEOL 6060) showed that the soaked polypyrrole samples had no observable CNTs but only salt crystals on both sides of the film (Figure 4-2). Therefore, soaking or sonicating the polymer in sCNTs suspension could not make the composite.

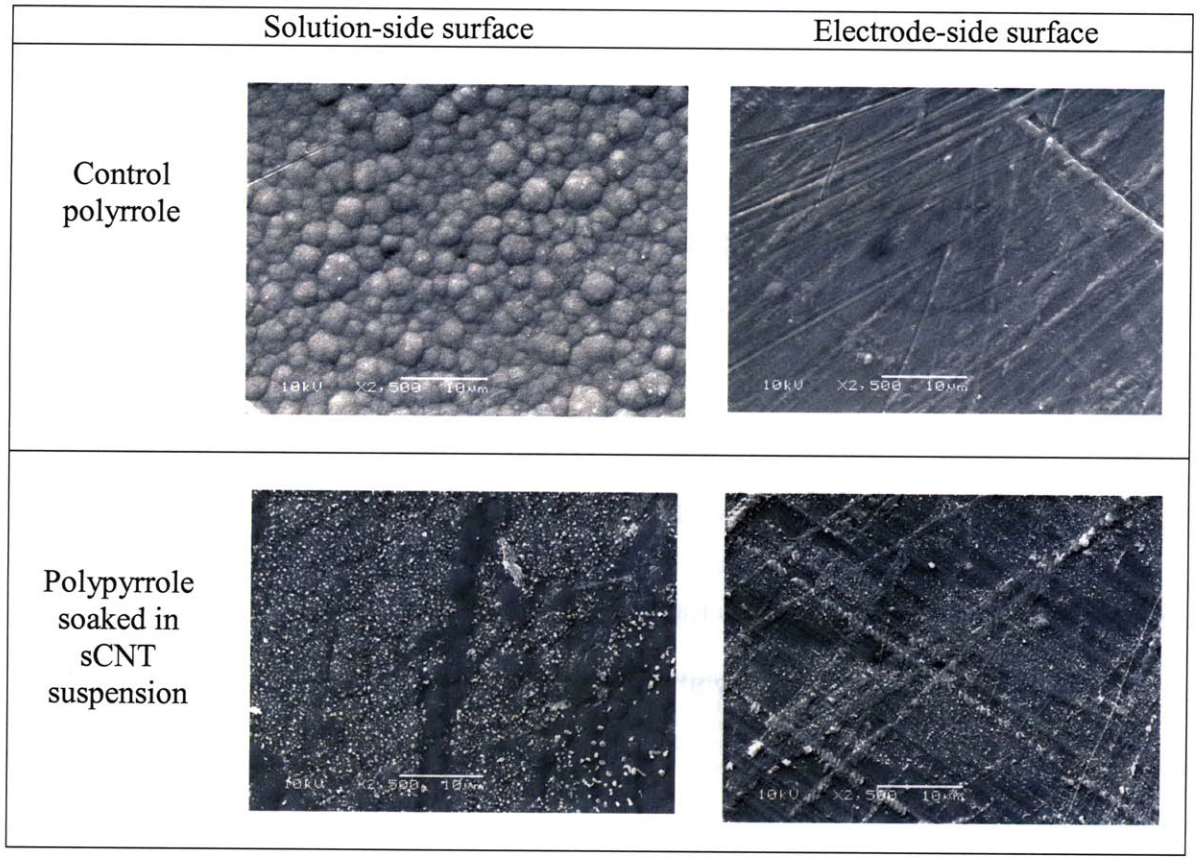

Figure 4-2. Surface SEM images showed that soaking polypyrrole films in CNT suspension did not successfully attach sCNTs to the polymer. Only salt crystals were seen after soaking.

4.2.3 Electrostatic Self-Assembly of CNTs

The sCNTs might also be attached to the polymer by electrostatic interactions. The negatively charged sCNTs could bind strongly to the polymer if it was applied with a positive voltage. As a result, an even layer of sCNTs would cover the polymer surface and the next layer of polymer could deposit on top to make a multilayer structure.

After one layer of polypyrrole was synthesized electrochemically, the glassy carbon electrode (25 mm × 25 mm) was applied with 0.7 V in the sCNT suspension for 15 minutes. The glassy carbon, with one polypyrrole layer and one CNT layer, was then

again placed in the polypyrrole deposition bath to form the next polymer layer. After repeating the deposition step three times and the electrostatic step twice, a five-layer polypyrrole-CNT multilayer was formed. However, applying 0.7 V on the glassy carbon seemed to attach the sCNTs not only to polypyrrole but also to the electrode. The multilayer films made by this method strongly adhere to the electrode, causing them to break during the peeling process.

To avoid ripping the composite during removal from the electrode, a free-standing polypyrrole film was then used instead as the base to attach sCNTs (on both sides) using the same voltage (Figure 4-3). Next, the film was placed in another bath to form the most outer polypyrrole layers. Although this technique attempted to make a five-layer polypyrrole-CNT composite using only half of the time compared to fabricating layers on top of the electrode surface, it was determined that polypyrrole base was not conductive enough to even attract any sCNTs to the surface or even deposit other polypyrrole layers. Viewing these samples under the SEM confirmed that there was no presence of the sCNTs or distinct polypyrrole layers.

Although the sCNTs did not electrostatically adhere to the polypyrrole, isotonic results showed that the PPy-sCNT films had less creep than the control film. Applying the film with 0.7 V in the sCNT suspension had even less creep than 0.65 V (Figure 4-4). Since the SEM showed no presence of sCNTs, the reduction in creep was not the effect of the sCNTs but rather the voltage application over half an hour might have degraded the polymer. The voltage applied within a polymer chain deteriorated its viscoelastic properties and therefore caused reduction in creep.

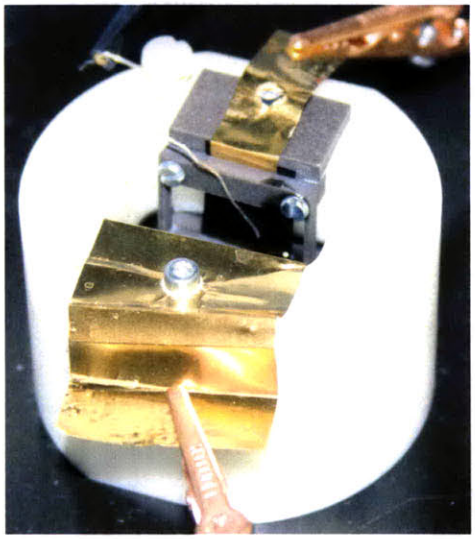

Figure 4-3. A free-standing polypyrrole film, stabilized by a plastic frame, was placed in the CNT suspension to attach CNTs to the surface by electrostatic.

In summary, attaching sCNTs by electrostatic self-assembly was intended to fabricate a composite with even thickness. However, applying voltage to form sCNT layers on glassy carbon made it difficult to peel off the composite compared to applying voltage directly to a free-standing polypyrrole film. Furthermore, if the electrostatic method attracted a thin layer of sCNTs, the amount would not increase as soon as the electrode became electrically neutralized. Therefore, this technique had limitations in controlling or measuring the amount of CNTs in the composite.

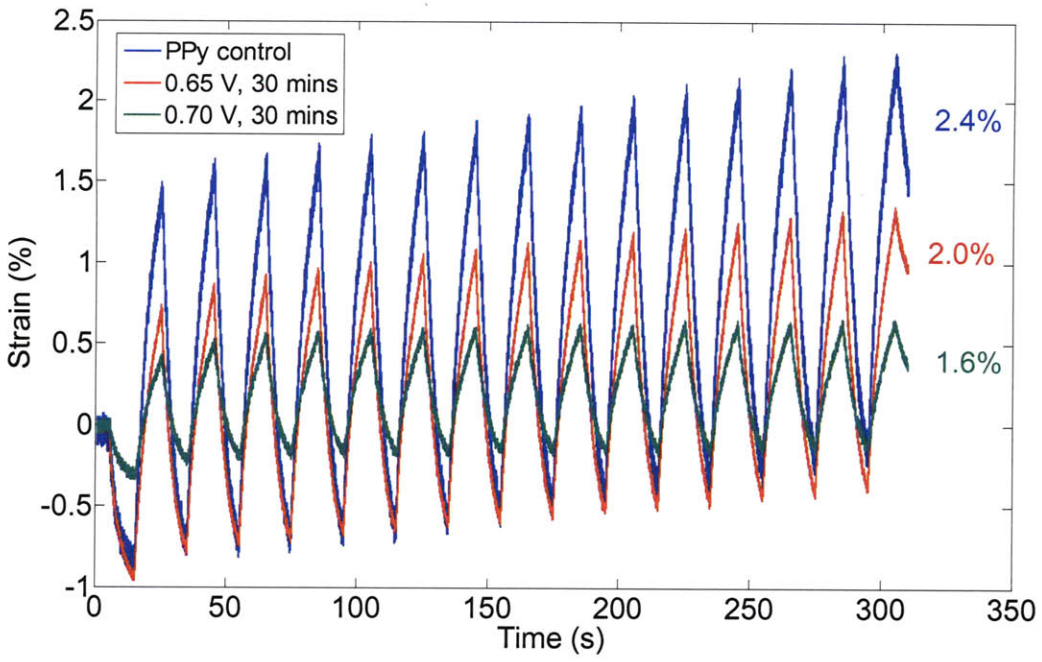

Figure 4-4. Applying the polypyrrole base with 0.7 V reduced the creep and strain compared to the control film. This was the result of polymer degradation from the voltage applied to electrostatically attach CNTs, but not the effect of any CNTs.

4.2.4 Multilayer Conducting Polymer-sCNT Composites by Drop-casting

The fabrication techniques previously mentioned could not successfully construct the composites to demonstrate the effect of sCNTs on conducting polymers. Dr. Ali Shaikh (visiting Professor) and Dr. Nate Vandesteeg introduced a multilayer composite structure composed of poly(3,4-ethylenedioxythiophene) (PEDOT) and cCNT layers [16]. The layer-by-layer approach allowed deposition of free-standing polymer layers and controllable amounts of cCNTs. Dr. Vandesteeg's study showed that the PEDOT-cCNT composite had lower creep rates and higher electrical conductivity than the PEDOT control film. This technique was developed further here to characterize how increasing

the amount of sCNTs affected the multilayer structure and mechanical properties of the composites.

In this study, the same layer-by-layer fabrication technique was repeated using the sCNTs. The PEDOT layers that sandwiched in the sCNTs were electrochemically deposited on a 25 mm × 25 mm glassy carbon at room temperature with a constant current of 0.5 mA using a potentiostat (AMEL Instruments Model 2053), 15 minutes for each layer. The PEDOT deposition solution consisted of 25 mL of 0.1 M EDOT in 0.1 M TEAP-propylene carbonate and 1% water. The sCNT layers in this study were drop-casted from an aqueous suspension because the sCNTs used here were processed differently from cCNTs. The suspension was dropped on top of each PEDOT layer (except the top layer) using a 1 mL syringe and the desired sCNT amount was estimated based on the concentration of the suspension 5 mg/mL. After depositing each PEDOT and sCNT layer, the composite with the glassy carbon was vacuum-dried and weighed on a digital scale (Mettler Toledo AG204) to calculate the percentage weight of the sCNTs (Figure 4-5 a). The aqueous suspension was chosen over propylene carbonate suspension because water has a lower boiling point so can dry faster in vacuum than propylene carbonate.

The composite was made for total nine layers, including five layers of PEDOT and four layers of sCNTs for 0%, 10%, and 20% sCNTs by weight. Drop-casting more than 20% of sCNTs in nine-layer PEDOT composites formed brittle films. Besides, because a 100% sCNT film was difficult to fabricate, a sCNT "control" was made by sandwiching four sCNT layers (80% wt.) in between two PEDOT support layers (Figure 4-5 b).

(a)

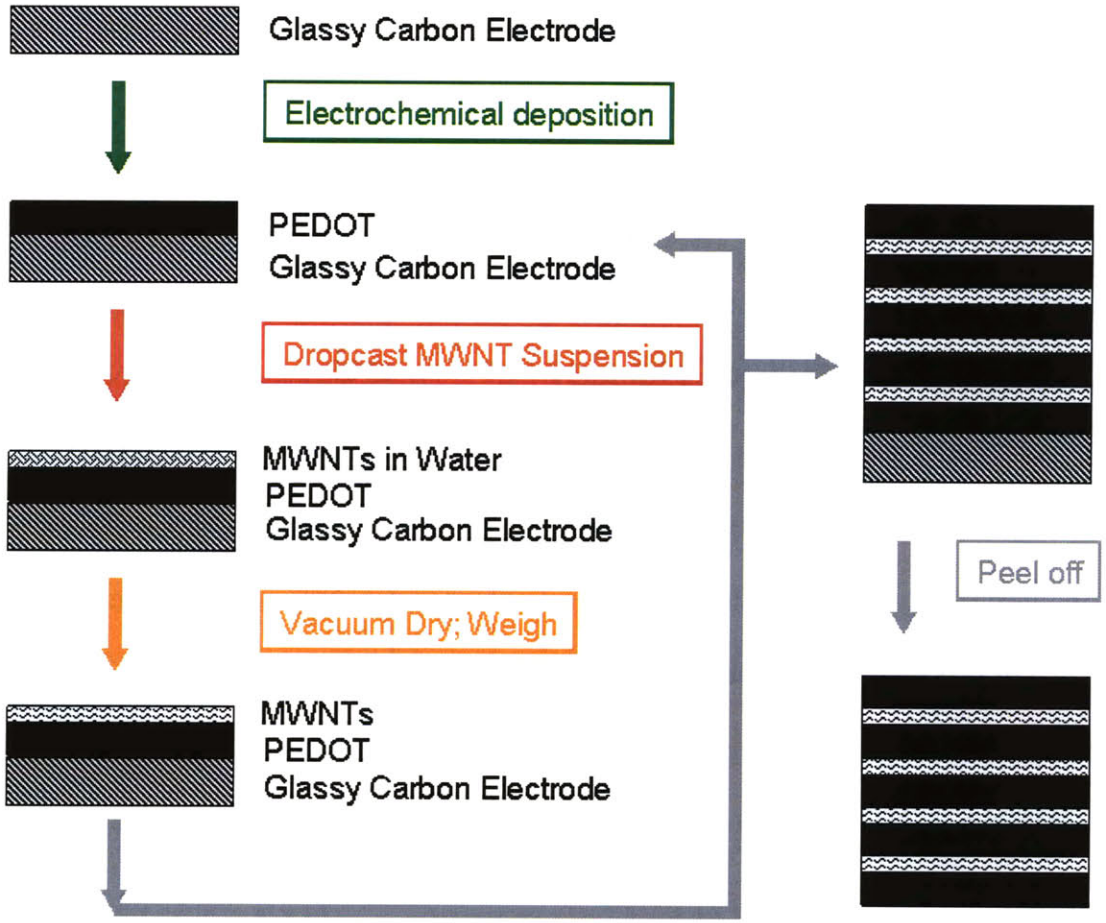

(b)

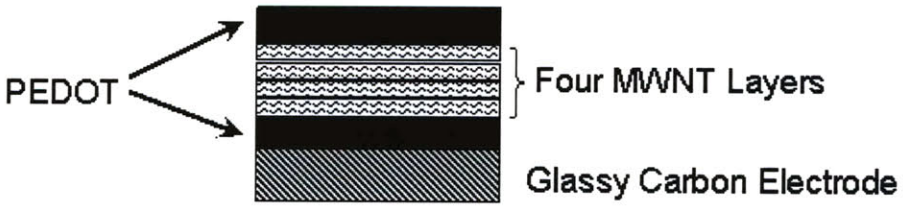

Figure 4-5. (a) The procedure for fabricating layer-by-layer PEDOT-sCNT composite films included electrochemical deposition of PEDOT layers and drop-casting sCNT water suspension. (b) The sCNT "control" film consisted four sCNT layers (80%) supported by two PEDOT layers.

For comparison, PPy-sCNT composites were also fabricated in multilayer structures. Because nine-layer PEDOT-sCNT composites were brittle and had separated layers when the sCNT content was higher than 20%, Dr. Shaikh fabricated the PPy-sCNT composites with only three layers of PPy sandwiching two layers of sCNTs, forming total five layers. The deposition setup for PPy layers were the same as the setup used for PEDOT layers, except the monomer added was 20 mL of distilled pyrrole. The drop-casting and weighing steps for PEDOT-sCNTs were repeated here. The PPy-sCNT composites were made for approximately 11%, 33%, 42%, and 60% of sCNTs by weight.

SEM was used to check the presence of sCNTs and how they orient in the composites. Figure 4-6(a) shows that the polypyrrole control film had distinct and connected layers with salt residues in between, appearing white in the SEM image. Figure 4-6(b-e) shows that composites with 30% and 60% sCNTs had cavities between polypyrrole layers. The cavities could be caused by the salt residues and/or sCNT clusters from the sCNT suspension, and these cavities could break the connections between polypyrrole layers.

The SEM images on cross sections of the composites could not clearly show the presence of the sCNTs because they were covered or mixed with salt crystals from the suspension. Therefore, SEM images from the sample surfaces were also taken. Figure 4-6(a) and (b) compared the surface facing the glassy carbon electrode, showing that the composite had sCNTs penetrating through while the control surface had no sCNTs. Figure 4-6(c) was the solution-side surface of a polypyrrole-CNT surface, showing no penetrating sCNTs. The electrode-side surface had scattered sCNTs penetrated through but the solution-side surface did not, because the negatively charged sCNTs were

attracted towards the glassy carbon electrode when positive voltage was applied to deposit the next polypyrrole layers. Similarly, scattered sCNTs and sCNT clusters were also seen on the electrode-side surface of the PEDOT-sCNT composite (Figure 4-8).

5-Layer PPy Control

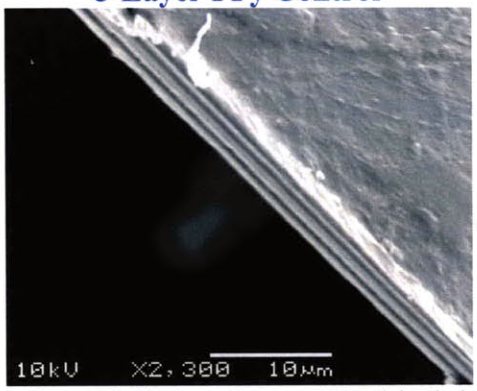

(a) The 5-layer PPy control showed distinct layers. The black layers were polypyrrole and the white layers were salt residues.

5-Layer PPy-sCNTs Composite – 30% sCNTs

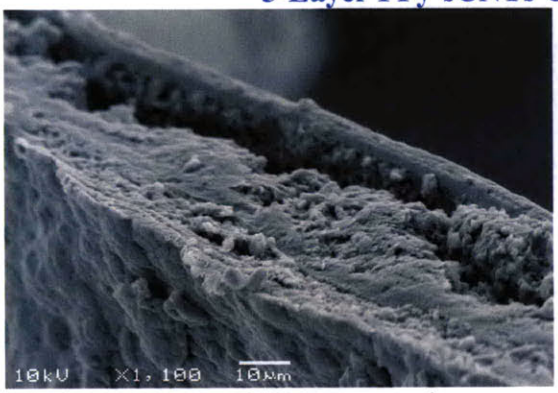

(b) The 30% PPy-sCNTs composite showed cavity in the structure.

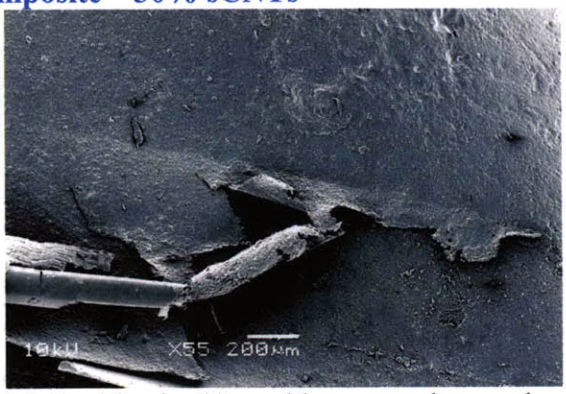

(c) Cavities in (b) could cause polypyrrole layers to separate.

5-Layer PPy-sCNTs Composite – 60% sCNTs

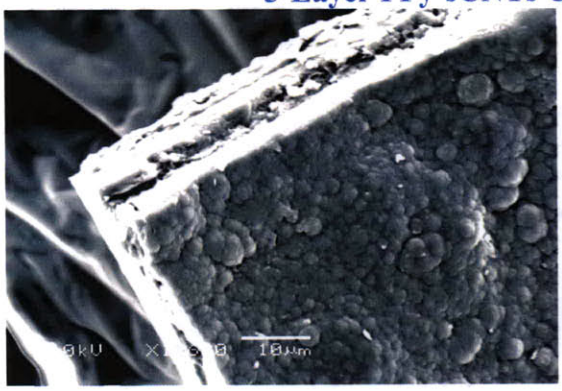

(d) The 60% sCNTs composite showed very thick sCNT layers between polypyrrole layers. The sCNT layers might also consist salt residues.

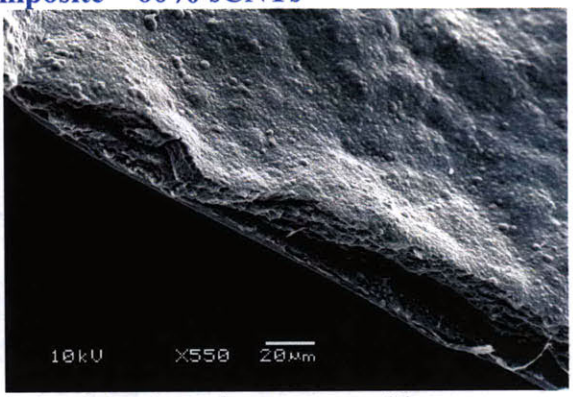

(e) Thick sCNT layers created large cavities between polypyrrole layers and bumpy surface structure.

Figure 4-6. Cross-sectional SEM images of (a) 5-layer polypyrrole control, (b-c) PPy-sCNTs composites with 30% and (d-e) 60% CNTs. The sCNTs layers created cavities in the composite, impeding ion movements during actuation.

(a)
The electrode-side surface of the 5-layer control.

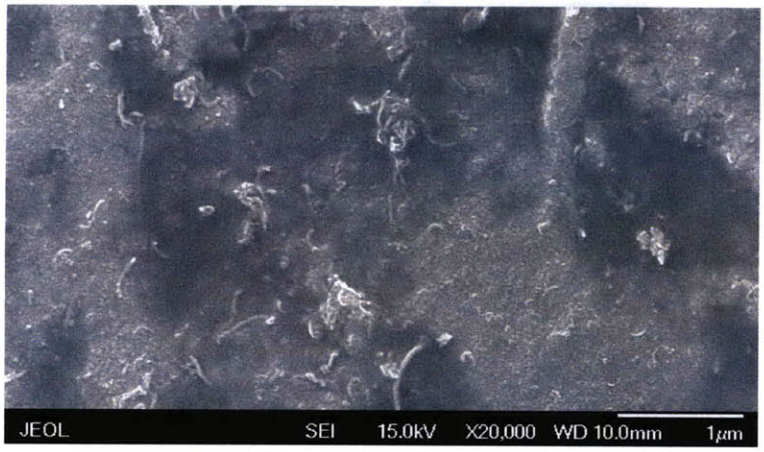

(b)
The electrode-side surface of a PPy-sCNT composite showed that the sCNTs penetrated through the polypyrrole layers in contact with the glassy carbon.

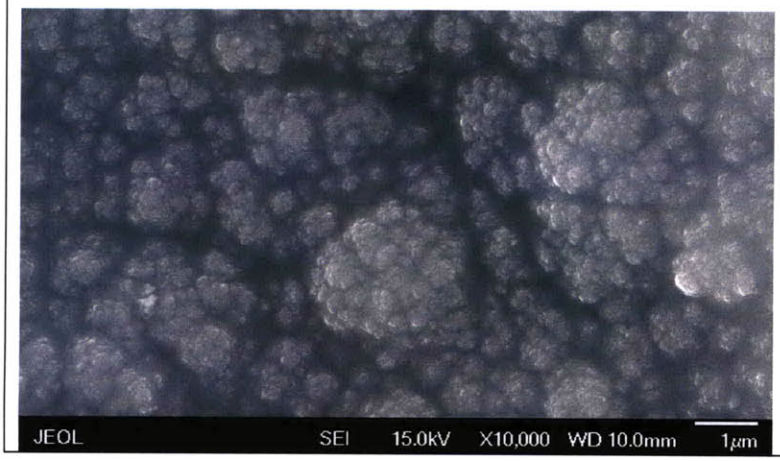

(c)
The solution-side surface of a PPy-sCNT composite showed no presence of sCNTs.

Figure 4-7. Surface SEM images showed that the side facing the electrode had sCNTs penetrating through but the side facing solution did not show any presence of sCNTs. (Images provided by Dr. Shaikh)

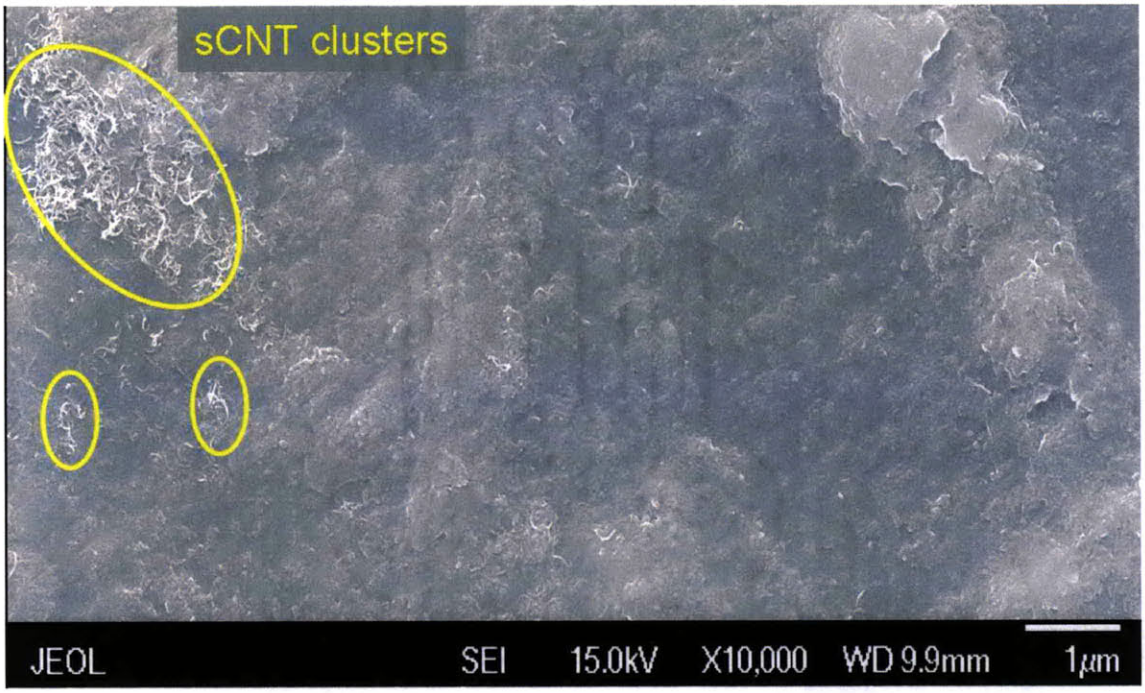

Figure 4-8. Electrode-side surface of a PEDOT-sCNT composite had sCNT clusters and scattered sCNTs penetrating through. (Image provided by Dr. Shaikh)

4.3 Properties of the sCNT Drop-casted Composites

4.3.1 Thickness, Conductivity, and Stiffness Results

The PEDOT-sCNT and PPy-sCNT composites with different quantities of sCNTs were compared in thickness, conductivity, stiffness, active stress, active strain, and creep rate. The thickness was measured using a micrometer (Mitutoyo IP-54 Absolute) and the conductivity was calculated using resistance from four-point probe resistivity measurements (Agilent 34411A Digit Multimeter). The stiffness was obtained by applying the samples with 1 Hz sinusoidal strain of 1% with preload of 1 MPa on the EDMA. Table 4-1 and Table 4-2 list how thickness, conductivity, and stiffness changed with increasing amount of sCNTs in both composites. As the amount of sCNTs increased, the thickness also increased overall. In PEDOT-sCNT composites, from 0% to 10% the thickness increased by 13 μm but from 10% to 20% the increase was nearly 20 μm. In PPy-sCNT composites the thickness also increased with the amount of sCNTs, and the composite with 42% sCNTs had thickness of 84 μm, thicker than the 60% film. The nonlinear increases in thickness implied that salt crystal residues from the deposition solutions and/or the sCNT clusters formed from drop-casting might have been included in the thickness measurements (Figure 4-6).

As the amount of sCNTs increased, the conductivity decreased. In PEDOT-sCNT composites the conductivity decreased from 34,780 S/m in 0% to 6,185 S/m in 80% sCNTs, and in PPy-sCNT it decreased from 8,032 S/m in 11% to 5,504 S/m in 60% sCNTs (Table 4-1; Table 4-2). One of the reasons why the conductivity decreased could be that connection between layers existed cavities, possibility caused by sCNT clusters or

loose PEDOT-sCNT layer bonding (Figure 4-6). Another reason could be that the sCNTs used here were functionalized so the way they were processed caused them to be less conductive than pristine CNTs. However, if pristine CNTs were used in the multilayer films to improve conductivity of the composites, the CNTs would not disperse in water to form a stable suspension and thus would not be ideal for drop-casting.

sCNT wt. (%) in PEDOT-sCNT	**Thickness (μm)**	**Conductivity (S/m)**
PEDOT-sCNT multilayer films (Figure 4-5a)		
0	17.5	34,780
10	30.5	25,655
20	50.0	14,925
sCNT "control" (Figure 4-5b)		
80	19	6,185

Table 4-1. As the amount of sCNTs increased in the PEDOT-sCNT composites, the thickness increased but the conductivity decreased.

sCNT wt. (%) in PPy-sCNT	**Thickness (μm)**	**Conductivity (S/m)**
11	20.7	8,032
30	40.0	7,597
42	84.0	1,757
60	46.3	5,504

Table 4-2. As the amount of sCNTs increased in the PPy-sCNT composites, the thickness increased but the conductivity decreased.

The conductivity of the PEDOT-sCNT composite was about three times higher than the conductivity of the PPy-sCNT composite with 10% sCNTs. Such a difference could be the result of different layer numbers in the two polymers. The PEDOT-sCNT composites had five PEDOT layers while the PPy-sCNT composites had only three PPy layers. The two extra polymer layers in PEDOT-sCNT films could make the composite more conductive.

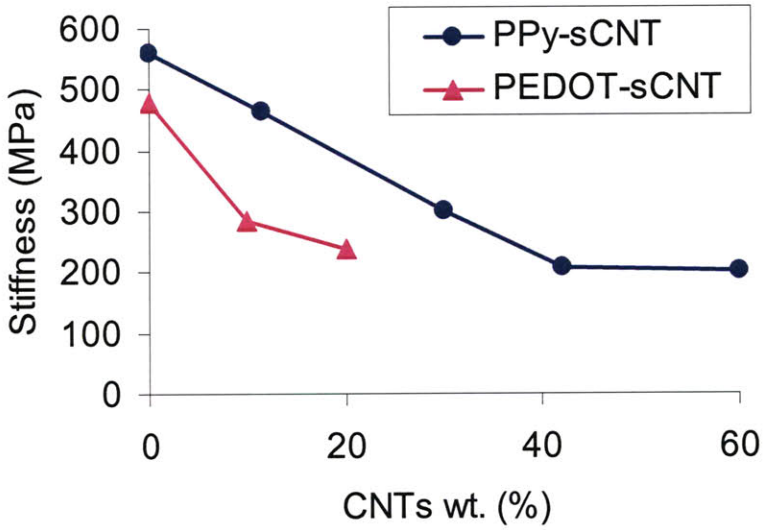

Figure 4-9. Stiffness of PPy-sCNTs composite decreased by half when the amount of sCNTs increased from 11% to 42%. Past 42%, the stiffness reached a plateau. The stiffness of PEDOT-sCNT composites also decreased with increasing amount of sCNT, but their stiffness was lower than PPy-sCNT composites.

The stiffness also decreased as more sCNTs were drop-casted in the composites (Figure 4-9). The sCNTs were stiffer than the polymers, causing individual polymer layers in the composites to become stiffer when sCNTs were added. However, the sCNTs

did not serve as good adhesive medium to connect the polymer layers well. At some parts of the film, especially where the salt crystals and/or sCNT clusters formed, the connection became so poor that polymer layers separated to cause decrease in the stiffness.

The PPy-sCNT composites were stiffer although they had two layers less than the PEDOT-sCNT composites (Figure 4-9). Besides the nature of the polymers, this could be because that distilled pyrrole but undistilled EDOT monomers were used for polymer layer depositions.

4.3.2 Actuation Results

Isotonic tests were done in BMIM-PF_6 with square pulses from -0.8 V to +0.8 V at 0.05 Hz for ten minutes (total 30 cycles). Peak strain was obtained by averaging the strain of the last 25 cycles. Creep rate was characterized by the slope of a straight line that fit the mean strain of each cycle after 150^{th} second. In Figure 4-10, the original strain was in grey and the strain at each voltage flip was in red. For each cycle the medium strain was found (in green) and the slope of the linear fit line in blue defined the creep rate.

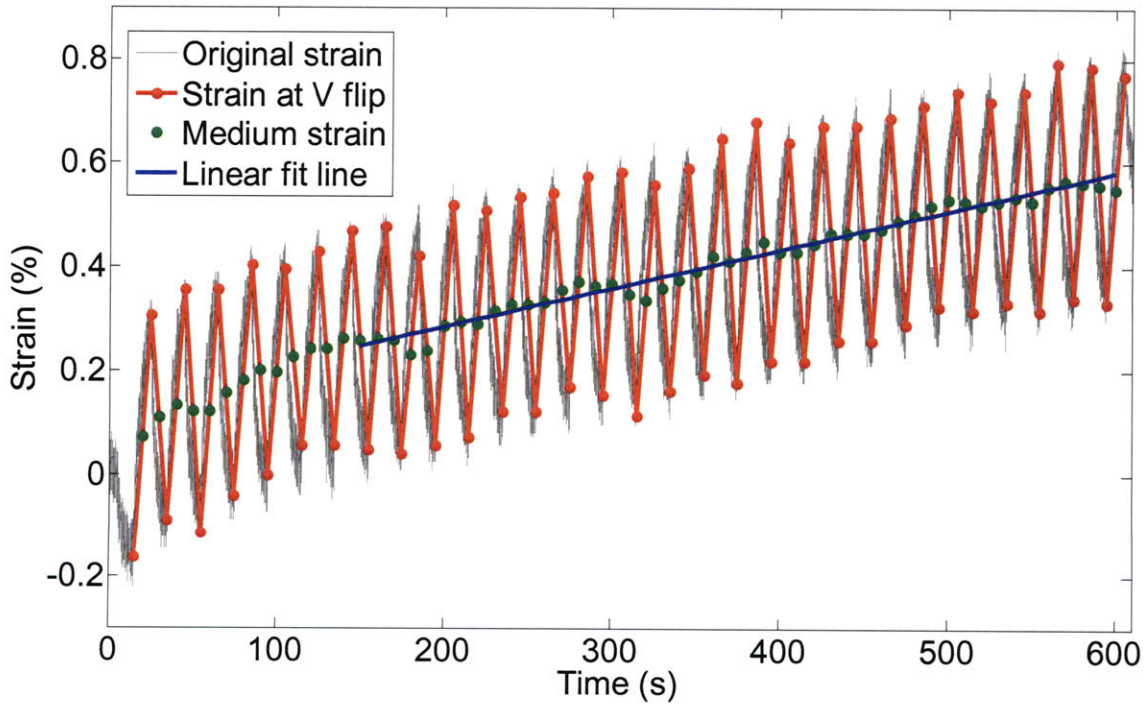

Figure 4-10. The blue straight line fit the medium strain (in green) of the strain when the voltage flipped (in red). The grey curve was the original strain. The slope of the blue line defines the creep rate.

(i.) Actuation results: nine-layer PEDOT-sCNT composites

The 80% sCNT "control" film was too brittle to be tested. Isotonic tests showed that increasing the amount of sCNTs decreased the creep rate. Figure 4-11 shows that the PEDOT control film had higher creep rate than the 10% CNT film, which had higher creep rate than the 20% CNT film. The reversible actuation in the 20% PEDOT-sCNT composite was accompanied by a reversible charge movement. This composite had more reversible charge movement than the PEDOT control, meaning that the same amount of charge diffused into the polymer bulk as the amount that moved out (Figure 4-12). Therefore, the green curve in Figure 4-12 shows that the overall trend in charge stayed flat. In contrast, in PEDOT control the overall trend in charge (in blue) decreased with time, implying that some cation remained in the polymer bulk when the voltage flipped from negative to positive.

In Figure 4-11, the 20% PEDOT-sCNT composite had significantly smaller strain than the PEDOT control. The average strain to charge ratio was 8.2×10^{-9} %·m^3/C in PEDOT control, 7.5×10^{-9} %·m^3/C in 10% sCNT composite, and 5.4×10^{-9} %·m^3/C in 20% sCNT composite. Like reduction in creep rate, the reduction in strain with increasing amount of sCNTs could also be associated with charge transfer. In Figure 4-12, the 20% sCNT composite also had smaller charge per volume than PEDOT control. The average charge per polymer volume was 52.2 MC/m^3 in PEDOT control and decreased to 28.0 MC/m^3 in the 20% PEDOT-sCNT composite.

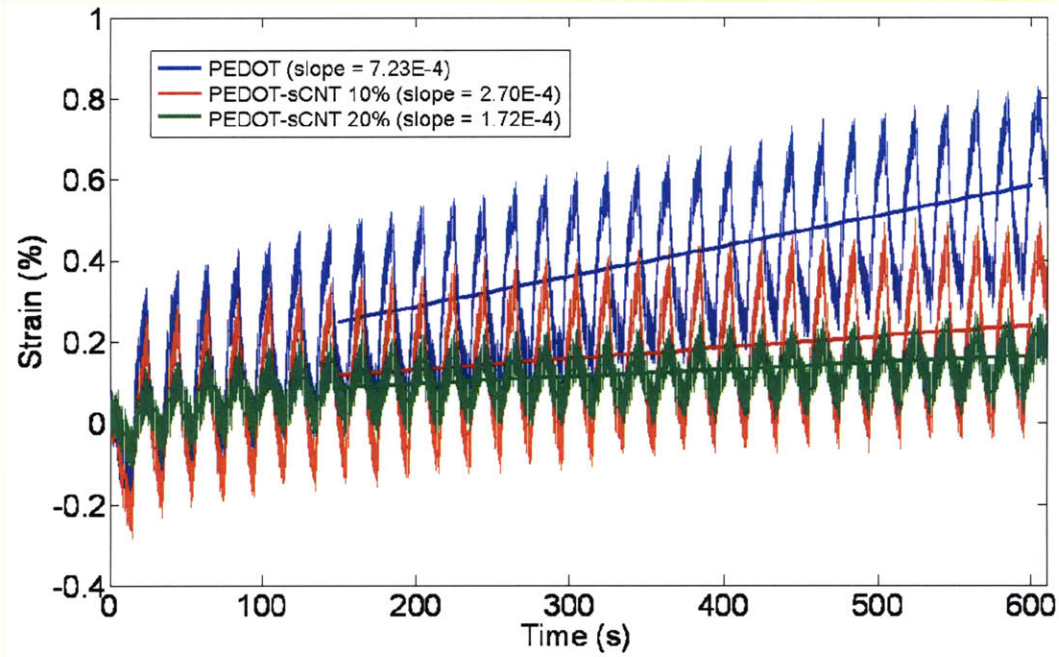

Figure 4-11. Increasing the amount of sCNTs reduced the creep and strain of the PEDOT composite. The 20% sCNT composite had no creep while the PEDOT control crept more than the 10% and the 20% sCNT composites. The straight lines defined the creep rate (Figure 4-10).

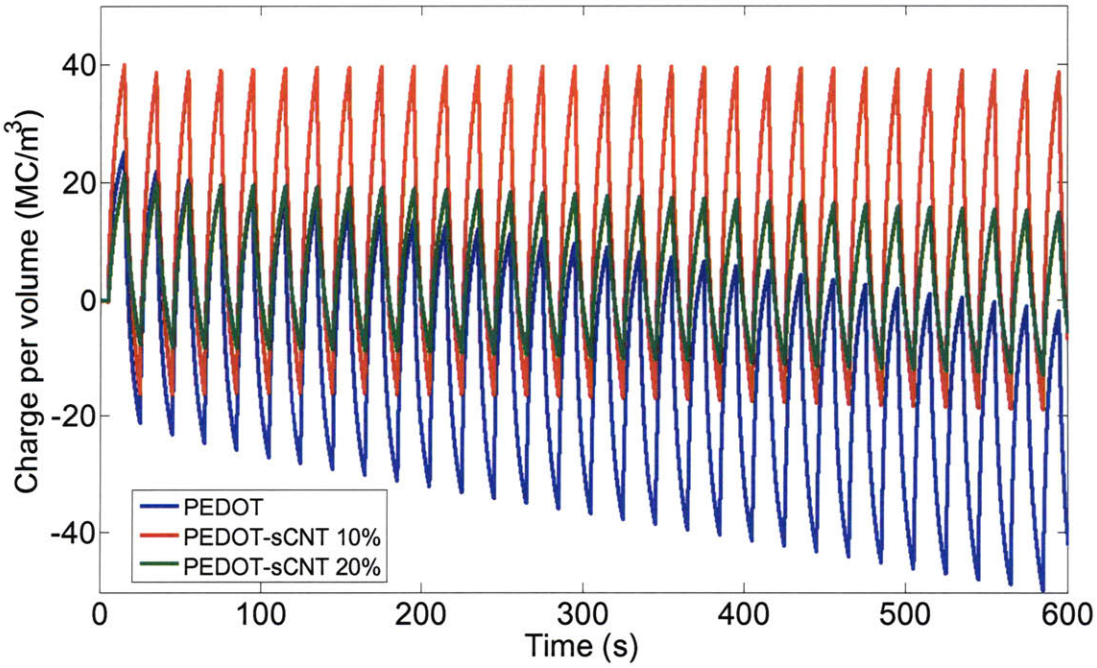

Figure 4-12. Increasing the amount of CNTs reduced charge transfer of the PEDOT composite but the charge movement was more reversibe. The 20% sCNT composite had much more reversible charge movement than the PEDOT.

The results suggested that the reduction in creep rate and active strain in the PEDOT-sCNT composite was associated with the charge transfer reversibility and the amount of ions diffused, respectively. It is unclear why exactly this phenomenon occurred. One possible explanation is that the reduction in charge transfer was the result of the sCNTs constraining the polymer that could be actuated freely, because the sCNTs were stiffer than the polymer. The polymer can be viewed as a network of springs. As the sCNTs were included, some of the springs got "replaced" by stiffer ones, leading to less strain and more reversibility. Figure 4-13 shows how the PEDOT control evenly actuated but the composite only actuated at the areas with no sCNT. As the actuatable area was less in the composite than in control, the charge transfer would also be less. Similarly, since the charge transfer was limited in the composite, the charge residues in the material that caused creep played negligible role.

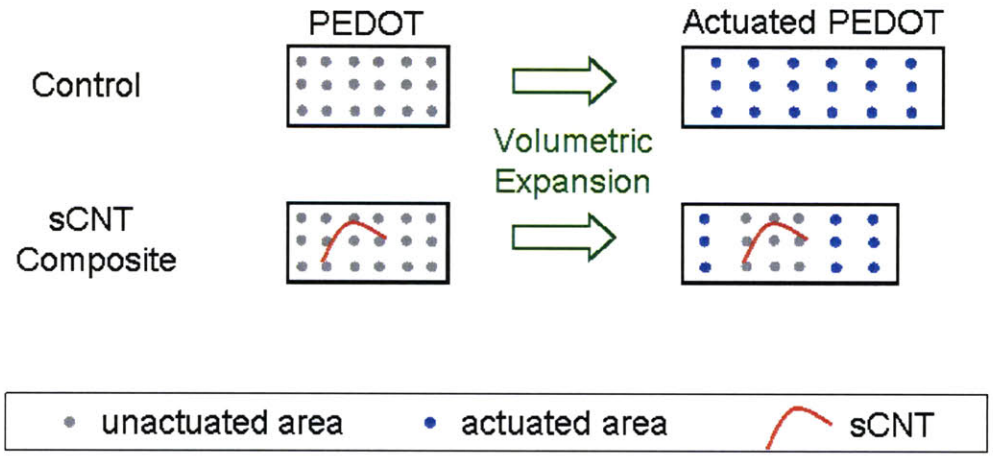

Figure 4-13. The illustration shows a speculated mechanism on how the sCNT impeded the composite from actuating freely. The PEDOT control could expand evenly while ions diffused into the polymer, but the composite could only actuate at the areas where the sCNTs were absent. The dots are used for position reference. Grey dots represent unactuated area, the blue dots represent actuated area, and the red curve represents a sCNT.

(ii.) Actuation results: Five-layer PPy-sCNT composites

Actuation results showed that as the sCNT content increased from 11% to 42%, the active stress at 1 MPa preload decreased from 0.58 to 0.27 MPa and the active strain at the same preload decreased from 0.24% to 0.16%. Past 42% the peak stress and strain reached a plateau (Figure 4-9; Figure 4-14). Although active stress and strain showed a decreasing trend with increasing amount of sCNTs, the magnitudes were low for polypyrrole due to use of degraded BMIM-PF_6 for actuation.

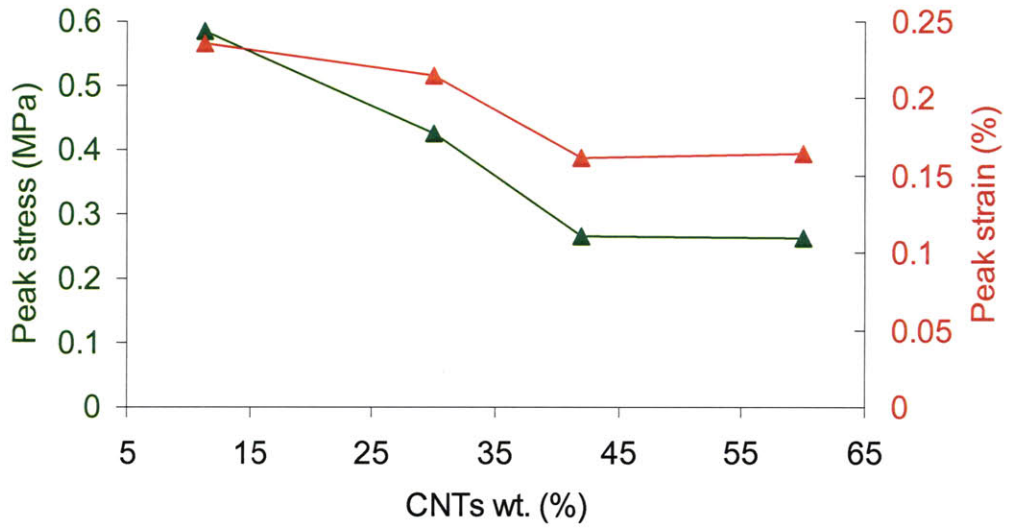

Figure 4-14. Peak stress (in green) and peak strain (in red) of polypyrrole/CNTs composite decreased when the amount of CNTs increased from 11% to 42%. Past 42%, both reached a plateau.

The active stress and strain decreased also for the same speculated mechanism as for PEDOT composites – for higher sCNT contents, less polymer area could be freely actuated. The plateaus past 42% sCNTs implied other ways the sCNTs might affect actuation. With very low amount of sCNTs, ions could diffuse through multiple layers, causing all or most polypyrrole layers to actuate. As the amount of drop-casted sCNTs

increased in the composite, the sCNTs started to impede the ions moving through inner polypyrrole layers, causing the active stress and strain to decrease. Past 42% sCNTs the stress and strain did not decrease further possibly because 42% of sCNTs completely blocked all the inner polypyrrole layers and only the most outer polypyrrole layer was actuated.

Similar to the actuation results in PEDOT-sCNT composites, the creep rate in the PPy-sCNT composite decreased as more sCNTs were drop-casted. The 11% composite crept the most (slope = 8.32E-5) and the 60% composite crept the least (slope = 3.26E-5) among the four different groups; the creep rate of the 33% and the 42% composites lied in between (slope = 3.95E-5 and 5.63E-5 respectively). The creep rate did not seem to reduce significantly with sCNT content past 33-42%. The reasoning that explained the possible mechanism in PEDOT-sCNT composites could be applied here. When the amount of sCNTs was increased, less PPy area was free to actuate and therefore the creep rate decreased (Figure 1-6). Past the "optimal" sCNT content of 33-42%, the polymer would not have "free" actuatable areas that could collectively cause creep.

4.3.3 Conclusions

The drop-casted multilayer technique successfully fabricated conducting polymer-sCNT composites. However, as shown in the SEM images it created an uneven thickness across the film due to the cavities and large particles formed in between layers. As a result, for example, the samples harvested for actuation tests from the 60% sCNT film might have more or less than 60% of sCNTs. This discrepancy could create experimental errors, especially in the multilayer groups that had large amount of sCNTs. For

application purpose, composites with inconsistent thickness or separated layers could limit the performance of the actuators.

The fact that the composite crept less and had more reversible charge movements than the control made the composite a more stable actuator material than pristine polymer. However, this advantage was accompanied with a decrease in active strain. The sCNTs layers not only impeded ionic movements within areas of the film, but also created cavities in the multilayer structure. These cavities could make brittle films that had bumpy surface or separated layers, which also limited the ionic movement from one polymer layer to the next. Combing the negative effects created by the sCNTs, having high sCNT content in the composite was not ideal to fabricate robust and powerful actuator materials. Based on the results, the "optimal" sCNT content was in the range of 33-42%.

4.4 Post-Deposition Actuation Improvements

In all the composite fabrication techniques described above, the multilayer structure by drop casting successfully demonstrated that the sCNTs reduced creep rate. However, the composite had lower active stress and strain than the controls. Following the mechanism illustrated in Figure 4-13, the stress or strain magnitude could be increased if the free polymer volume (represented in blue dots) could be increased, without changing the material composition. Two possible ways were proposed to achieve this – one way was to increase the preload applied to the polymer for actuation, and the other way was to permanently stretch the composite after fabrication. Both methods intended to expand "free" polymer volume to allow more ionic movements, which lead to higher stress (or strain).

4.4.1 Actuation at Increasing Preloads

The five-layer PPy-sCNTs composites were actuated isometrically at preloads 1, 1.5, 3, 5, 7, and 10 MPa to investigate how stress changed with increasing preloads. The actuation setup was the same as in Section 4.2.4.

The results showed that the peak stress exponentially increased with preload, verifying that stretching the composite for higher preload expanded the "free" polymer area to allow more ionic movements (Figure 4-13). As more ions diffused through the polymer, the peak stress was also increased. The increase in peak stress was most effective at preloads from 1 to 3 MPa because stretching the composite at stresses higher than this range might have caused necking in the polymer.

At preloads from 1 MPa to 10 MPa, the peak stress increased by 444% in the composite with 11% CNTs, but the increase was only 133% in the composite with 60% CNTs (Figure 4-15). This phenomenon could be explained again by the mechanism illustrated in Figure 4-13. The 11% composite had more "free" polymer spaces to actuate than the 60% composite. As the preload increased, these "free" polymer spaces expanded and allowed more ion diffusion than the 60% film.

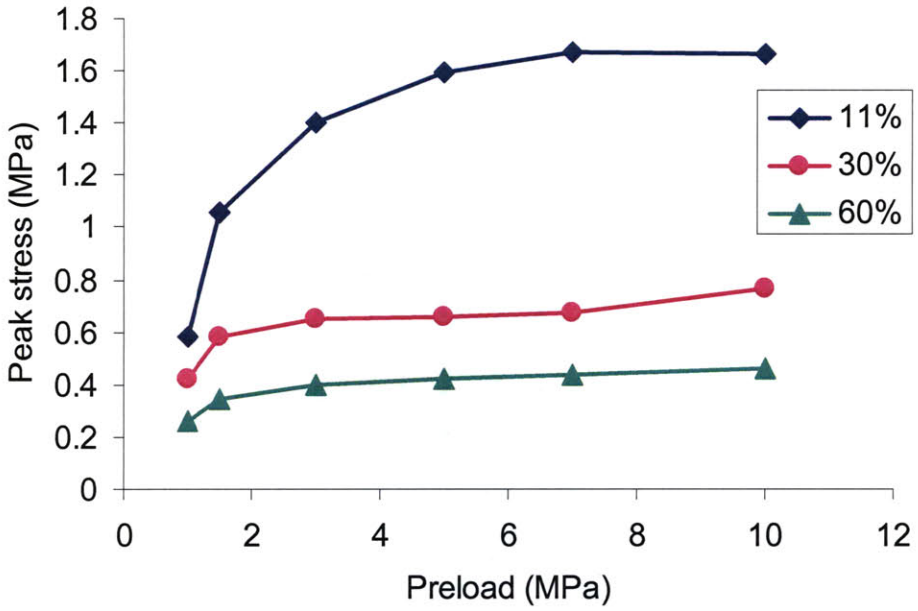

Figure 4-15. The peak stress in five-layer polypyrrole-CNTs composite increased with increasing preload. In the composite with 11% CNTs the peak stress increased much more with preload than in the 60% composite.

4.4.2 Stretched PPy-sCNT Composite

Pytel et al. demonstrated that the linear active strain of polypyrrole could be controlled by stretching that caused chain orientation [23]. The PPy-sCNT composite used for this study was made by drop-casting one droplet of 1 mg/ml sCNT dichloromethane suspension onto the surface of a free-standing polypyrrole film. The

suspension was air-dried so the sCNTs could adhere to the polypyrrole surface. The composite was then clamped in between the two rollers of a Durston Rolling Mills and stretched manually by about 10%. The rollers were turned on to compress the composite (Figure 4-16). Unstretched and stretched PPy-sCNT composites were actuated isotonically, and SEM images were taken to show how stretching affected the surface features of the films.

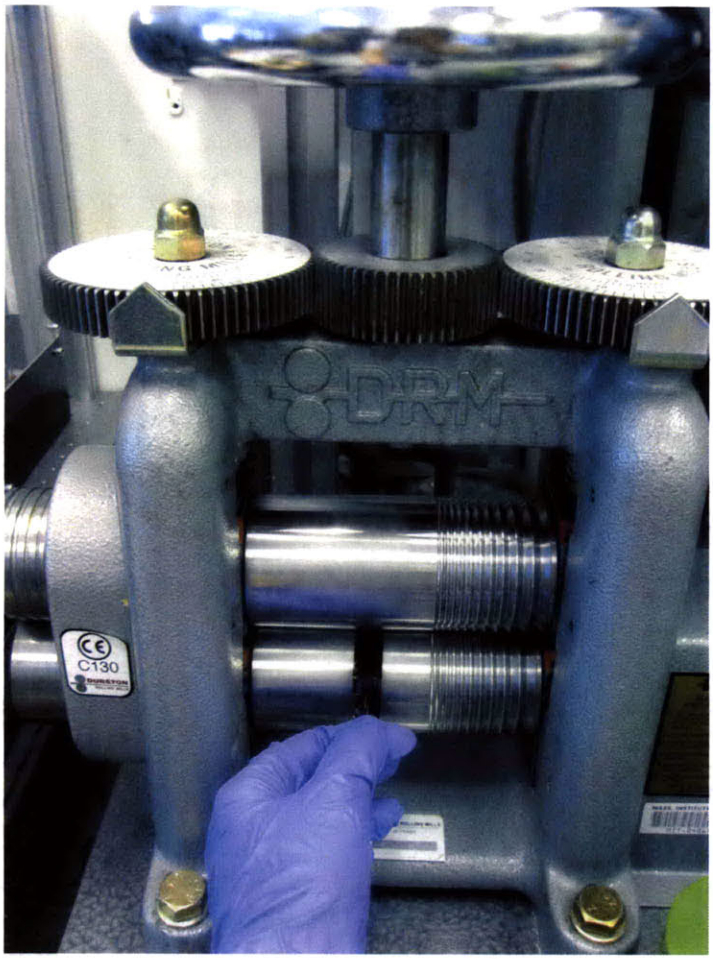

Figure 4-16. The PPy-sCNT composite was manually stretched by approximately 10% and then rolled on a Durston Rolling Mill.

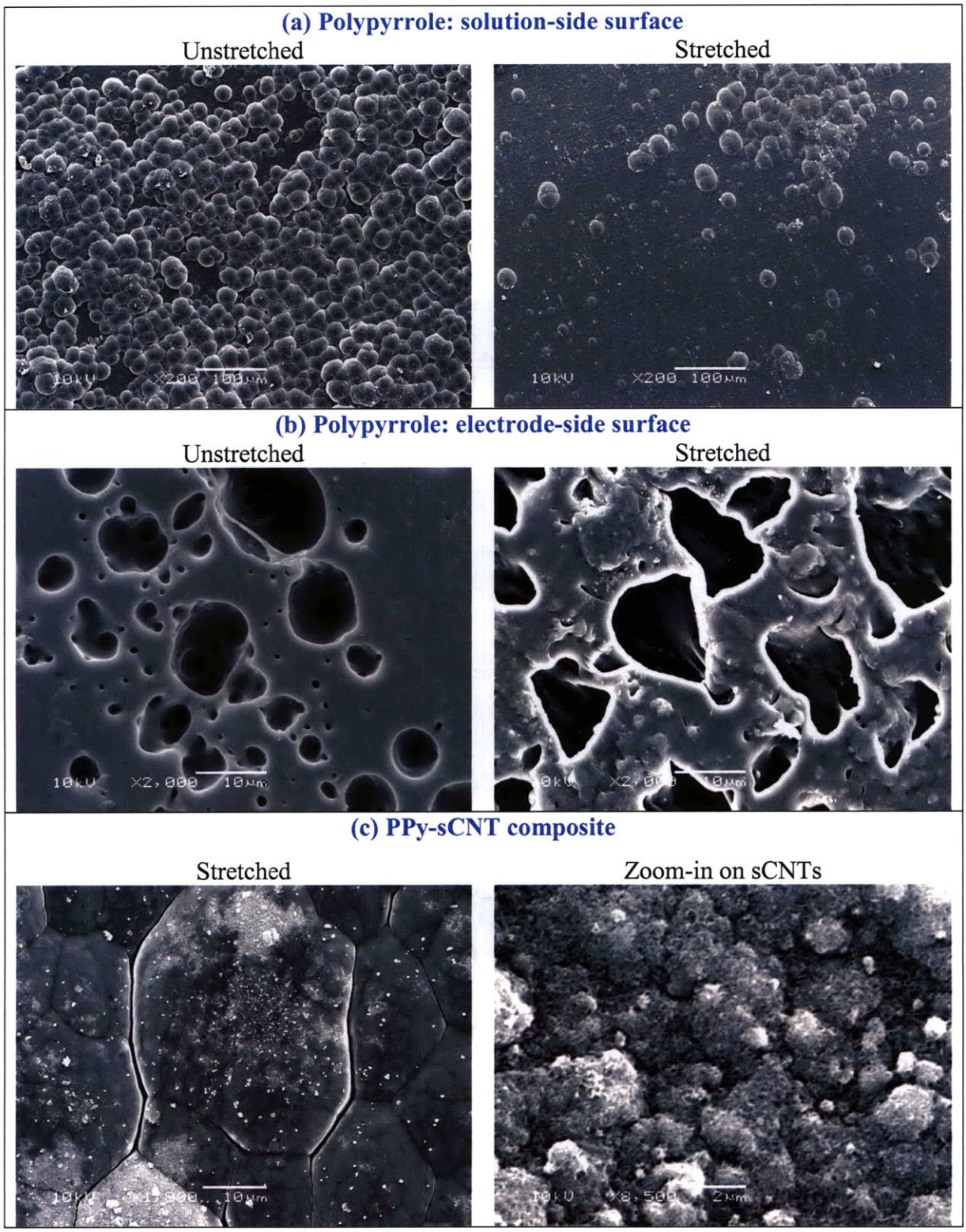

Figure 4-17. SEM images showed that stretching changed the surface features on both the (a) solution- and (b) electrode-side surfaces of polypyrrole. (c) shows that stretching elongated the "bubble" features of the solution-side surface and the sCNTs clusters (appear white) scattered across the film.

SEM images in Figure 4-17(a) showed that stretching reduced the bumpy features and created stretch marks on the solution-side of polypyrrole surface. On the electrode-side, stretching caused the circular holes to elongate in the direction of stretch (Figure 4-17b). And the stretched PPy-sCNT composite in (c) also showed elongated features, with sCNT clusters scattered across the film. The changes in surface features suggested that stretching caused permanent deformation in the films. If the sCNTs were less dense on the polymer surface, stretching may cause the sCNTs to align in the direction of stretch.

	Conductivity (S/m)	**Stiffness (MPa)**	**Creep Rate (%/s)**	**Strain (%)**	**Max Strain Rate (%/s)**
Unstretched PPy-sCNT	25,806	230	8×10^{-4}	1.01	0.15
Stretched PPy-sCNT	32,841	368	3×10^{-4}	0.45	0.08

Table 4-3. List of results showed how unstretched PPy-sCNT composite compared to the stretched PPy-sCNT composite in conductivity, stiffness, creep rate, strain, and maximum strain rate parallel to the stretch axis.

Table 4-3 shows how unstretched PPy-sCNT compared to the stretched PPy-sCNT composite in conductivity, stiffness, creep rate, strain, and maximum strain rate parallel to the stretch axis. The conductivity increased by 27% and the stiffness increased by 56% after rolling. Besides these two improvements, rolling reduced the creep rate by more than half. However, the tradeoffs from rolling include decreases in strain and maximum strain rate. These deteriorations in actuation performance occurred possibly

because stretching caused necking in the composite, leading the material to become stiffer. As a result, the stretched composite could not go as much volumetric expansion as the unstretched composite while voltages were applied. Pytel et al. reported that a film stretched 96% improved in conductivity parallel to stretch and improved in active strain perpendicular to stretch axis [23]. This study confirmed improvement in conductivity in the direction parallel to stretch, and further research can analyze the composite in the direction perpendicular to stretch to achieve both reducing creep and increasing active strain in polypyrrole. Further research can also attempt analyses 45^{o} to the stretch axis to investigate if both conductivity and active strain can be improved after stretching.

4.5 Conclusions and Future Work

The stable sCNT suspension allowed more consistent and repeatable composite fabrication that required hours of processing time. Most attempted fabrication techniques – including (1) direct deposition of sCNT with conducting polymer, (2) soaking or sonicating polymer in sCNTs suspension, (3) electrostatic attachment of sCNTs on polypyrrole – could not successfully demonstrate how the sCNTs affected conducting polymer properties. The drop-casted multilayer structure was able to show that the sCNTs could make the polymer a better actuator material by reducing creep rate. However, the stress and strain magnitudes were reduced due to limited "free" polymer spaces that were not constrained by the sCNTs. Although these magnitudes could be improved by stretching the composite, stress higher than 3 MPa should be avoided to prevent the material from necking. High preload was most effective to give high stress magnitudes in composite with around 11 to 20% CNTs, which was also an ideal amount to reduce creep rate and form adhesive layers. Stretching that caused permanent deformations improved the composite's conductivity, stiffness and creep rate. However, it also created necking to impede polymer actuation.

The studies presented here did not attempt to align the sCNTs in the composites. Most polymer-CNTs composites have aligned CNTs so that they could be easily modeled, in our case, as laminated structure [22]. Future work can align the sCNTs in different directions to investigate how they affect the composite comparing to composites with randomly aligned CNTs. Possibly aligning the CNTs can also resolve the thickness inconsistency problem caused by drop-casting.

CHAPTER 5

Summary

Performance of conducting polymer actuators can be affected by various factors. This thesis demonstrates that actuation driven by large ions resulted in higher active stress than by small ions. The active stress (or strain) was further increased by increasing the temperature, which speeded up the ionic movement and caused thermal expansion to allow more charge uptake in the polymer bulk. While the active stress and strain were increased with temperature, creep rate reduction was also achieved by addition of sCNTs to improve the properties of conducting polymer actuators. The sCNTs, stiffer than the polymer, constrained the composites from going as much volumetric expansion as a control polymer did. This tradeoff was compensated by applying a high preload (up to 3 MPa) during actuation so more polymer space was available for charge uptake. Although the sCNTs reduced creep rate, having sCNT content more than 30% by weight in the composite resulted in brittle films or separated layers in multilayer structures.

This thesis shows that various properties of conducting polymers could be improved by heating, post-deposition processing, addition of sCNTs, and stretching. However, potential applications of the polymer actuators require the performances to be repeatable over a long period of time. Future studies can conduct longevity tests to investigate the effects of the same factors. For example, although the active strain of polypyrrole at 83°C was shown to be four times higher than at room temperature, the polymer might have been degraded by the high temperature and would show a train decrease if the actuation lasted for hours.

References

[1] T.F. Otero, H. Grande, T. A. Skotheim, R. L. Elsenbaumer, J. R. Reynolds, and M. Dekker. In Electrochemical Devices: Artificial Muscle Based on Conducting Polymers, volume 2, pages 1015-1017. Marcel Dekker, New York, 1998.

[2] I. Hunter, S. Lafontaine. "A Comparison of Muscle with Artificial Actuators". *Tech. Dig. IEEE Solid State Sensors Acutators Workshop,* pages 178-185, 1992.

[3] J. D. W. Madden, N. A. Vandesteeg, P. A. Anquetil, P. G. A. Madden, A. Tak-shi, R. Z. Pytel, S. R. Lafontaine, P. A. Wieringa, and I. W. Hunter. "Artificial Muscle Technology: Physical Principles and Naval Prospects". *IEEE Journal of Oceanic Engineering*, 29(3):706-728, 2004.

[4] P. Anquetil. Large Contraction Conducting Polymer Molecular Actuators. PhD thesis, Massachusetts Institute of Technology, 2004.

[5] L. Bay, K. West, P. Sommer-Larsen, S. Skaarup, and M. Benslimane. "A Conducting Polymer Artificial Muscle with 12% Linear Strain". *Advanced Materials*, 15(4):310–313, February 2003.

[6] S. Hara, T. Zama, W. Takashima, and K. Kaneto. "Tfsi-doped polypyrrole actuator with 26% strain". *Journal of Materials Chemistry*, volume 14, pages 1516–1517, 2004.

[7] J. Madden, I. W. Hunter, and R. J. Gilbert. "Development of an Artificial Muscle Fiber Composed of the Conducting Polymer Actuator Polypyrrole". *Gastroenterology*, 122(4):A164–A164, 2002.

[8] C. M. Li, C. Q. Sun, W. Chen, and L. Pan. "Electrochemical thin film deposition of polypyrrole on different substrates". *Surface and Coating Technology*, 198(1-3): 474-477, 2005.

[9] N. Vandesteeg. *Synthesis and Characterization of Conducting Polymer Actuators*. Ph.D. thesis defense slides. Massachusetts Institute of Technology, Cambridge, MA, 2006.

[10] J. D.W. Madden. *Conducting Polymer Actuators*. Ph.D. Thesis, Massachusetts Institute of Technology, Cambridge, MA, 2000.

[11] A. Chen. *Large Displacement Fast Conducting Polymer Actuators*. M.S. Thesis, Massachusetts Institute of Technology, Cambridge, MA, 2006.

[12] R. Z. Pytel. *Artificial Muscle Morphology*. Ph.D. Thesis, Massachusetts Institute of Technology, Cambridge, MA, 2007.

[13] Perkin Elmer Dynamic Mechanical Analyzer DMA 7 Method Guide.

[14] B T Kulakowski. Dynamic Modeling and Control of Engineering Systems. Cambridge Press, 2007.

[15] R. Pytel, E. L. Thomas, and I. W. Hunter. "In situ observation of dynamic elastic modulus in polypyrrole actuators". Polymer, Volume 49, 2008-2013, 2008.

[16] N. Vandesteeg. Synthesis and Characterization of Conducting Polymer Actuators. Ph.D. thesis defense slides. Massachusetts Institute of Technology, Cambridge, MA, 2006.

[17] J. D.W. Madden, P. G.A. Madden, and I. W. Hunter. "Polypyrrole Actuators: Modeling and Performance". Smart Structures and Materials 2001: Electroactive Polymer Actuators and Devices Proc SPIE, Vol. 4329, 72; DOI:10.1117/12.432688, 2001.

[18] P. V. Pillai, and I. W. Hunter. "Stochastic System Identification of the Compliance of Conducting Polymers". Materials Research Society Symposium Proc. Vol. 1134, 2009.

[19] Y. Keng, P. V. Pillai and I. W. Hunter. "Characterizing the Effect of Temperature Increase on Polypyrrole Active Strength and Stress Rate." ASME Conference on Smart Materials, Adaptive Structure and Intelligent Systems, SMASIS2009-1258, 2009.

[20] M. Cole and J. Madden. "The Effect of Temperature Exposure on Polypyrrole Actuation". Materials Research Society Symposium Proc. 0889-W04-04, 2005.

[21] Y. Keng, P. V. Pillai and I. W. Hunter. "The Effect of Ion Delivery on Polypyrrole Strain and Strain Rate under Elevated Temperature". Materials Research Society Symposium Proc. 1222-DD02-10, 2009.

[22] P. J. F. Harris. Carbon Nanotube Composites. International Materials Reviews, 49(1): 31-43, 2009.

[23] R. Pytel, E. Thomas, and I. W. Hunter. "Anisotropy of Electroactive Strain in Highly Stretched Polypyrrole Actuators." 18(4): 861-863, 2006.

Appendix A.
Temperature controller source code in Visual Basic

```
Private Sub Start_Click(ByVal sender As System.Object, ByVal e As
System.EventArgs) Handles Start2.Click

    Control2.Start()

    Timer1.Enabled = True
    Start2.Enabled = False
       'TargetTemp.Enabled = False
    Pause2.Enabled = True
    Continue2.Enabled = True

    'With SaveTemp
    '.WriteLine("%" & Now)
    '.WriteLine("% Note: " & note.Text)
    '.WriteLine("% Kp = " & KpText.Text & "; Ki = " & KiText.Text & ";
     Kd = " & KdText.Text)
    '.WriteLine("% Desired Temperature = " & TargetTemp.Value & "C")
    '.WriteLine("")
    '.WriteLine("Temp=[")
    'End With
    'SaveVolt.WriteLine("Volt=[")

End Sub


Private Sub Pause_Click(ByVal sender As System.Object, ByVal e As
System.EventArgs) Handles Pause2.Click

    Control2.Suspend()
    Continue2.Enabled = True
    Timer1.Enabled = False
    Pause2.Enabled = False
    power.WriteString("OUTP OFF")


    'TargetTemp.Enabled = True
    'With SaveTemp
    '.WriteLine("];")
    '.WriteLine("[m1,m2]=size(Temp);")
    '.WriteLine("t=0:" & (Val(Hour.Text) * 3600 + Val(Minute.Text) *
     60 + Val(Second.Text)) & "/m1:" & (Val(Hour.Text) * 3600 +
     Val(Minute.Text) * 60 + Val(Second.Text)) & "-" & (Val(Hour.Text)
     * 3600 + Val(Minute.Text) * 60 + Val(Second.Text)) & "/m1;")
    '.WriteLine("figure;")
    '.WriteLine("plot(t,Temp)")
    '.WriteLine("title('" & note.Text & "')")
    '.WriteLine("xlabel('Time (Second)')")
    '.WriteLine("ylabel('Temperature (Celcius)')")
    '.WriteLine("")
```

```
        '.WriteLine("")
        '.WriteLine("")
        'End With
        'SaveVolt.WriteLine("];")

End Sub

Sub Control()

    Dim I As Integer
    Dim rdgs As Object

    ' Call power supply
    ioMgrP = New Ivi.Visa.Interop.ResourceManager
    power = New Ivi.Visa.Interop.FormattedIO488
    power.IO = ioMgrP.Open("GPIB0::5::INSTR")

    ' Call data acquisition box
    ioMgr = New Ivi.Visa.Interop.ResourceManager
    dataq = New Ivi.Visa.Interop.FormattedIO488
    dataq.IO = ioMgr.Open("GPIB0::2::INSTR")

    Dim TrigCount As Integer

    ' power on the instrument
    ' dataq.WriteString("*RST")

    ' Configure the instrument
    dataq.WriteString("CONF:TEMP RTD,85, (@102)")

    Et = 0
    E1 = 0
    ' T1 = 0

    Do
        With dataq
            ' Do 2 10-sec scans
            .WriteString("TRIGger:SOURCE TIMER")
            .WriteString("TRIGger:TIMer 5")
            .WriteString("TRIGger:COUNT 1")

            ' Trigger scan and retrieve readings
            .WriteString("INITiate")

            ' Show unit (default unit C)
            ' .WriteString("FORMat:READing:UNIT ON")
            ' Get the number of data counts (points because only one
              channel)
            .WriteString("TRIGger:COUNt?")
            TrigCount =
            .ReadNumber(Ivi.Visa.Interop.IEEEASCIIType.ASCIIType_I2,
            True)
        End With


        Do
            With dataq
```

```
        dataq.WriteString("DATA:POINTS?")
        I =
        .ReadNumber(Ivi.Visa.Interop.IEEEASCIIType.ASCIIType_I4,
        True)
    End With
Loop Until I = TrigCount


For I = 1 To TrigCount
    With dataq
        .WriteString("DATA:REMove? 1")
        rdgs =
      .ReadList(Ivi.Visa.Interop.IEEEASCIIType.ASCIIType_BSTR,
        ",")
        dataArray = rdgs(0)
        CurrentTemp1.Text = (dataArray)
        'SaveTemp.WriteLine(dataArray)
        CurrentTemp.Refresh()
    End With
Next I

' PID controller
With power
    E = TargetTemp1.Value - CurrentTemp1.Text

    ' Propportional control
    Ep = E
    Kp = txtKp.Text
    ' Volt = Kp * E

    ' Integral Control
    Et = Et + E
    Ki = txtKi.Text

    ' Derivative Control
    E2 = E
    ' de = E2 - E1
    de = Abs(E1 - E2)
    E1 = E2

   ' T2 = Hour.Text * 3600 + Minute.Text * 60 + Second.Text
    ' dt = T2 - T1
    ' T1 = T2
    ' Label10.Text = dt

    Ed = de ' / dt
    Kd = txtKd.Text

    Volt = Kp * Ep + Ki * Et + Kd * Ed

    Label12.Text = Volt

    If Volt >= 4.0 Then
        Volt = 4.0
    End If

    If Volt <= -25.0 Then
```

```
                Volt = -25.0
            End If

            .WriteString("OUTP ON")
            If Volt >= 0 Then
                .WriteString("INST:SEL P6V")
                ' .WriteString("APPL P6V, 4.0, 3.5")
            Else
                .WriteString("INST:SEL N25V")
            End If
             .WriteString("VOLTage:LEVel:IMMediate:AMPLitude " &
             CStr(Volt))

        End With

        'SaveVolt.WriteLine(Volt)
    Loop
End Sub


Private Sub Continue_Click(ByVal sender As System.Object, ByVal e As
System.EventArgs) Handles Continue2.Click

    Control2.Resume()

    Timer1.Enabled = True
    Pause2.Enabled = True
    'TargetTemp.Enabled = False
    'With SaveTemp
    '.WriteLine("%" & Now)
    '.WriteLine("% Note: " & note.Text)
    '.WriteLine("% Desired Temperature" & TargetTemp.Value &
      "Celcius")
    '.WriteLine("")
    '.WriteLine("Temp_" & TargetTemp.Value & "C=[")
    'End With
    Continue2.Enabled = False

End Sub


Private Sub Timer1_Tick(ByVal sender As System.Object, ByVal e As
System.EventArgs) Handles Timer1.Tick

   Second.Text = Val(Second.Text) + Val(1)

    If Second.Text = 60 Then
        Minute.Text = Val(Minute.Text) + Val(1)
        Second.Text = 0
    End If

    If Minute.Text = 60 Then
        Hour.Text = Val(Hour.Text) + Val(1)
        Minute.Text = 0
        Second.Text = 0
```

```
        End If
    End Sub


Private Sub ZeroTimer_Click(ByVal sender As System.Object, ByVal e As
System.EventArgs) Handles ZeroTimer.Click

        Hour.Text = "0"
        Minute.Text = "0"
        Second.Text = "0"

End Sub
```

Appendix B.
MATLAB Code

I. Stiffness calculation

```
%%% Take cycle 3-10; cut off the first two cycles
CN = 10;   % Total number of cycles
CNN = CN-2;
ti = (2*((length(RawData)-1)/SamplingFrequency)/CN);
% Find the starting time of the third cycle
tf = (length(RawData)-1)/SamplingFrequency;   % last time point
[min_difference_ti, array_position_ti] = min(abs(Time - ti));
% Find position of ti in "Time"
[min_difference_tf, array_position_tf] = min(abs(Time - tf));
% Find position of tf in "Time"
TimeN = [ti:1/SamplingFrequency:tf];
% Create a new time array "TimeN" starting with ti

%%%%% Time for the average of the last 10 cycles
TimeAF = (tf-ti)/CNN;   % Find the average time for each cycle
TimeAve = (0:1/SamplingFrequency:TimeAF);

%%%%% Average Stress for the last 8 cycles
StressN = Stress(array_position_ti:array_position_tf,:);
% StressN take stresss points corresponding to TimeN
[m,n]=size(StressN);
StressPt = m/CNN;
Scount1=0; Scount2=1; STotal = 0;
for n=1:CNN
    S = StressN(StressPt*Scount1+1:StressPt*Scount2);
    Scount1=Scount2; Scount2=Scount2+1;
    STotal = STotal + S;
end
SMean = STotal/CNN;
SMeanSet = SMean-SMean(1,1);   % Stress array for the average cycles
StressAmp = max(SMean)-min(SMean)

%%%%% Average Strain for the last 8 cycles
StrainN = Strain(array_position_ti:array_position_tf,:);
% StrainN take stresss points corresponding to TimeN
[mm,nn]=size(StrainN);
StrainPt = mm/CNN;
Stcount1=0; Stcount2=1; StTotal = 0;
for n=1:CNN
    St = StrainN(StrainPt*Stcount1+1:StrainPt*Stcount2);
    Stcount1=Stcount2; Stcount2=Stcount2+1;
    StTotal = StTotal + St;
end
StMean = StTotal/CNN;
StMeanSet = StMean-StMean(1,1);   % Stress array for the average cycles
StrainAmp = max(StMean)-min(StMean)

Stiffness2 = StressAmp/StrainAmp
```

II. Strain and strain rate calculation

```
%%Take cycle 6-30; cut off the first 5 cycles
Period = 20;    % 20seconds per cycle
NumberC = 30;    % 30 cycles
Wait = 5;    % Wait for 5 seconds before starting and before ending
Cutoff = 5;  % Cut off the first 5 cycles
Take = NumberC-Cutoff;
ti = Cutoff*((length(RawData)-1)/SamplingFrequency-
2*Wait)/NumberC+Wait;    % Find the starting time of the third cycle
tf = (length(RawData)-1)/SamplingFrequency-5;    % last time point
[min_difference_ti, array_position_ti] = min(abs(Time - ti));
% Find position of ti in "Time"
[min_difference_tf, array_position_tf] = min(abs(Time - tf));
% Find position of tf in "Time"
TimeN = [ti:1/SamplingFrequency:tf];
% Create a new time array "TimeN" starting with ti

%% Time for the average of the last 25 cycles
TimeAF = (tf-ti)/Take;    % Find the average time for each cycle
TimeAve = (0:1/SamplingFrequency:TimeAF);
% Time array for the averaged cycle

%%%% Strain:
%% Average Strain for the last 25 cycles
StrainN = Strain(array_position_ti:array_position_tf,:);
% StrainN take stresss points corresponding to TimeN
[mm,nn]=size(StrainN);
StrainPt = mm/Take;
Stcount1=0; Stcount2=1; StTotal = 0;
for n=1:Take
    St = StrainN(StrainPt*Stcount1+1:StrainPt*Stcount2);
    Stcount1=Stcount2; Stcount2=Stcount2+1;
    StTotal = StTotal + St;
end
StMean = StTotal/Take;
StMeanSet = StMean-min(StMean);


%%%%%%% UP(=Strain increase) ONLY %%%%%%%%
TimeUP = TimeAve((length(TimeAve)/2+1):length(TimeAve));
% Time array for an UP cycle
StMeanSetUP = StMeanSet(length(StMeanSet)/2+1:length(StMeanSet));
MaxStrainUP = max(StMeanSetUP);

%% UP Strain Rate
StMeanSetUP_PerSec =
StMeanSetUP(1:SamplingFrequency:size(StMeanSetUP));
% Strain at each second
StMeanSetUP_PerSec_average = tril(toeplitz([1/2 1/2
zeros(1,size(StMeanSetUP_PerSec)-2)]))*StMeanSetUP_PerSec;
StMeanSetUP_PerSec_average =
StMeanSetUP_PerSec_average(2:size(StMeanSetUP_PerSec_average));
% Average strain btw each second
StrainRateUP = diff(StMeanSetUP_PerSec);    % Strain Rate
```

```
MaxStrainRateUP = max(StrainRateUP);    % UP Maximum strain rate


%%%%%%% DOWN(=Strain decrease) ONLY %%%%%%%%
TimeDOWN = TimeAve(1:(length(TimeAve)/2));
% Time array for an DOWN cycle
StMeanSetDOWN = StMeanSet(1:length(StMeanSet)/2);
StMeanSetDOWNf = -StMeanSet(1:length(StMeanSet)/2);
% Flip the DOWN part
StMeanSetDOWNf = StMeanSetDOWNf - StMeanSetDOWNf(1);
% Force to start with "0"
MaxStrainDOWNf = max(StMeanSetDOWNf);

MaxStrain = (MaxStrainUP+MaxStrainDOWNf)/2

%% DOWN Strain Rate
StMeanSetDOWN_PerSec =
StMeanSetDOWNf(1:SamplingFrequency:size(StMeanSetDOWNf));
% Strain at each second
StMeanSetDOWN_PerSec_average = tril(toeplitz([1/2 1/2
zeros(1,size(StMeanSetDOWN_PerSec)-2)]))*StMeanSetDOWN_PerSec;
StMeanSetDOWN_PerSec_average =
StMeanSetDOWN_PerSec_average(2:size(StMeanSetDOWN_PerSec_average));
% Average strain btw each second
StrainRateDOWN = diff(StMeanSetDOWN_PerSec);    % Strain Rate
MaxStrainRateDOWN = max(StrainRateDOWN);    % DOWN Maximum strain rate
MaxStrainRate = (MaxStrainRateDOWN+MaxStrainRateUP)/2

ReStrain = [StMeanSetDOWNf;StMeanSetUP];


%% Creating a time array for each min and max point
Strain = Strain - Strain(1);
Cycles = NumberC;    % Number of cycles
FlipTime = Period/2;    % Time it takes for voltage to flip
FirstLowTime = Wait + FlipTime;
AverageTime = FirstLowTime:FlipTime:2*FlipTime*Cycles+FlipTime;

NCycle = 0:1:Cycles*2-1;
StrainSec = Strain((FirstLowTime +
NCycle.*FlipTime).*SamplingFrequency+1);    % Strain at each flip time

for a = 1:1:size(StrainSec,1)-1
      AverageStrain(a) = (StrainSec(a)+ StrainSec(a+1))./2;
end
AverageT =
(AverageTime(1)+AverageTime(2))/2:FlipTime:AverageTime(length(AverageTi
me));
AverageStrain = AverageStrain-AverageStrain(1);
```

III. Creep rate calculation

```
%% Creep Characterization
%%% Creating a time array for each min and max point
Strain = Strain - Strain(1);
Cycles = 30;    % Number of cycles
FlipTime = 10;    % Time it takes for voltage to flip
FirstLowTime = 5 + FlipTime;
AverageTime = FirstLowTime:FlipTime:2*FlipTime*Cycles+FlipTime;

NCycle = 0:1:Cycles*2-1;
StrainSec = Strain((FirstLowTime +
NCycle.*FlipTime).*SamplingFrequency+1);    % Strain at each flip time

for a = 1:1:size(StrainSec,1)-1
AverageStrain(a) = (StrainSec(a)+ StrainSec(a+1))./2;
end

%AverageStrain=AverageStrain.*100;
AverageT =
(AverageTime(1)+AverageTime(2))/2:FlipTime:AverageTime(length(AverageTi
me));



AverageStrainL = AverageStrain-AverageStrain(1);
Strain_6=Strain-Strain(1);
hold on
plot(Time,Strain)
AverageStrain(:)
hold on
plot(AverageTime,StrainSec,'r')
hold on
plot(AverageT,AverageStrain,'g')
```

IV. Charge calculation

```
%%% Average Charge
ChargeN = Charge(array_position_ti:array_position_tf,:);
% ChargeN take charge points corresponding to TimeN
[aa,bb]=size(ChargeN);
ChargePt = aa/Take;
Ccount1=0; Ccount2=1; CTotal = 0;
for n=1:Take
    C = ChargeN(ChargePt*Ccount1+1:ChargePt*Ccount2);
    Ccount1=Ccount2; Ccount2=Ccount2+1;
    CTotal = CTotal + C;
end
CMean = CTotal/Take;
CMeanV = CMean/(SampleWidth*SampleLength*SampleThickness);
CMeanSet = CMeanV-min(CMeanV);
MaxCMeanV = max(CMeanSet)
% plot(CMeanSet)

%%%%%%%% UP ONLY %%%%%%%%
TimeUP = TimeAve(1:(length(TimeAve)/2));    % Time array for an UP cycle
CMeanSetUP = CMeanSet(1:length(CMeanSet)/2);
CMeanSetUP = CMeanSetUP - CMeanSetUP(1);    % Force to start with "0"
MaxChargeUP = max(CMeanSetUP)

%%% UP Charge Rate
CMeanSetUP_PerSec = CMeanSetUP(1:SamplingFrequency:size(CMeanSetUP));
% Strain at each second
CMeanSetUP_PerSec_average = tril(toeplitz([1/2 1/2
zeros(1,size(CMeanSetUP_PerSec)-2)]))*CMeanSetUP_PerSec;
CMeanSetUP_PerSec_average =
CMeanSetUP_PerSec_average(2:size(CMeanSetUP_PerSec_average));
% Average strain btw each second
ChargeRateUP = diff(CMeanSetUP_PerSec);    % Strain Rate
MaxChargeRateUP = max(ChargeRateUP)    % Maximum strain rate

%%%%%%%% DOWN ONLY %%%%%%%%
TimeDOWN = TimeAve((length(TimeAve)/2+1):length(TimeAve));
% Time array for an DOWN cycle
CMeanSetDOWN = CMeanSet(length(CMeanSet)/2+1:length(CMeanSet));
MaxChargeDOWN = max(CMeanSetDOWN)

%%% DOWN Charge Rate
CMeanSetDOWN_PerSec =
CMeanSetDOWN(1:SamplingFrequency:size(CMeanSetDOWN));
% Strain at each second
CMeanSetDOWN_PerSec_average = tril(toeplitz([1/2 1/2
zeros(1,size(CMeanSetDOWN_PerSec)-2)]))*CMeanSetDOWN_PerSec;
CMeanSetDOWN_PerSec_average =
CMeanSetDOWN_PerSec_average(2:size(CMeanSetDOWN_PerSec_average));
% Average Charge btw each second
ChargeRateDOWN = diff(CMeanSetDOWN_PerSec);    % Strain Rate
MaxChargeRateDOWN = abs(max(ChargeRateDOWN))    % Maximum strain rate

MaxCharge = (MaxChargeUP+MaxChargeDOWN)/2
```